Comparative Analysis of ACE-FTS, OSIRIS & PEARL FTIR Ozone Measurements

Sallam Saka

University of Toronto, Department of Physics

Supervisor: Professor Kaley Walker

Mentor: Dr Paul Jeffery

August 6, 2025

Abstract

This study presents a comprehensive comparative analysis of stratospheric ozone measurements from the Atmospheric Chemistry Experiment Fourier Transform Spectrometer (ACE-FTS), the Optical Spectrograph and Infrared Imager System (OSIRIS), and the ground-based Polar Environment Atmospheric Research Laboratory Fourier Transform Infrared Spectrometer (PEARL FTIR). Using coincident measurement pairs (≤500 km, ≤8 hours apart), ozone profiles and columns were evaluated through statistical metrics including absolute/relative differences, Pearson correlation coefficients, and temporal divergence trends. Key findings reveal strong agreement between all instruments for ozone column comparisons. Profile comparisons also showed good agreement and consistent seasonal patterns. Temporal analysis indicated no significant long-term divergence between instruments. These results validate the consistency of ACE-FTS and OSIRIS satellite measurements against ground-based PEARL FTIR data, reinforcing their reliability for atmospheric ozone monitoring, particularly in the high Arctic.

Table of Contents

1 INTRODUCTION **4**

1.1 Background 4

1.2 Instruments 5

1.2.1 ACE-FTS *5*

1.2.2 OSIRIS *5*

1.2.3 PEARL FTIR *7*

2 METHODOLOGY **7**

2.1 Coincidence Criteria and Comparison Metrics 7

3 RESULTS **8**

3.1 Preliminary Findings 8

3.2 Profile comparisons 13

3.2.1 OSIRIS vs ACE-FTS Profile Comparisons *13*

3.2.1.1 Global OSIRIS vs ACE-FTS Profile Comparisons 13

3.2.1.2 Above PEARL OSIRIS vs ACE-FTS Comparisons 18

3.2.2 Satellite-based vs PEARL FTIR Profile Comparisons *22*

3.2.2.1 ACE-FTS vs PEARL FTIR Profile Comparisons 22

3.2.2.2 OSIRIS vs PEARL FTIR Profile Comparisons 27

3.3 Column comparisons 31

3.3.1 Partial Column Altitude Range *31*

3.3.1.1 Partial Column Upper Bound Choice 31

3.3.1.2 Partial Column Lower Bound Choice 31

3.3.2 OSIRIS vs ACE-FTS Column Comparisons *32*

3.3.2.1 Global OSIRIS vs ACE-FTS Column Comparisons 32

3.3.2.2 Above PEARL OSIRIS vs ACE-FTS Column Comparisons 35

3.3.3 Satellite-based vs PEARL FTIR Column Comparisons *38*

3.3.3.1 ACE-FTS vs PEARL FTIR Column Comparisons 38

3.3.3.2 OSIRIS vs PEARL FTIR Column Comparisons 41

3.3.4 Time Series Column Comparisons *44*

4 CONCLUSION **45**

5 APPENDIX **46**

6 REFERENCES **53**

1 Introduction

1.1 Background

The atmosphere is a mixture of gases and aerosols that surround the earth and extends up to thousands of miles away from earth, reducing in density the farther away it is (NOAA, 2024). The atmosphere serves a variety of functions such as containing the oxygen we breathe and keeping Earth sufficiently warm which are vital for human life (NOAA, 2024). Nitrogen is the most abundant gas in the atmosphere, forming ~78% of gases in the atmosphere, followed by Oxygen and Argon, forming ~21% and ~1% of the atmosphere, respectively (NOAA, 2024). Water vapour is also found in the atmosphere ranging from 0-4% of the atmosphere along with other gases that are scarcer in the atmosphere (NOAA, 2024). One of the atmosphere's minor constituents is Ozone (O_3), yet it is one of the most important atmospheric gases (Salawitch et al., 2023). About 10% of ozone resides in the troposphere, while the rest is in the stratosphere (Salawitch et al., 2023). The main reason for the importance of ozone is its ability to absorb ultraviolet light, specifically, UV-C and UV-B radiation which are dangerous to all life forms (Salawitch et al., 2023). For humans, the radiation could cause skin cancer, cataracts, and suppress the immune system (Salawitch et al., 2023). The crucial role of ozone in the atmosphere makes it an important gas to monitor, along with other atmospheric gases (Salawitch et al., 2023).

One of the methods used in monitoring atmospheric composition is remote sensing and spectroscopy. Atmospheric remote sensing and spectroscopy is routinely performed by satellite-based instruments and ground-based instruments around the world. A major limitation of satellite-based instruments is that they are not accessible to on-site supervision. In comparison, ground-based instruments are routinely supervised in-person. This downside of satellite-based instruments restricts the ability of scientists to verify proper functioning of the instruments to data retrieved remotely from the instruments. This verification process requires an independent data source against which to compare the satellite data which is provided by the ground-based instruments. Measurements can also be validated by comparing satellite measurements to each other. Every year, there is an intensive validation campaign done in the Arctic, specifically, at the Polar Environment Atmospheric Research Laboratory (PEARL) in Eureka, Nunavut (80°N, 86°W) (Kerzenmacher et al., 2005; Batchelor et al., 2010; Adams et al., 2012). These campaigns consist of atmospheric measurements using various instruments such as Fourier Transform Spectrometers, UV-Vis Spectrometers, Ozonesonde launches, etc (Department of Physics, University of Toronto, n.d.; Kerzenmacher et al., 2005). The collection of these measurements provides an extensive data to use for comparison with the measurements retrieved from satellite-based instruments. One of the Fourier Transform Spectrometers at PEARL, referred to as PEARL FTIR in this paper, and will act as an independent source of data for comparison with the satellite-based instruments, ACE-FTS and OSIRIS. Specifically, I will be comparing ozone profile and column data between each pair of these instruments using various computational and visualization techniques.

1.2 Instruments

1.2.1 ACE-FTS

Atmospheric Chemistry Experiment (ACE), also known as SCISAT-1, is a Canadian satellite mission intended for remote sensing of Earth's atmosphere (Bernath, 2005). SCISAT was launched into a circular orbit at an altitude of 650km and inclination of 74° on 12 August 2023 (Bernath, 2005). The purpose of ACE is to understand the chemical and dynamical processes that control the distribution of ozone in the stratosphere and upper troposphere, explore the relationship between atmospheric chemistry and climate change, study the effects of biomass burning on free troposphere and measure aerosols and clouds to reduce the uncertainties in their effects on the global energy balance (Bernath, 2005). To achieve its goals, the satellite contains 2 instruments, ACE-FTS (ACE Fourier Transform Spectrometer) and ACE-MAESTRO (ACE Measurement of Aerosol Extinction in the Stratosphere and Troposphere Retrieved by Occultation) (Bernath, 2005). ACE-FTS is a high resolution (0.02 cm^{-1}) Fourier transform spectrometer, operating in the wavenumber range of 750-4400 cm^{-1} (Bernath, 2005). During the satellite's sunrise and sunset, ACE-FTS measures solar absorption spectra of the atmosphere in the limb viewing geometry, looking towards the sun, with a vertical resolution of 4km. ACE-FTS is also augmented by two imagers which provide measurements of atmospheric extinction, all three instruments share one sun tracker (Bernath, 2005). The satellite completes an identical cyclic pattern of measurements annually as seen in Figure 1. Together, ACE-FTS, ACE-MAESTRO and its imagers provide a comprehensive amount of atmospheric data.

1.2.2 OSIRIS

The Optical Spectrograph and Infrared Imager System (OSIRIS), along with a sub-mm/mm radiometer (SMR), is on-board the ODIN satellite which was launched on 20 February 2001 into a circular Sun-synchronous 620 km orbit elevation (Llewellyn, 2004; Murtagh, 2002). The satellite is intended for investigations in aeronomy and astronomy. The objective of the aeronomy mission is to study stratospheric ozone science, mesospheric ozone science, summer mesosphere science and mechanisms involved in coupling of atmospheric regions (Murtagh, 2002). OSIRIS is composed of 2 different parts, the Optical Spectrograph (OS) and the Infrared Imager (IRI) (Llewellyn, 2004). The OS collects data that includes Rayleigh-scattered sunlight spectra within the wavelength range of 280-800nm and atmospheric emission features such as airglow and auroral emissions (Llewellyn, 2004). The IRI data also includes Rayleigh-scattered sunlight and airglow near 1270 nm and 1530 nm wavelengths (Murtagh, 2002). The satellite is pointed at the limb of the earth, towards its movement direction, allowing it to collect scattered sunlight (Llewellyn, 2004). The OSIRIS data used in this paper is from the OS. The ODIN satellite also completes an identical cyclic measurement pattern annually as seen in Figure 2.

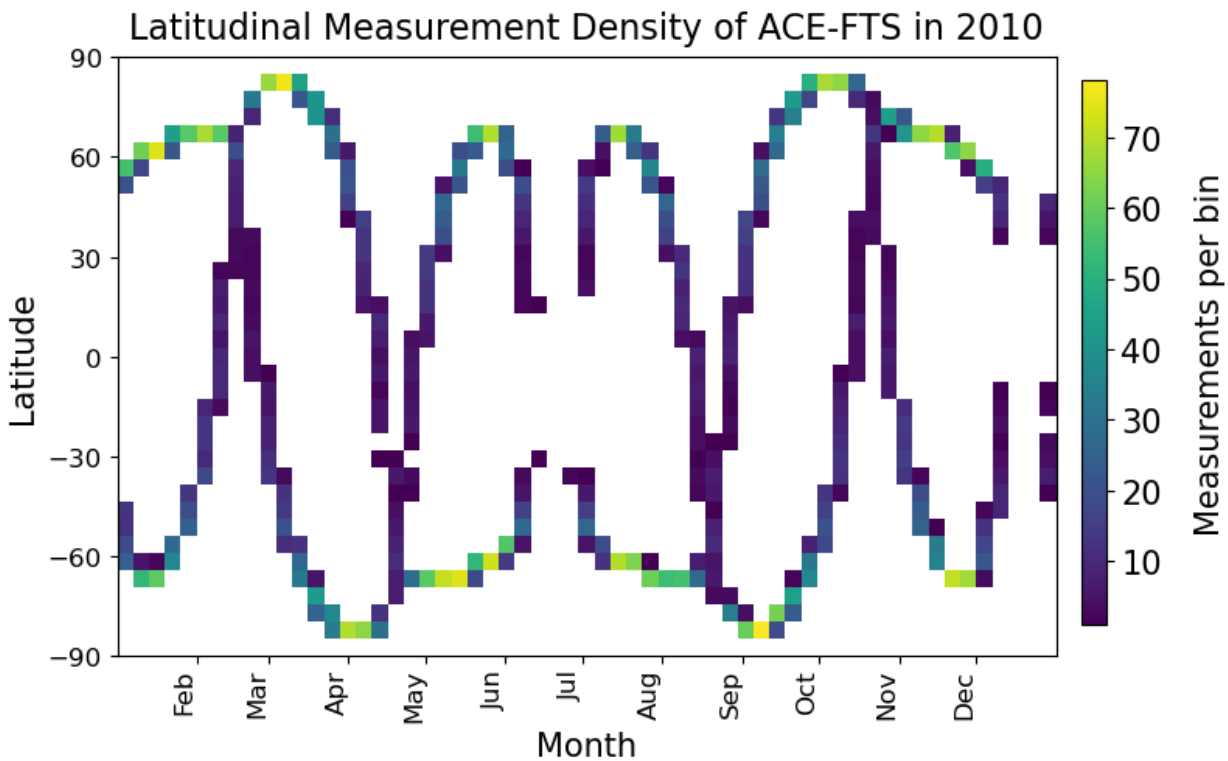

Figure 1. Representative yearly latitudinal measurement density of ACE-FTS.

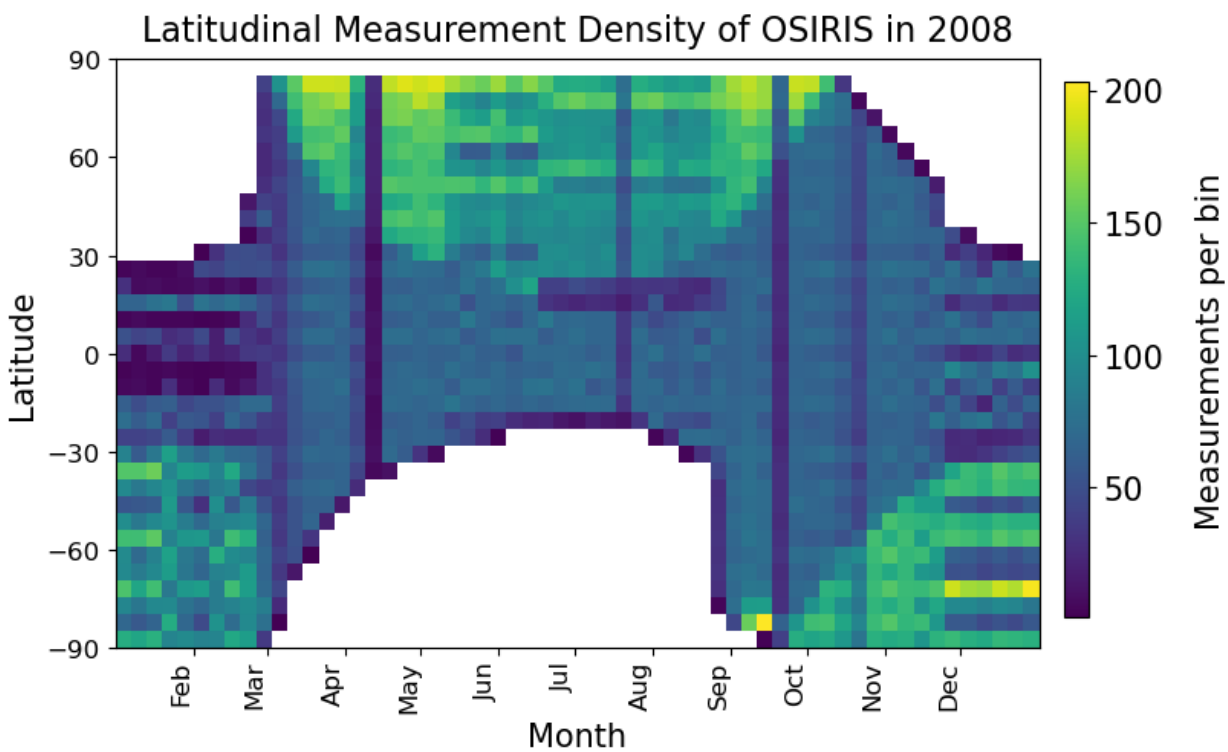

Figure 2. Representative yearly latitudinal measurement density of OSIRIS.

1.2.3 PEARL FTIR

Polar Environment Atmospheric Research Laboratory Fourier-Transform Infra-Red Spectrometer (PEARL FTIR), also referred to as Bruker FTIR, is a ground-based Michelson interferometer (Batchelor, 2009). PEARL FTIR was permanently installed at PEARL in 2006 (Adams, 2012). It operates between the wavenumber ranges of 1850-10000 cm^{-1} 600-6000 cm^{-1} at a high resolution of up to 0.0024 cm^{-1} (Batchelor, 2009). PEARL FTIR makes direct sun-absorption measurements during sunlit times in the Arctic (about 21st February – 20th October) using a sun tracker installed on the roof of its enclosure to direct sunlight to itself (Batchelor, 2009; Griffin, 2017). PEARL FTIR has also been used in several studies for comparison against various instruments (Griffin, 2017; Batchelor, 2010; Adams, 2012).

2 Methodology

2.1 Coincidence Criteria and Comparison Metrics

Comparisons were made between individual pairs of coincident measurements for each pair of instruments (i.e. OSIRIS vs ACE-FTS, OSIRIS vs PEARL FTIR, ACE-FTS vs PEARL FTIR). The criteria used to assess whether two measurements could be similar enough to be appropriate for comparison was that each pair of measurement must be a maximum of 500 km and 8 hours apart. These criteria are used throughout this paper. The distance criterion represents the great-circle distance between the measurement locations. The great-circle distance was computed using the haversine distance formula below:

$$\text{Longitudinal difference: } \Delta\lambda = \lambda_2 - \lambda_1$$

$$\text{Latitudinal difference: } \Delta\phi = \phi_2 - \phi_1$$

$$a = \sin^2\left(\frac{\Delta\phi}{2}\right) + \cos(\phi_1) \cdot \cos(\phi_2) \cdot \sin^2\left(\frac{\Delta\lambda}{2}\right)$$

$$\text{Great-circle distance: } d = 2 \cdot \arcsin\left(\sqrt{a}\right) \cdot 6371$$

The choice of these criteria was originally due to a suggestion, however, further experimentation with different criteria showed that the chosen criteria yield the satisfactory results because it is narrow enough to minimize outliers but wide enough to get a representative sample of measurement pairs. To compare measurement pairs, various statistics were computed and visualized which are shown in Table 1. As a standard of this paper, the instrument on the left of "and/vs", in "OSIRIS and/vs PEARL FTIR", "ACE-FTS and/vs PEARL FTIR" and "OSIRIS and/vs ACE-FTS" will be the "S_1" instrument, while the other instrument would be "S_2" when performing computations.

Statistic	Formula
Absolute Difference	$S_1 - S_2$
Relative Difference	$200\% \times \frac{S_1 - S_2}{S_2 + S_2}$
Pearson Correlation Coefficient	$\mathrm{r} = \frac{\sum_{i=1}^{n}(S_{1i} - \bar{S_1})(S_{2i} - \bar{S_2})}{\sqrt{\sum_{i=1}^{n}(S_{1i} - \bar{S_1})^2}\sqrt{\sum_{i=1}^{n}(S_{2i} - \bar{S_2})^2}}$
Mean Absolute Difference	$\frac{(\sum_{i=1}^{n} Absolute\ Difference_i)}{n}$
Mean Relative Difference	$\frac{(\sum_{i=1}^{n} Relative\ Difference_i)}{n}$

Table 1. Formulas of Comparison Statistics.

3 Results

3.1 Preliminary Findings

Prior to finding coincident measurements, computing comparison metrics and visualizing the computed values, the data of each satellite were visualized and explored individually. This exploratory data analysis allows for familiarization with the data and ensures data quality. The ACE-FTS data were initially filtered using the data quality flags outlined in Sheese et al. (2015) by only using data with a flag value of 0 which is deemed by Sheese et al. to have no known issues. Figures 3 and 4 below made from the ACE-FTS and OSIRIS data, respectively, showcase the latitudinal (x-axis) and altitudinal (y-axis) distribution of ozone in units of ppmv during various seasons. The time range of 2006 to 2020 was chosen because this is the time range where all three instruments have recorded measurements.

In Figure 3, it is very evident that most of the ozone is measured to reside in the stratosphere, specifically, between about 20-45km altitudes which is an expected result (Salawitch et al., 2023). This pattern is also reproduced from the OSIRIS plot in Figure 4. Additionally, the latitudes where ozone is most concentrated shifts seasonally in both plots. For example, at higher Northern Hemisphere latitudes, during the Northern Hemisphere spring season, ozone VMR is noticeably higher compared to Northern Hemisphere winter which is also expected due to increased ozone transport from the tropics (Salawitch et al., 2023). These plots serve as good verification that the

measurements taken by the instruments align with expectations and capture similar ozone distribution patterns.

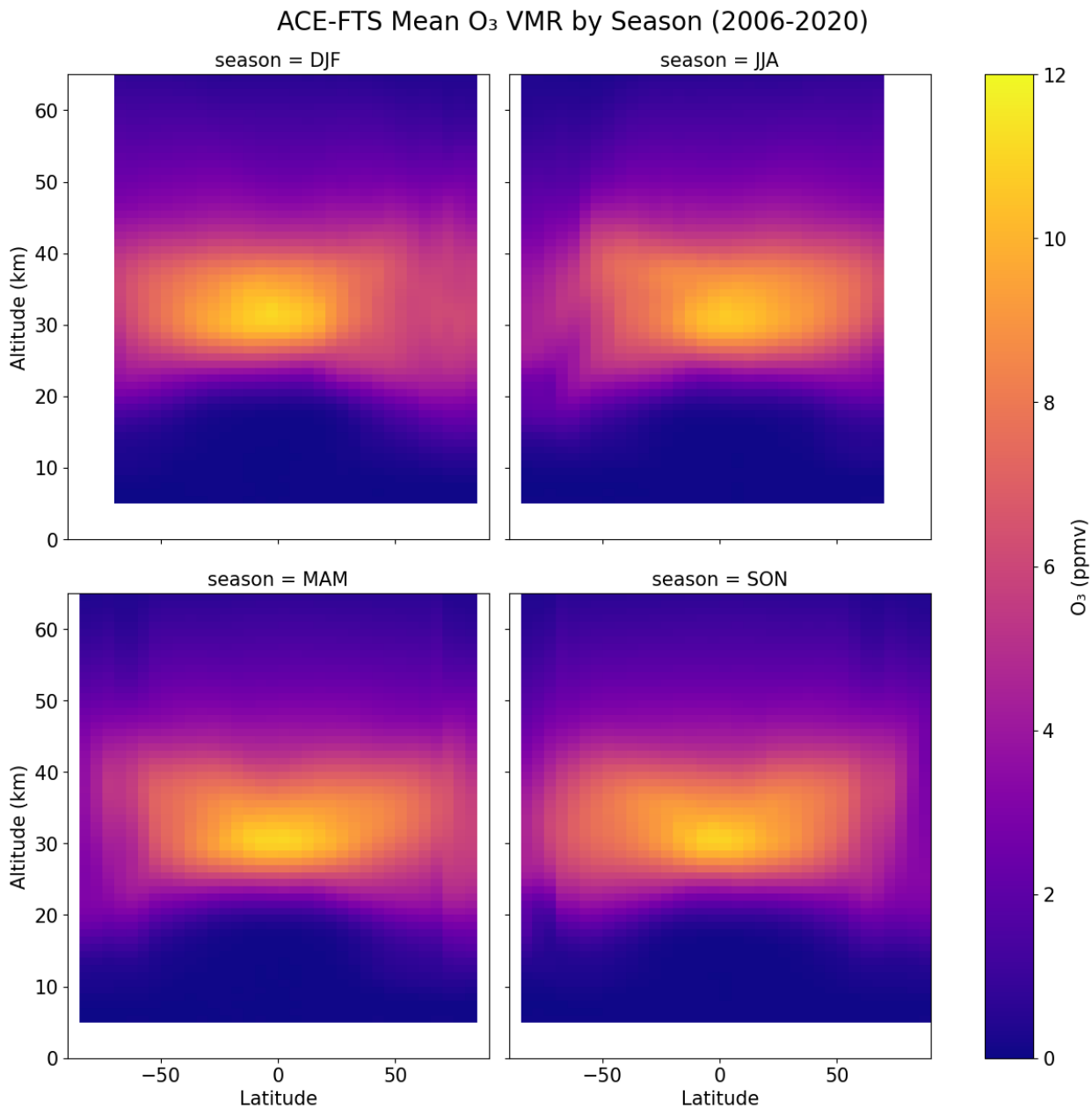

Figure 3. Climatology plot depicting latitudinal and altitudinal distribution of mean ozone VMR by ACE-FTS between 2006 and 2020.

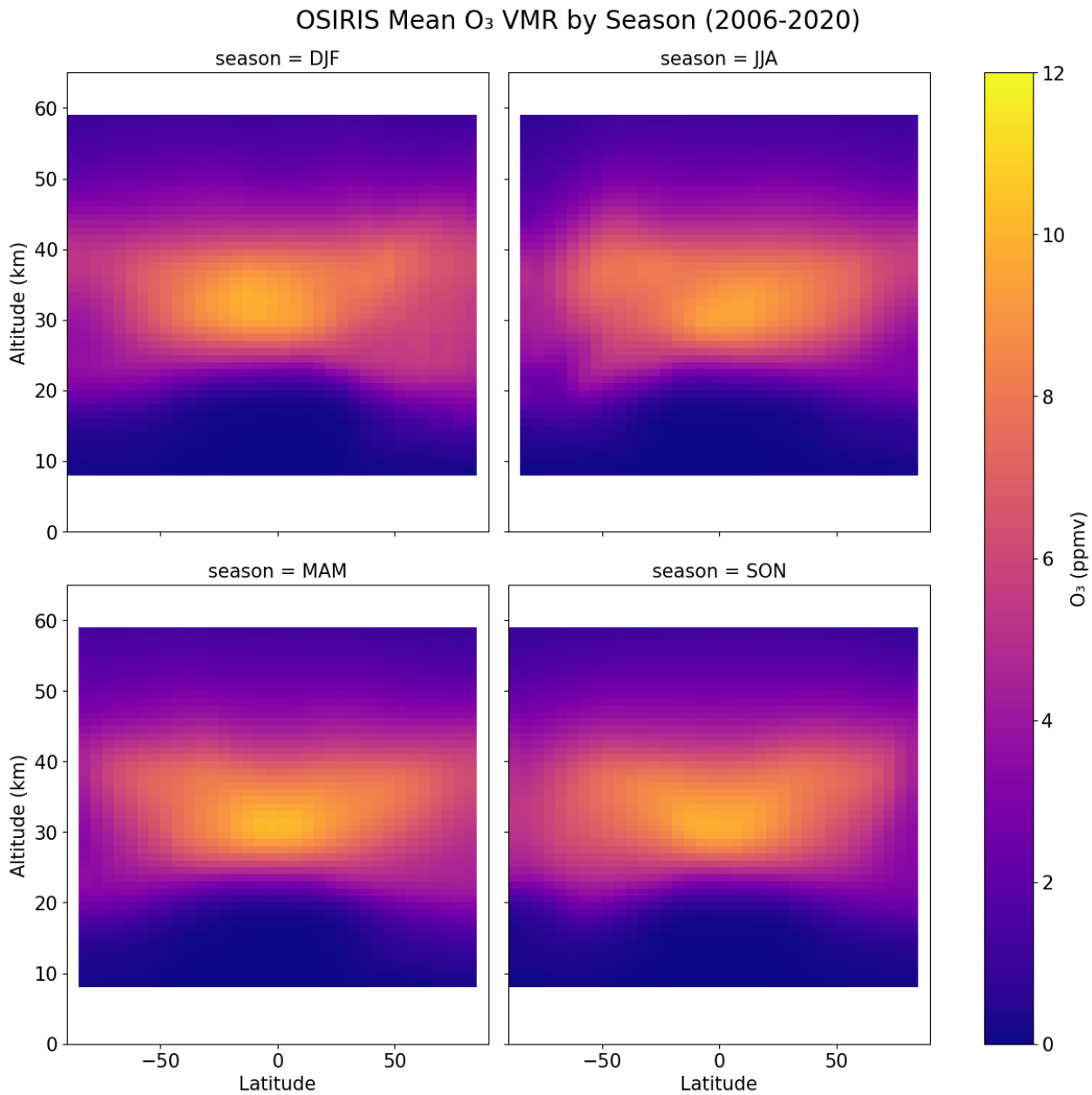

Figure 4. Climatology plot depicting latitudinal and altitudinal distribution of mean ozone VMR by OSIRIS between 2006 and 2020.

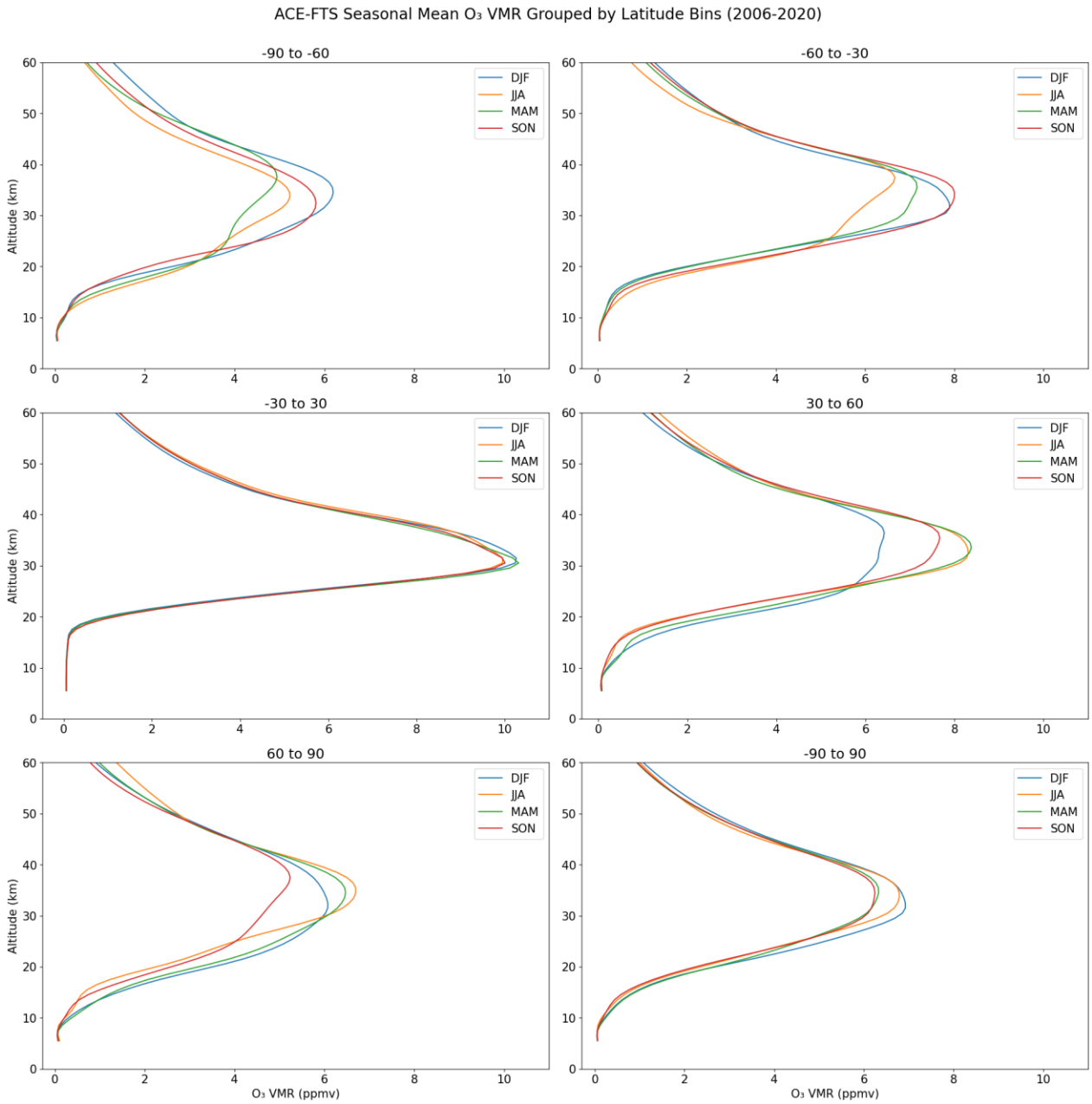

Figure 5. Line plots depicting seasonal mean ozone VMR measurements by ACE-FTS in six different latitude bins between 2006 and 2020.

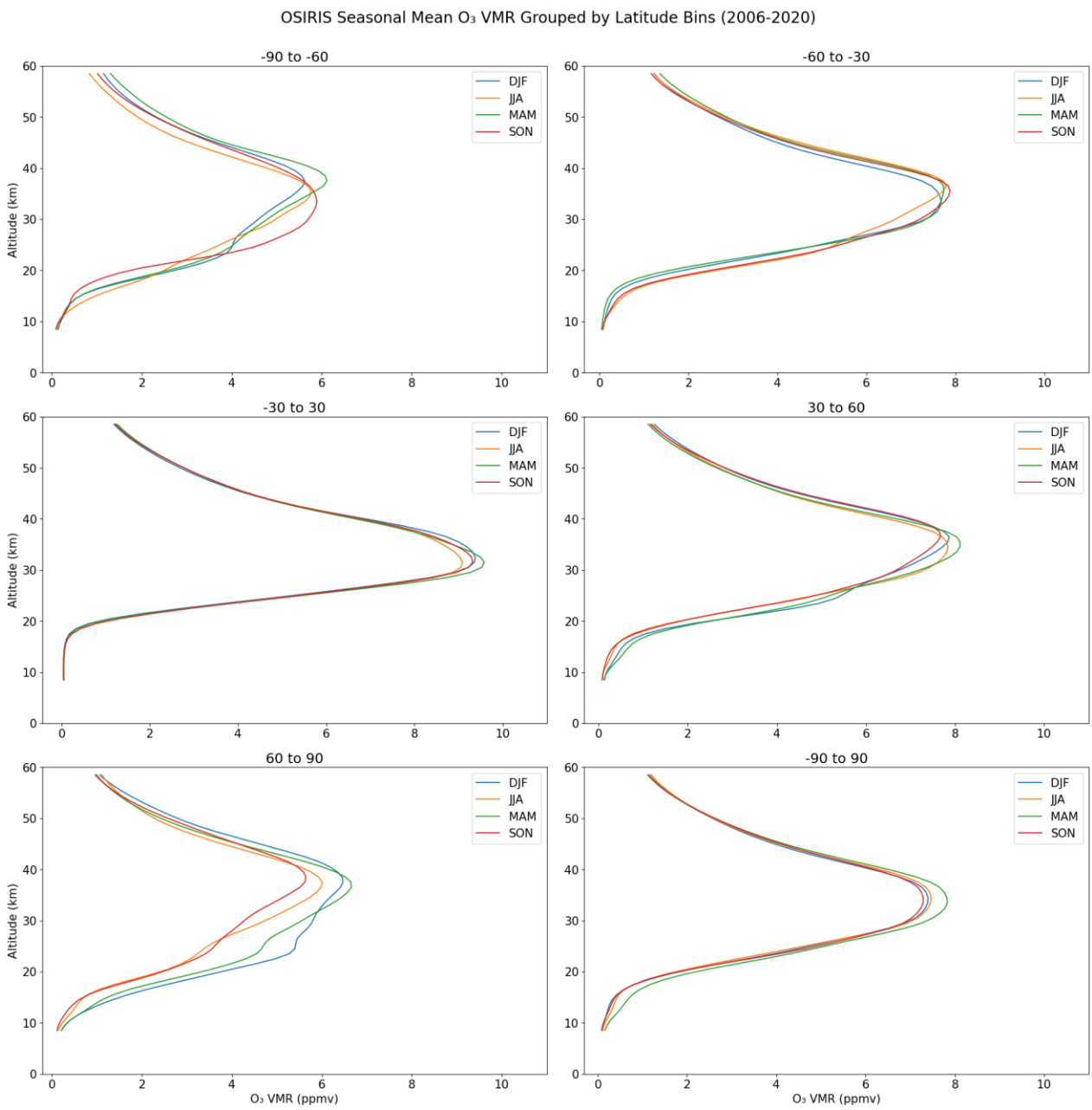

Figure 6. Line plots depicting seasonal mean ozone VMR measurements by OSIRIS in six different latitude bins between 2006 and 2020.

Figures 5 and 6, computed from ACE-FTS and OSIRIS data, respectively, compare mean ozone profiles seasonally, within six different latitude bins. General ozone patterns such as high ozone VMR in the tropics and lower ozone VMR at the poles are captured by both plots. However, these series of plots reveal some discrepancies that are difficult to notice from the climatology plot. For example, the mean ozone VMR at the tropics is higher in the ACE-FTS dataset for every season. Furthermore, the global ozone mean tends to be higher in the OSIRIS plot. There are many other minor discrepancies in the plots in other latitude bands. These discrepancies arise from the different

temporal and spatial measurement densities of the instruments as well as the different measurement techniques. To control for the differences that arise due to the difference in temporal and spatial measurement densities, comparing individual pairs of coincident measurements is crucial which will be the methodology adopted in ensuing sections.

3.2 Profile comparisons

The plots below will be focused on the stratospheric layer of the atmosphere. Firstly, a plot of all individual coincident profiles of each instrument alongside its paired partner will be shown. Subsequently, absolute and relative difference plots aggregated over all seasons will be shown which will be followed be a Pearson correlation coefficient plot. For all the plots mentioned above, they will be followed by a seasonal equivalent. For pairs of coincident measurements, data from all available time periods were included in the analysis. Some notation included in the plots are: N and r which represent number of coincidences and Pearson correlation coefficient, respectively. Additionally, dashed boundaries around line plots represent one standard deviation from the mean. All these plots will be discussed simultaneously as they are shown.

3.2.1 OSIRIS vs ACE-FTS Profile Comparisons

Two sets of comparisons of OSIRIS to ACE-FTS profiles were done. The first set of comparisons had no spatial restrictions while the other set was restricted to being a maximum of 500 km great-circle distance away from PEARL.

3.2.1.1 Global OSIRIS vs ACE-FTS Profile Comparisons

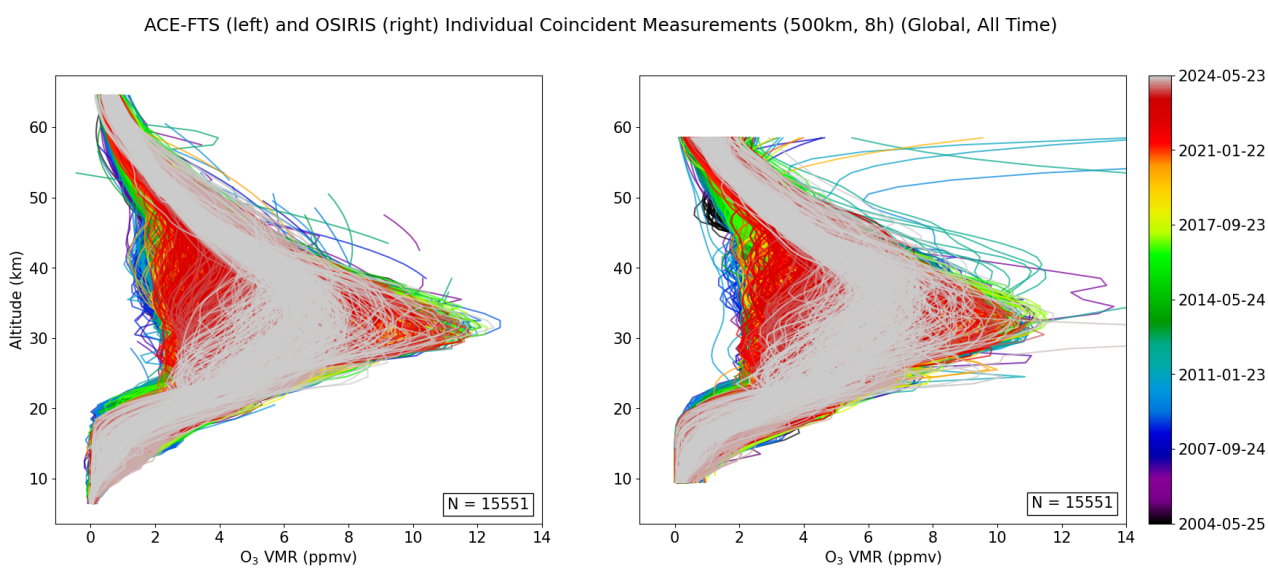

Figure 7. Line plots of individual global coincident ozone profiles from ACE-FTS (left) and OSIRIS (right).

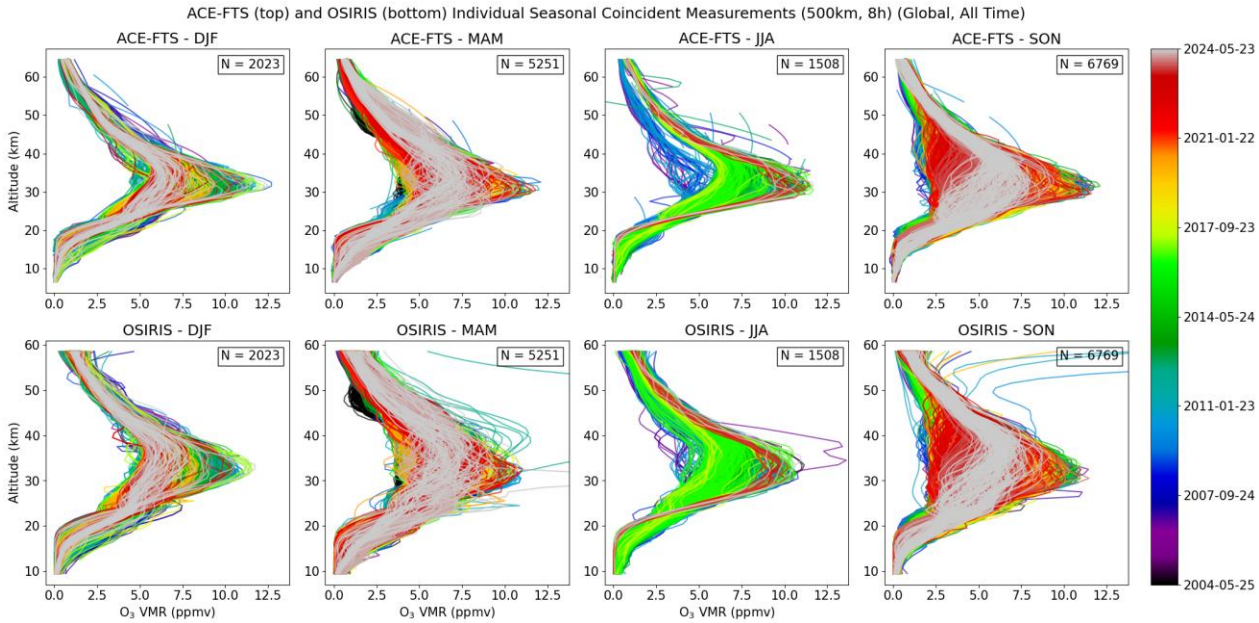

Figure 8. Seasonal line plots of individual global coincident ozone profiles from ACE-FTS (top) and OSIRIS (bottom).

Figure 7 highlights several prominent features, including a narrower peak in the ACE-FTS measurements and the presence of more extreme values in the OSIRIS plot which both indicate more variability in the OSIRIS measurements. Figure 8 shows that these features are present in all seasons but mostly present in the Northern Hemisphere fall and spring seasons.

Figure 9 suggests that the measurements are very similar with their average absolute differences being confined within -0.40 to 0.25 ppmv at all altitudes. Figure 10 shows that the pattern of agreement between the instruments at the various altitudes is similar across all seasons, so, no season is specifically responsible for the range of average absolute differences.

Figures 11 and 12 support the insights derived from Figures 9 and 10. Firstly, they show that the mean relative differences are mostly confined to between -10% and 5% for most altitudes. The increase in relative differences at the edges of the stratosphere result from exaggerated small differences in ozone measurements due to little ozone being present. Like the absolute difference seasonal plots, the pattern of agreement of measurement across various altitudes is similar between the seasons.

Figures 13 and 14 confirms the pattern observed in the relative and absolute difference plots. They show that the measurements are very correlated in the stratosphere, and more specifically, the ozone layer (~15-35 km) before the correlation drops off at the edges of the stratosphere. The seasonal correlation plots indicate that in Northern Hemisphere winter and summer, the correlation decreases faster.

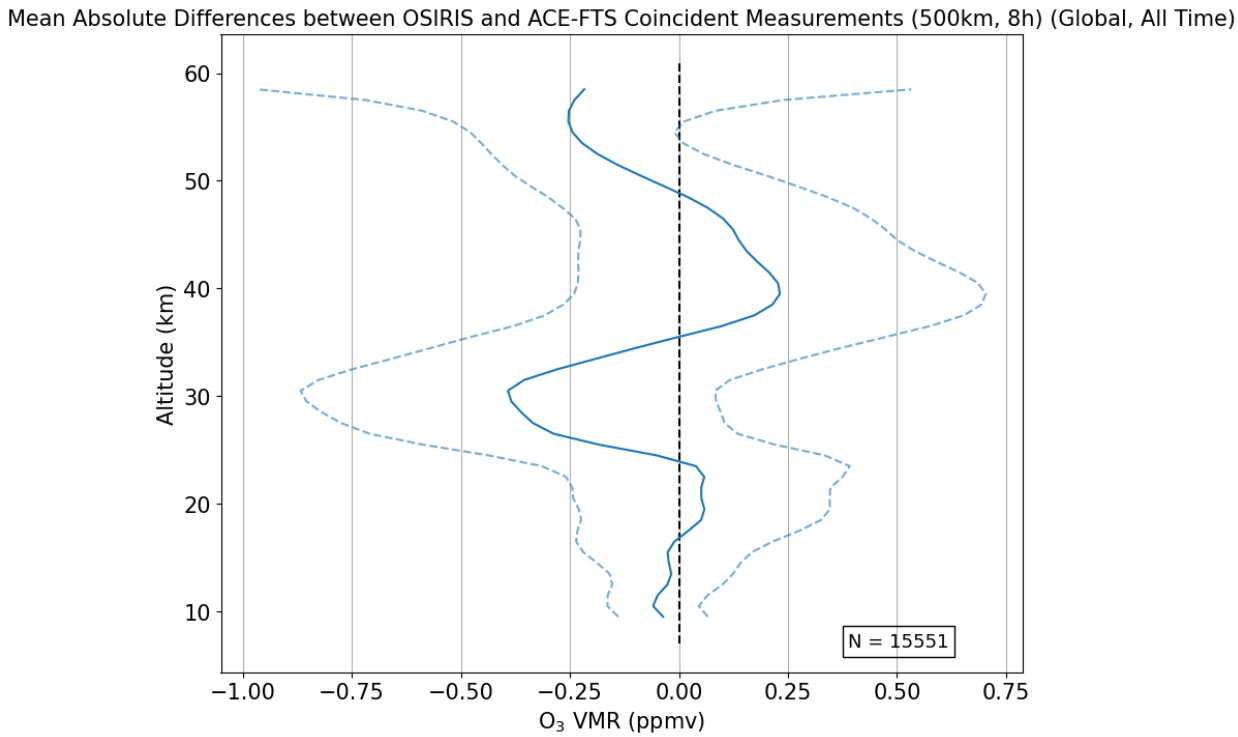

Figure 9. Line plot of the mean absolute difference of all OSIRIS and ACE-FTS global coincident ozone measurements at each altitude.

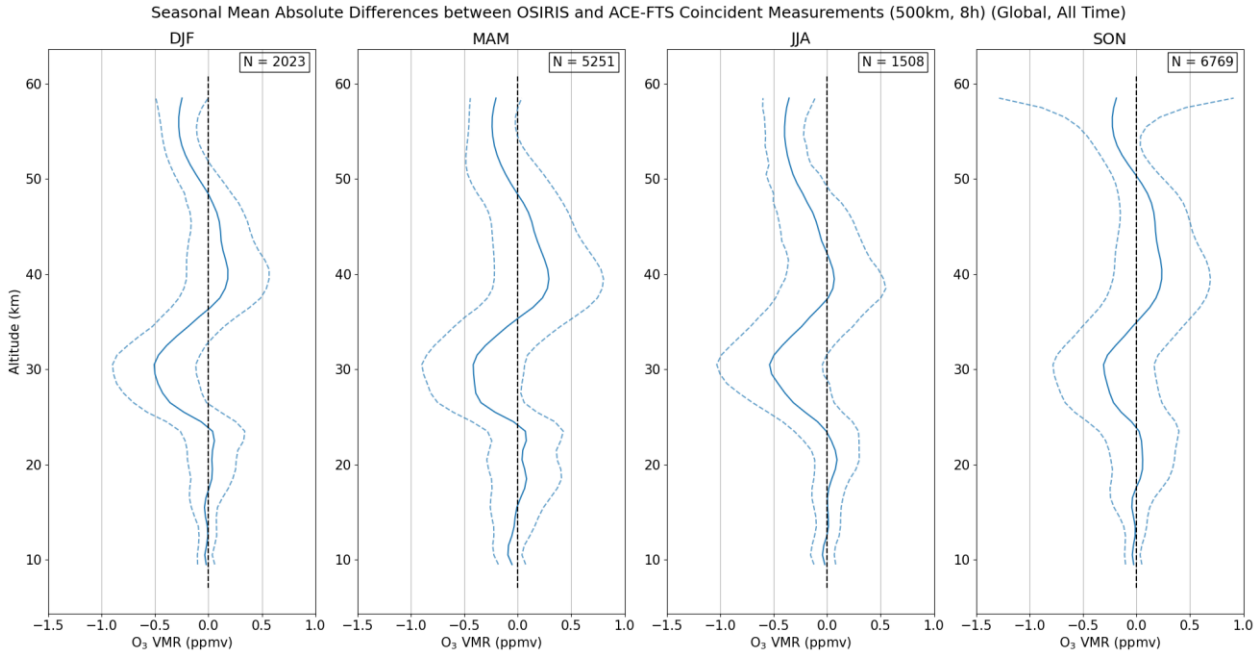

Figure 10. Seasonal line plots of the mean absolute difference of all OSIRIS and ACE-FTS global coincident ozone measurements at each altitude.

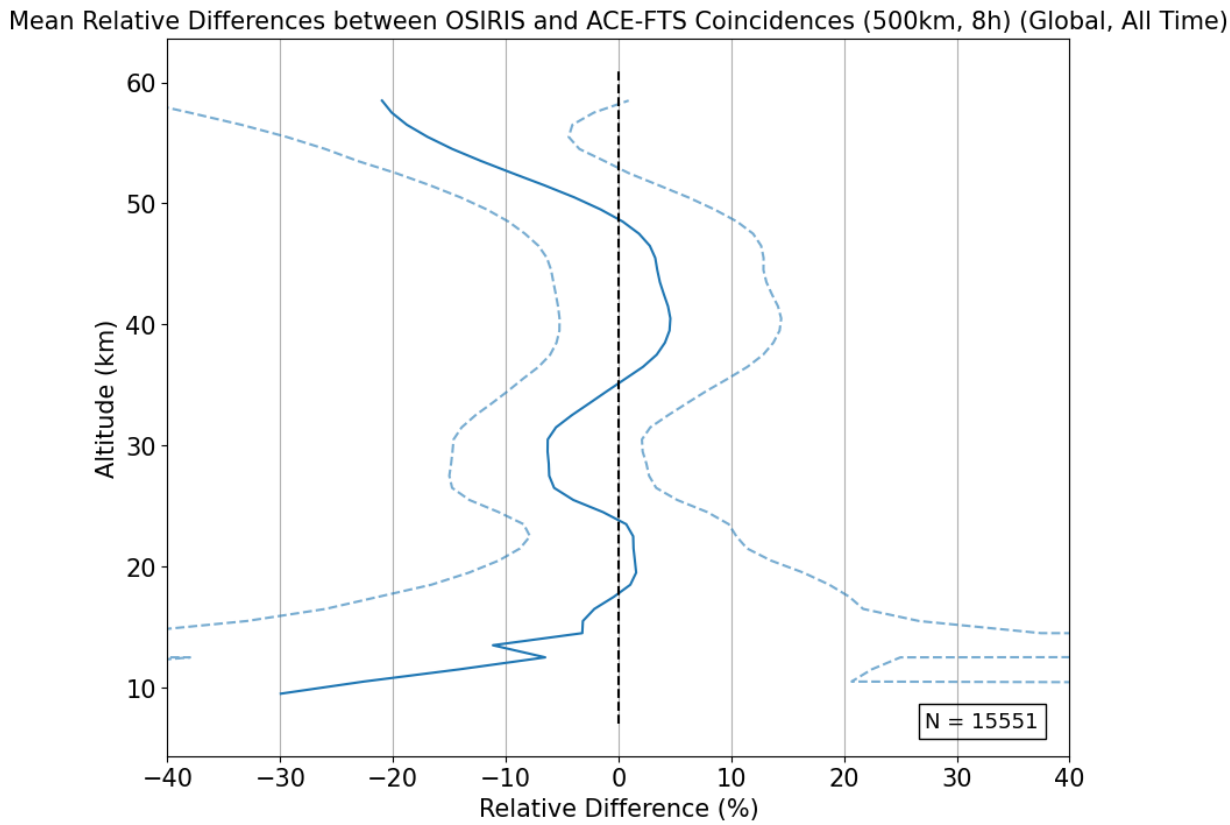

Figure 11. Line plot of the mean relative difference of all OSIRIS and ACE-FTS global coincident ozone measurements at each altitude.

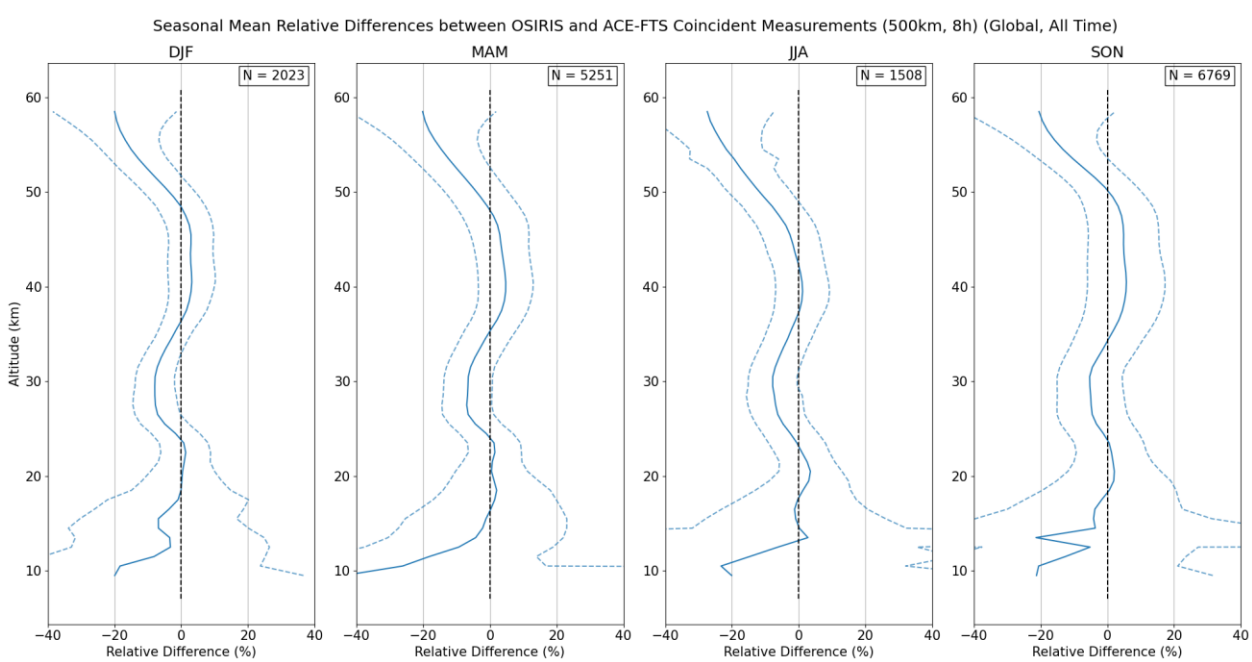

Figure 12. Seasonal line plots of the mean relative difference of all OSIRIS and ACE-FTS global coincident ozone measurements at each altitude.

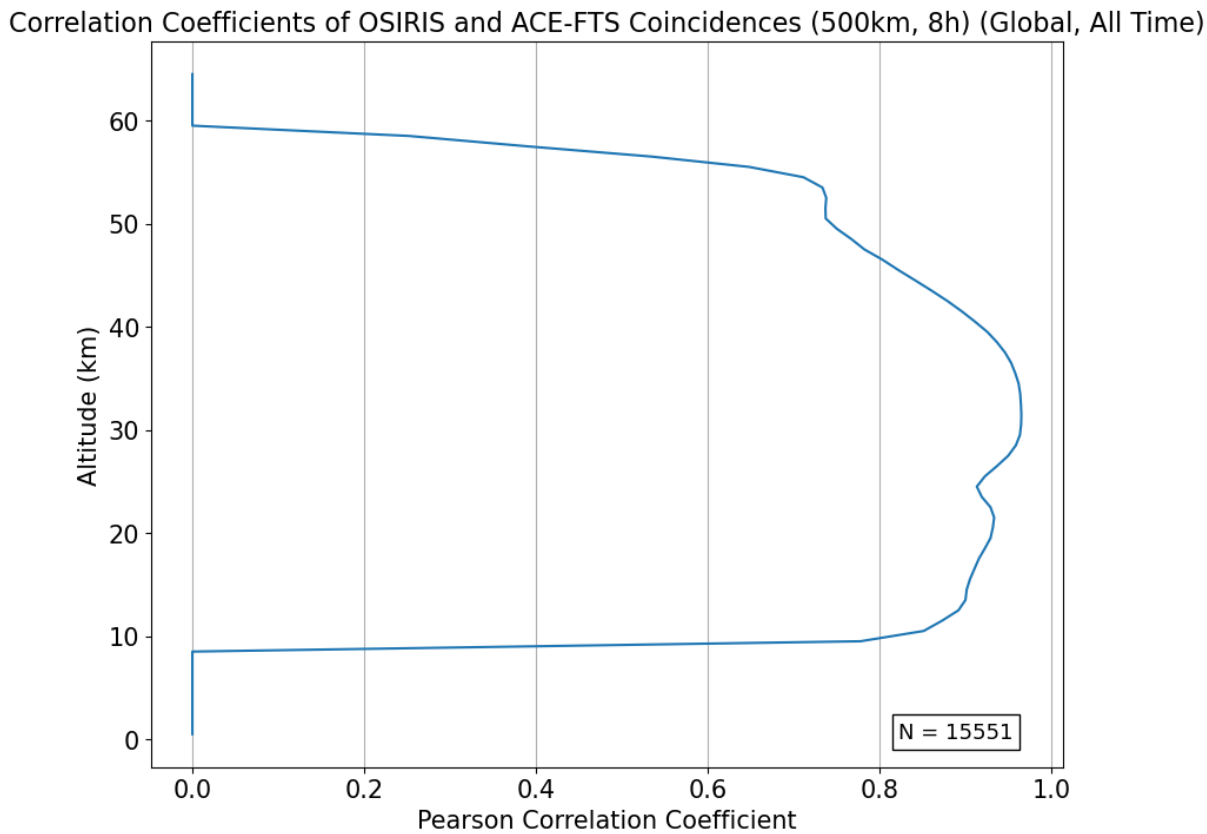

Figure 13. Line plot of the Pearson correlation coefficient of all OSIRIS and ACE-FTS global coincident ozone measurements at each altitude.

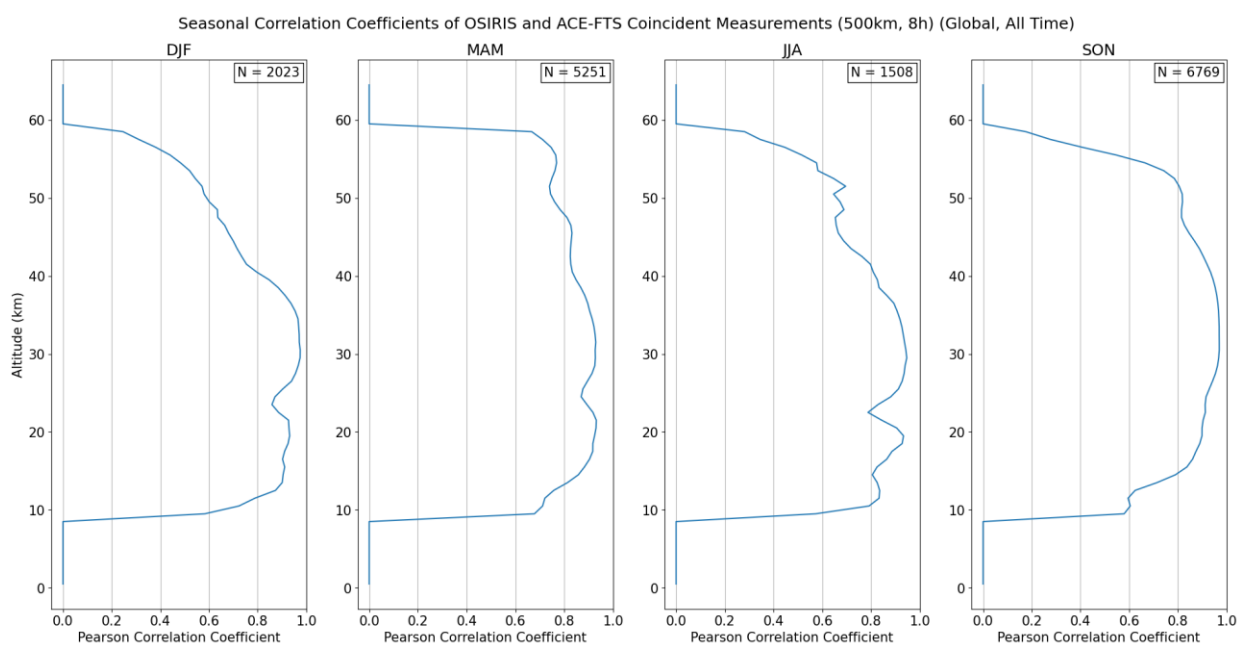

Figure 14. Seasonal line plots of the Pearson correlation coefficient all OSIRIS and ACE-FTS global coincident ozone measurements at each altitude spanning all available time periods.

3.2.1.2 Above PEARL OSIRIS vs ACE-FTS Comparisons

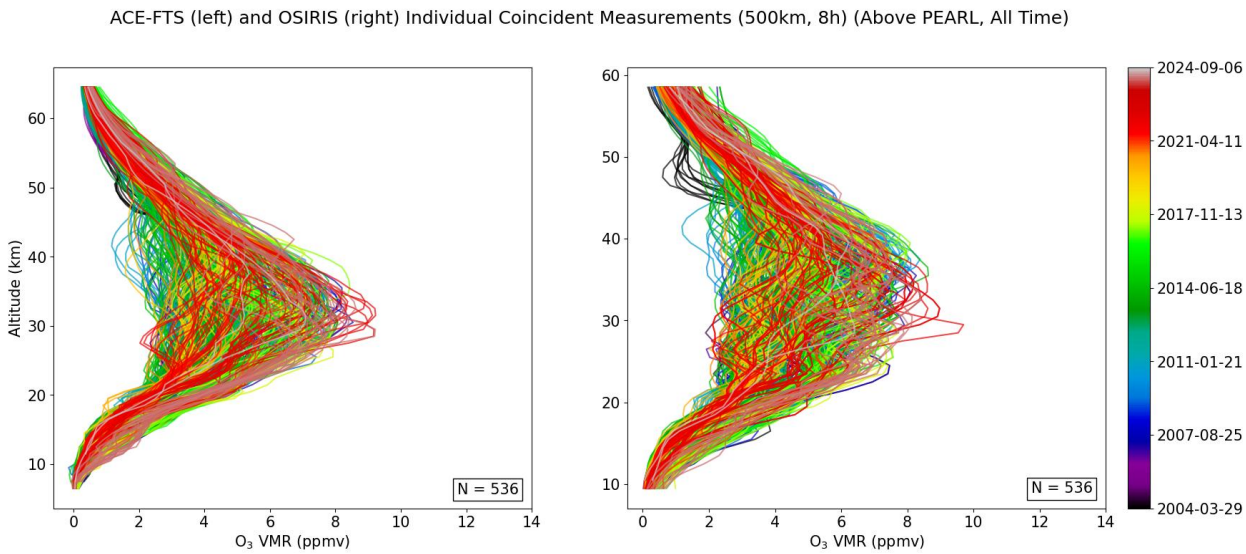

Figure 15. Line plots of individual coincident ozone profiles above PEARL from ACE-FTS (left) and OSIRIS (right).

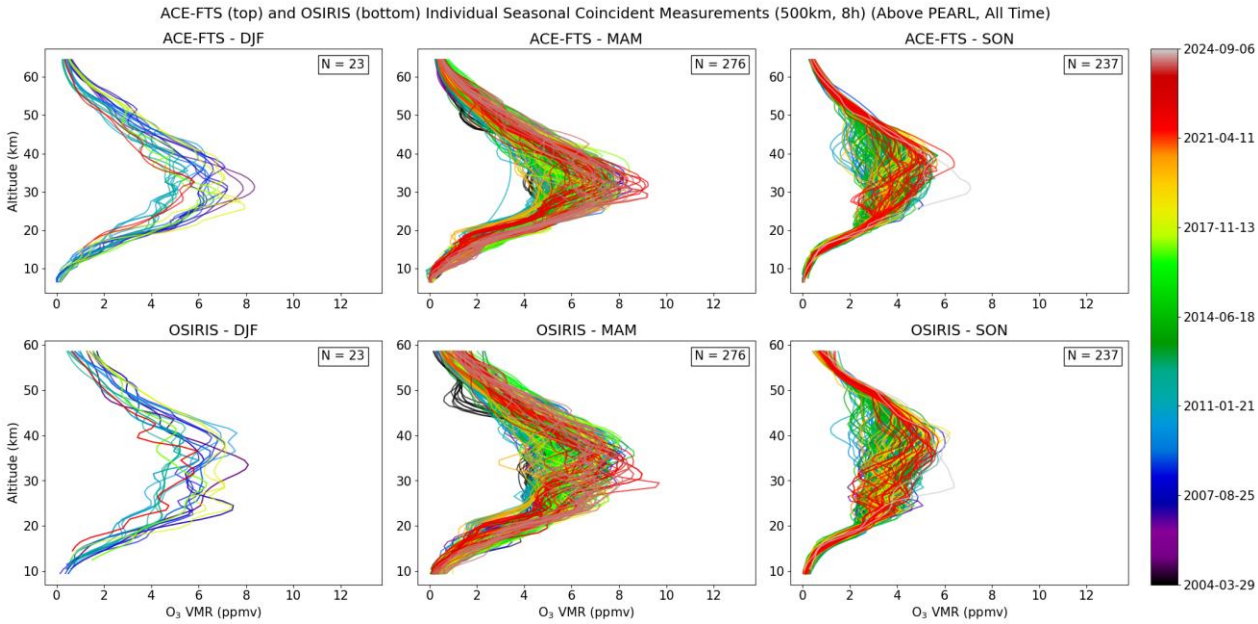

Figure 16. Seasonal line plots of individual coincident ozone profiles above PEARL from ACE-FTS (top) and OSIRIS (bottom).

In comparison to Figures 7 and 8, the individual measurements in Figures 15 and 16 show less outliers, however, OSIRIS measurements still show more variability. The seasonal plots between the satellites in Figure 16 also seem to match more closely compared to the Figure 8. Additionally, the seasonal plots show that there are no coincident measurements between the instruments above

PEARL in Northern Hemisphere summer which is a result of the SCISAT's orbit affecting spatial measurement density which can be observed from Figure 1.

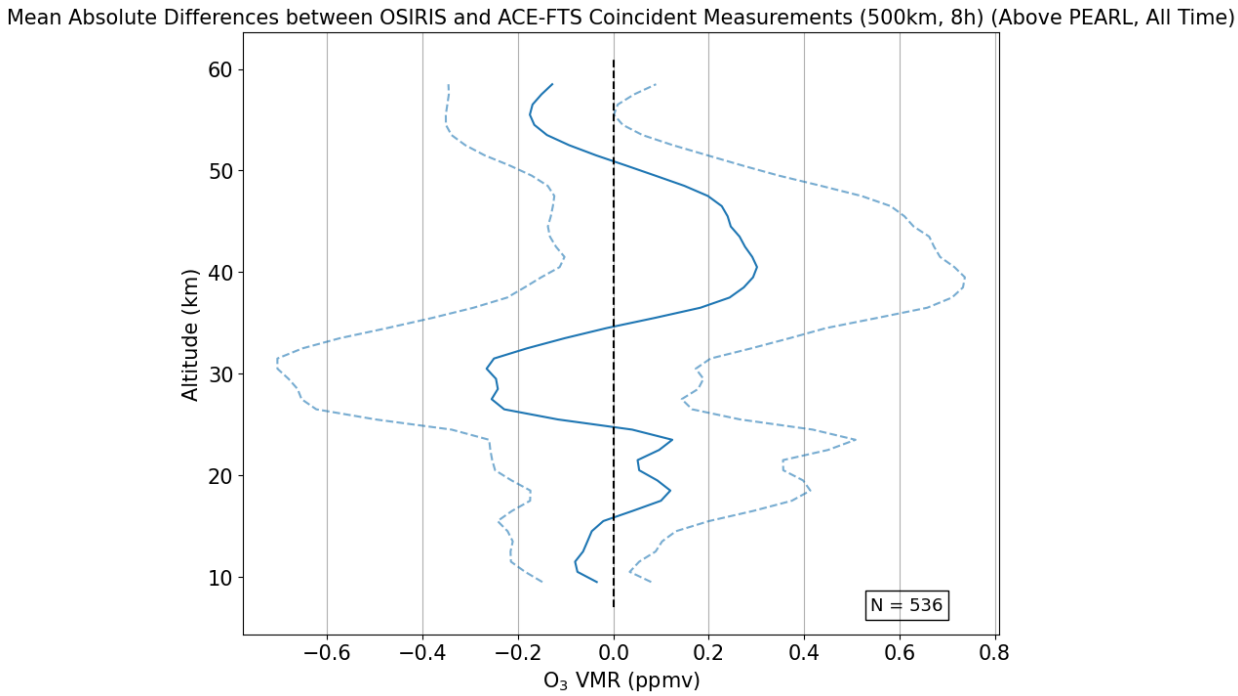

Figure 17. Line plot of the mean absolute difference of all OSIRIS and ACE-FTS coincident ozone measurements above PEARL at each altitude.

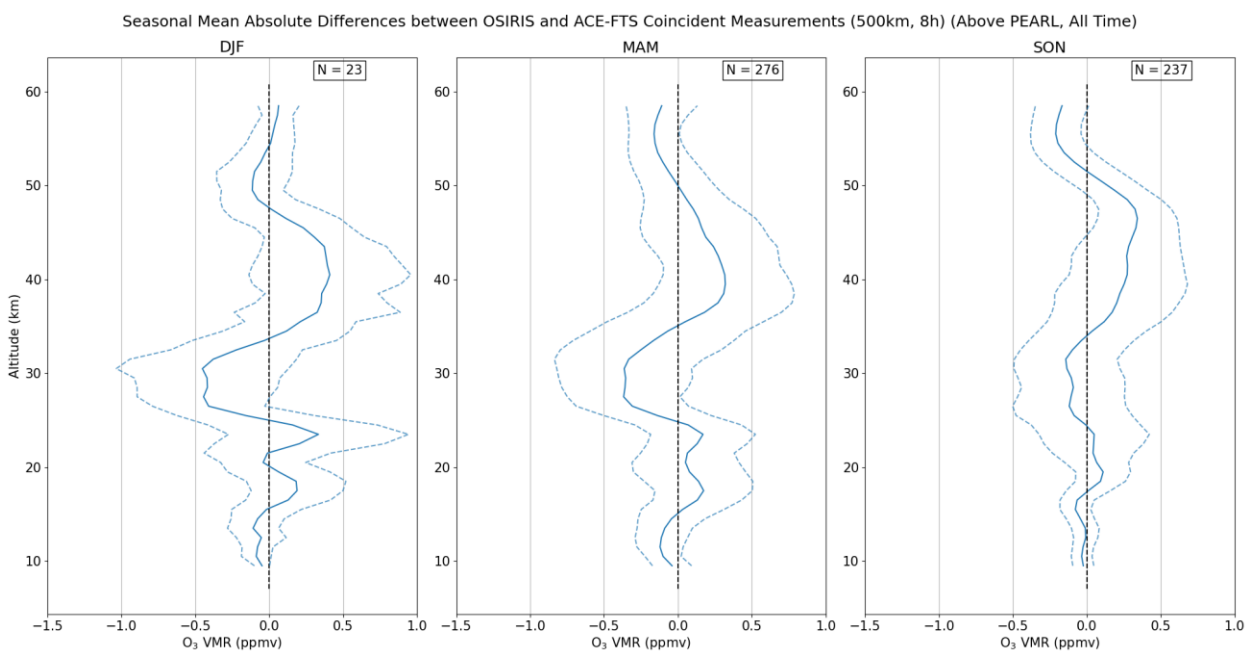

Figure 18. Seasonal line plots of the mean absolute difference of all OSIRIS and ACE-FTS coincident ozone measurements above PEARL at each altitude.

Figures 17 and 18 communicate the same pattern of agreement between the instruments observed in Figures 9 and 10.

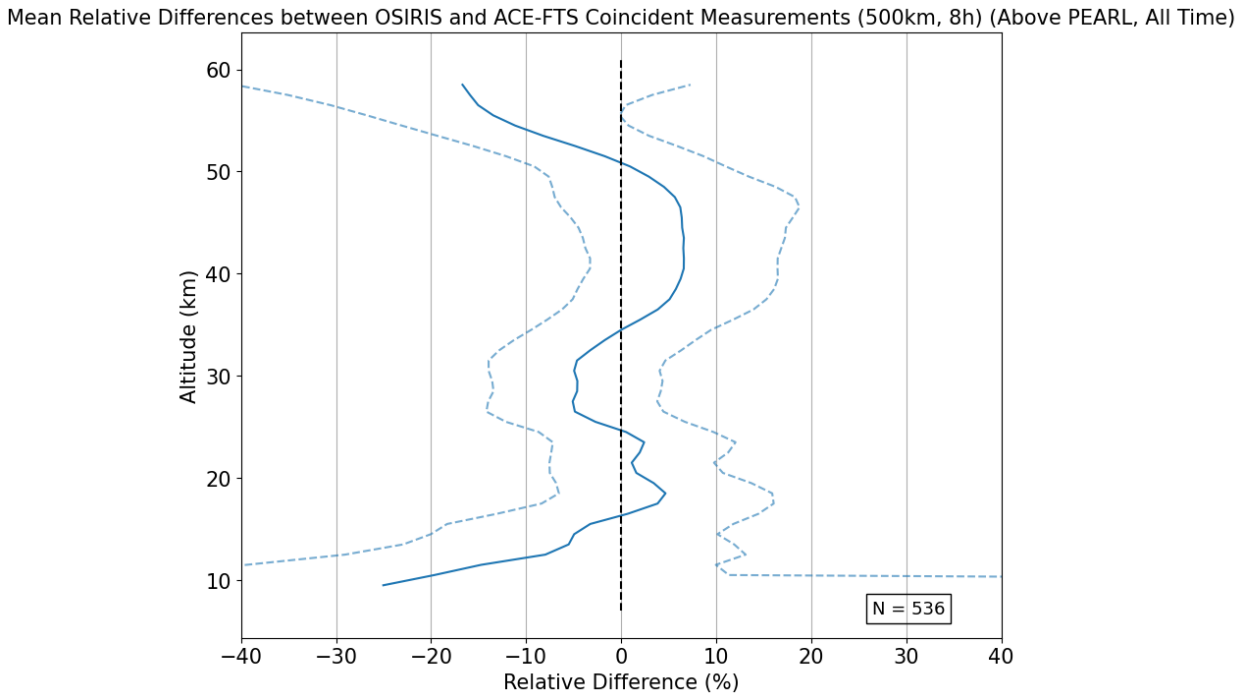

Figure 19. Line plot of the mean relative difference of all OSIRIS and ACE-FTS coincident ozone measurements above PEARL at each altitude.

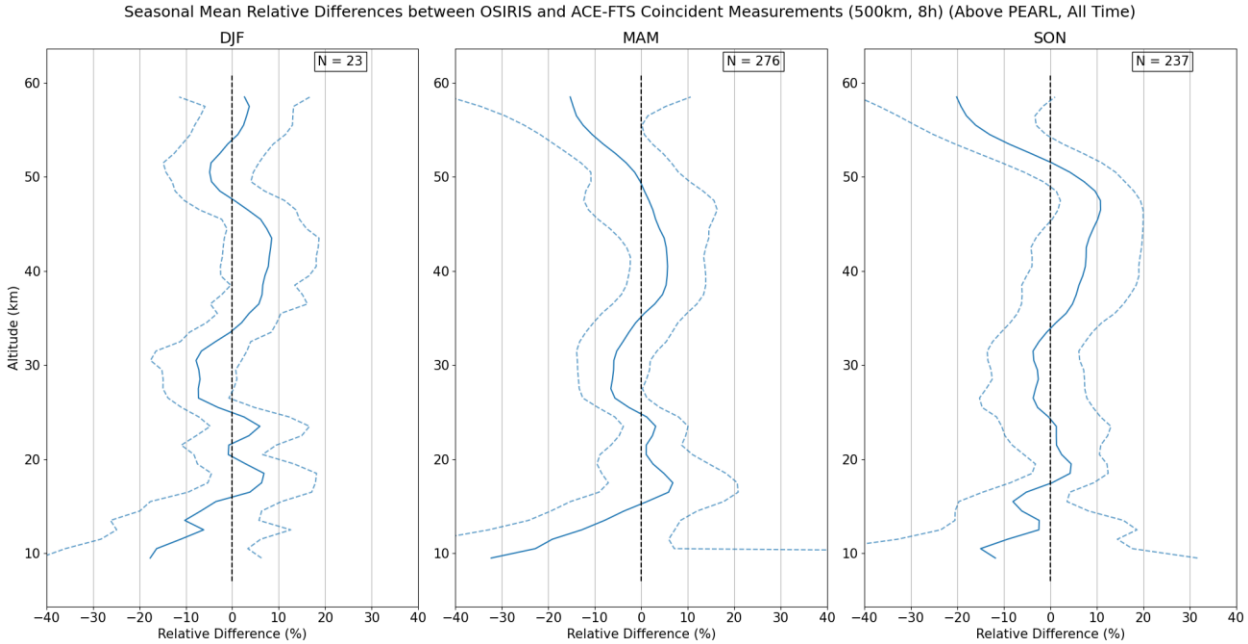

Figure 20. Seasonal line plots of the mean relative difference of all OSIRIS and ACE-FTS coincident ozone measurements above PEARL at each altitude.

Figures 19 and 20, in comparison to Figures 11 and 12, show less of an increase in relative difference at the edges of the stratosphere. Other patterns are similarly manifested in these plots.

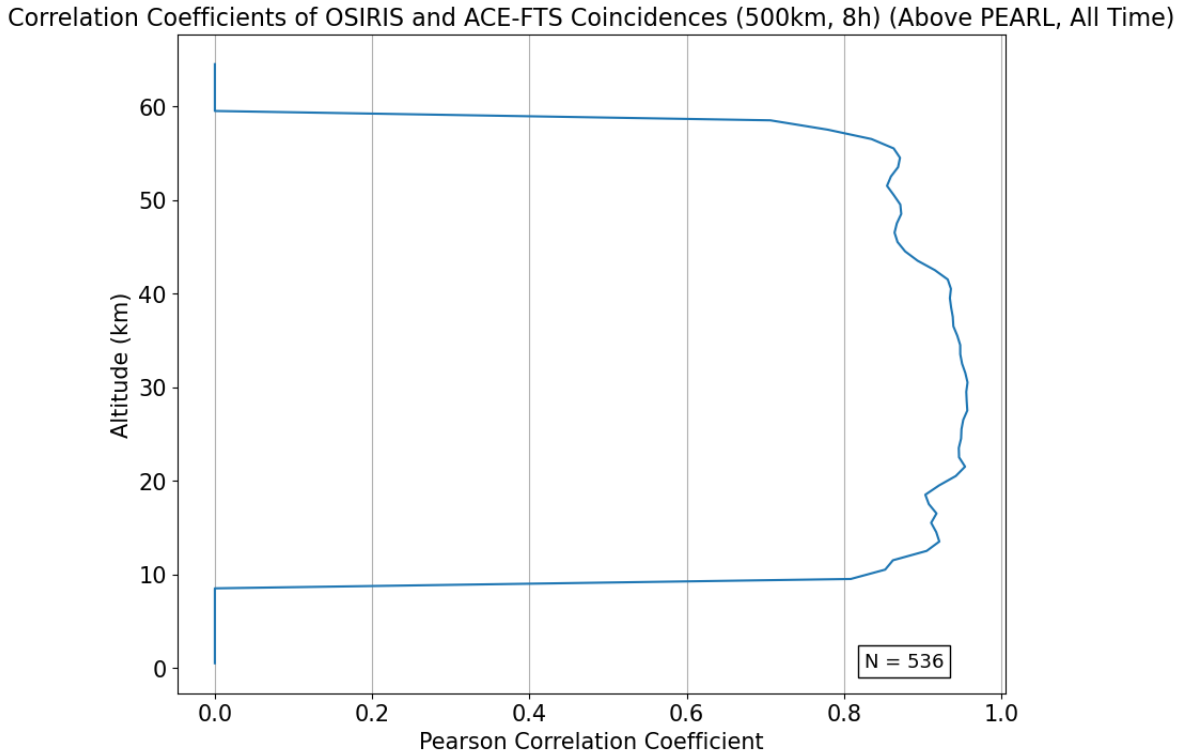

Figure 21. Line plot of the Pearson correlation coefficient of all OSIRIS and ACE-FTS coincident ozone measurements above PEARL at each altitude.

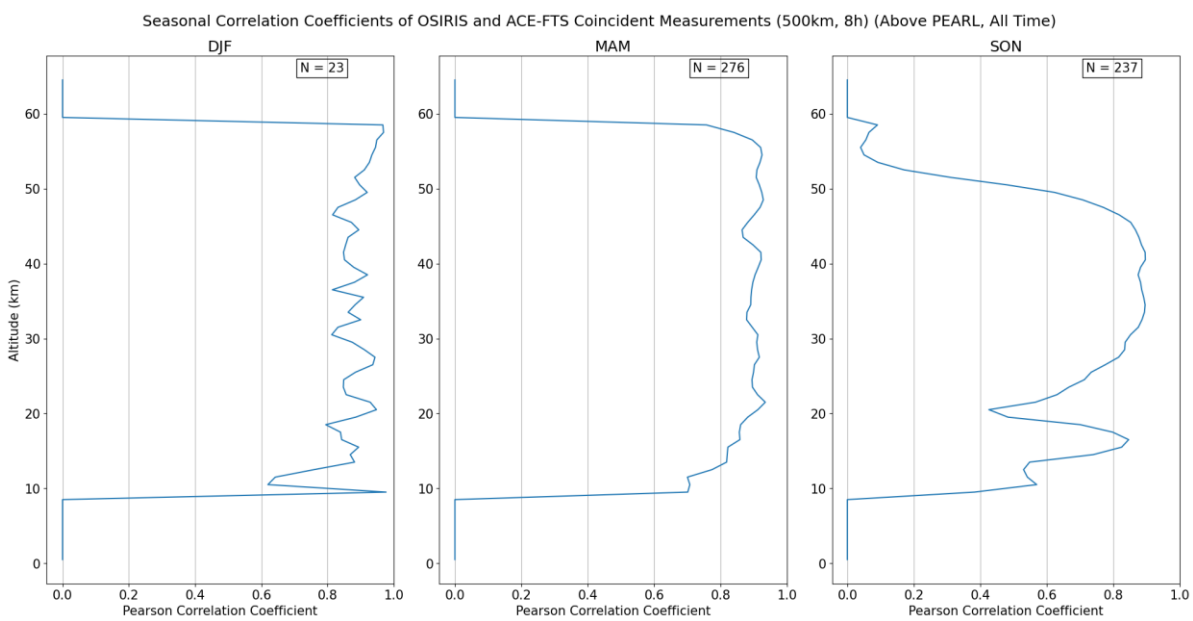

Figure 22. Seasonal line plots of the Pearson correlation coefficient all OSIRIS and ACE-FTS coincident ozone measurements above PEARL at each altitude.

Excluding Northern Hemisphere fall season, the Pearson correlation coefficient plots show that the measurements above PEARL have high correlation (above 0.8) throughout the stratosphere unlike global coincident measurements. These plots suggest more strongly that the measurements above PEARL are more strongly correlated compared to global measurements. Although, the measurements above PEARL are less correlated during Northern Hemisphere fall.

3.2.2 Satellite-based vs PEARL FTIR Profile Comparisons

To ensure accurate comparisons, satellite profiles were linearly interpolated to the same altitude grid as the PEARL FTIR data which has a more sporadic altitude grid.

3.2.2.1 ACE-FTS vs PEARL FTIR Profile Comparisons

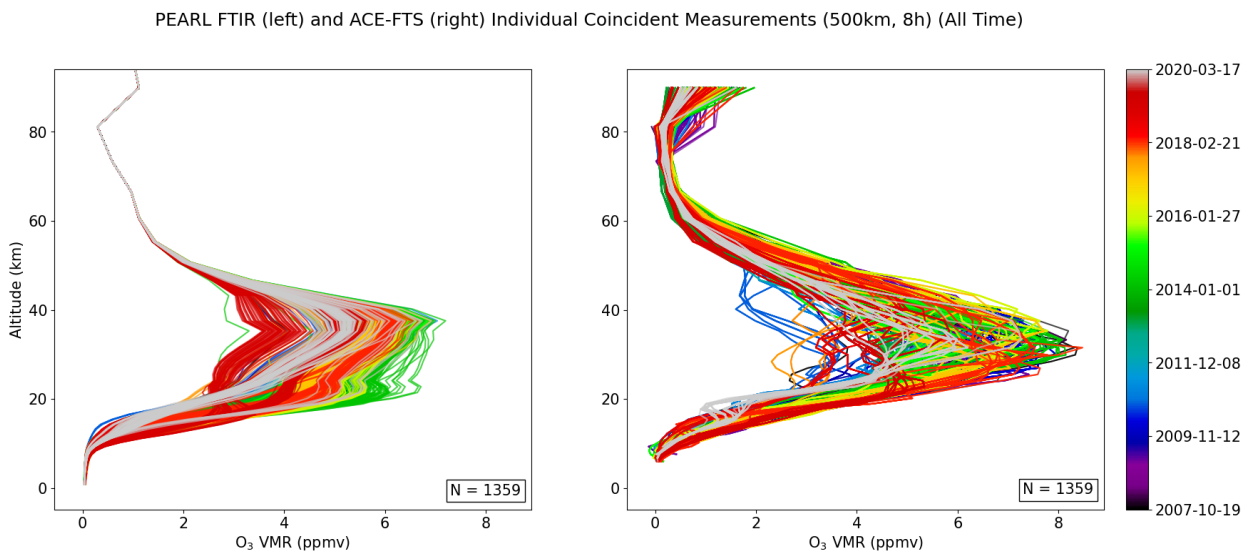

Figure 23. Line plots of individual coincident ozone profiles from PEARL FTIR (left) and ACE-FTS (right).

Figure 24 shows that there are no ACE-FTS measurements within pearl during Northern Hemisphere summer. In the other seasons, ACE-FTS has a narrower and slightly misaligned peak, indicating less variability around the peak. However, it has more variability at higher altitudes due to PEARL FTIR measurement's being less sensitive to the atmospheric composition at higher altitudes. The PEARL FTIR measurements converge unto the apriori estimate of atmospheric composition at higher altitudes due to the decrease in sensitivity. Given that most of the ozone is in the stratosphere, analysis of measurements in higher altitudes will be brief, if any.

Figure 25 shows good agreement between the coincident measurements, most of the differences are confined between -0.5-0.5 ppmv. The seasonal plot in Figure 26 shows that during Northern Hemisphere fall, the absolute difference plot has a negative peak beginning from about 22km to 43km, meaning that ACE-FTS measurements are lower on average than the PEARL FTIR measurements. The other seasons have the usual oscillation around 0 with no significant mean absolute difference outlier.

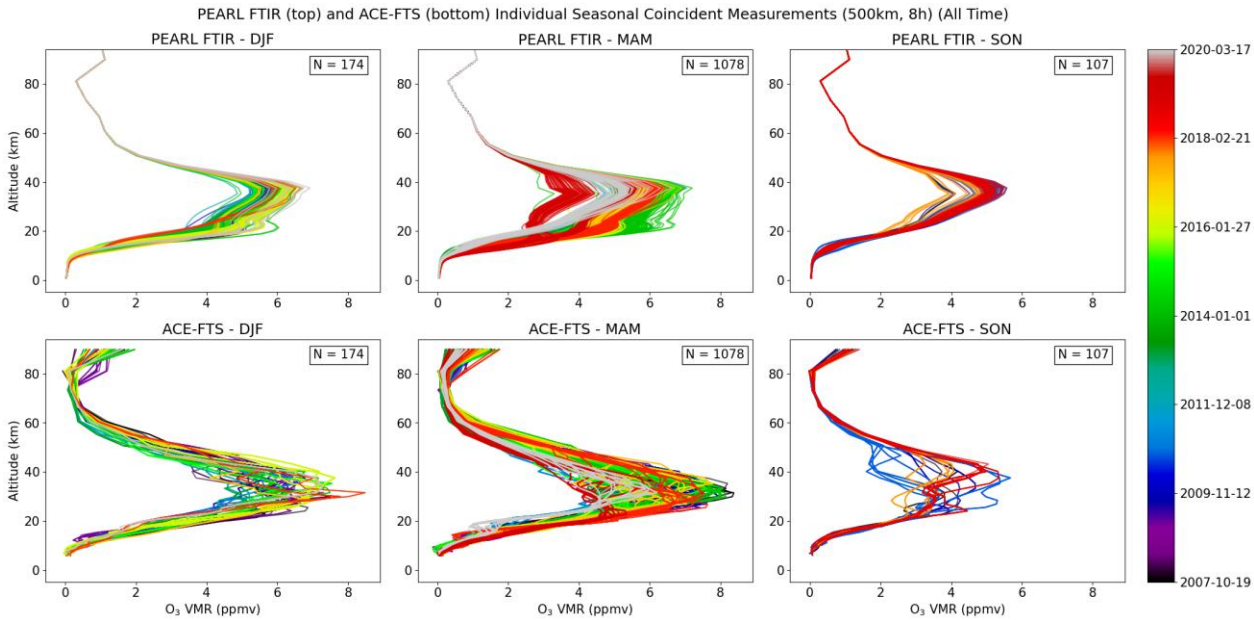

Figure 24. Seasonal line plots of individual coincident ozone profiles from PEARL FTIR (top) and ACE-FTS (bottom).

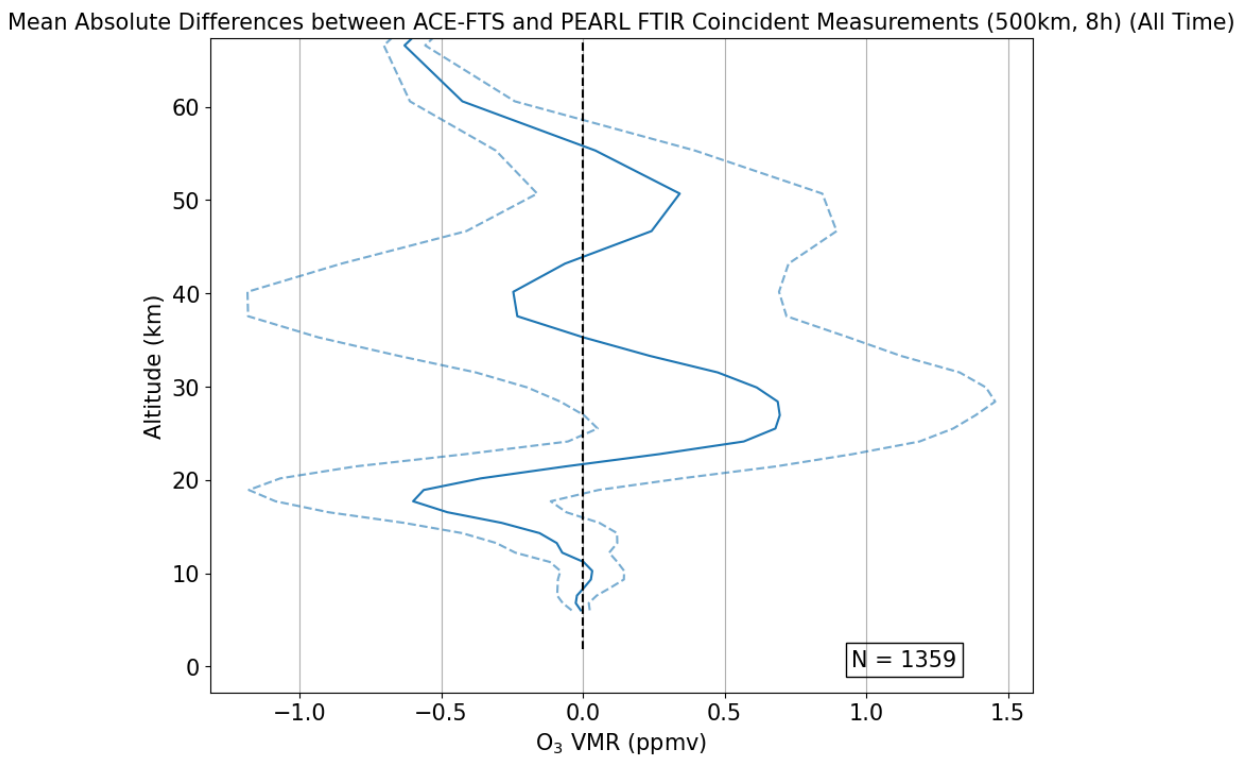

Figure 25. Line plot of the mean absolute difference of all ACE-FTS and PEARL FTIR coincident ozone measurements at each altitude.

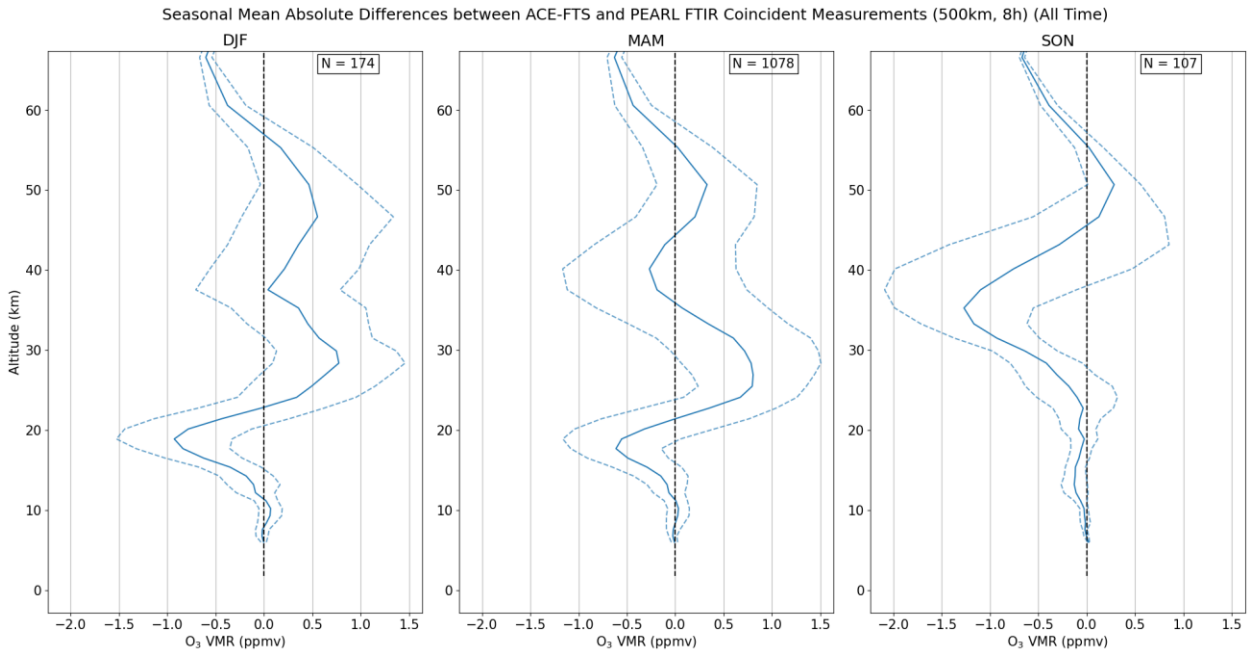

Figure 26. Seasonal line plots of the mean absolute difference of all ACE-FTS and PEARL FTIR coincident ozone measurements each altitude.

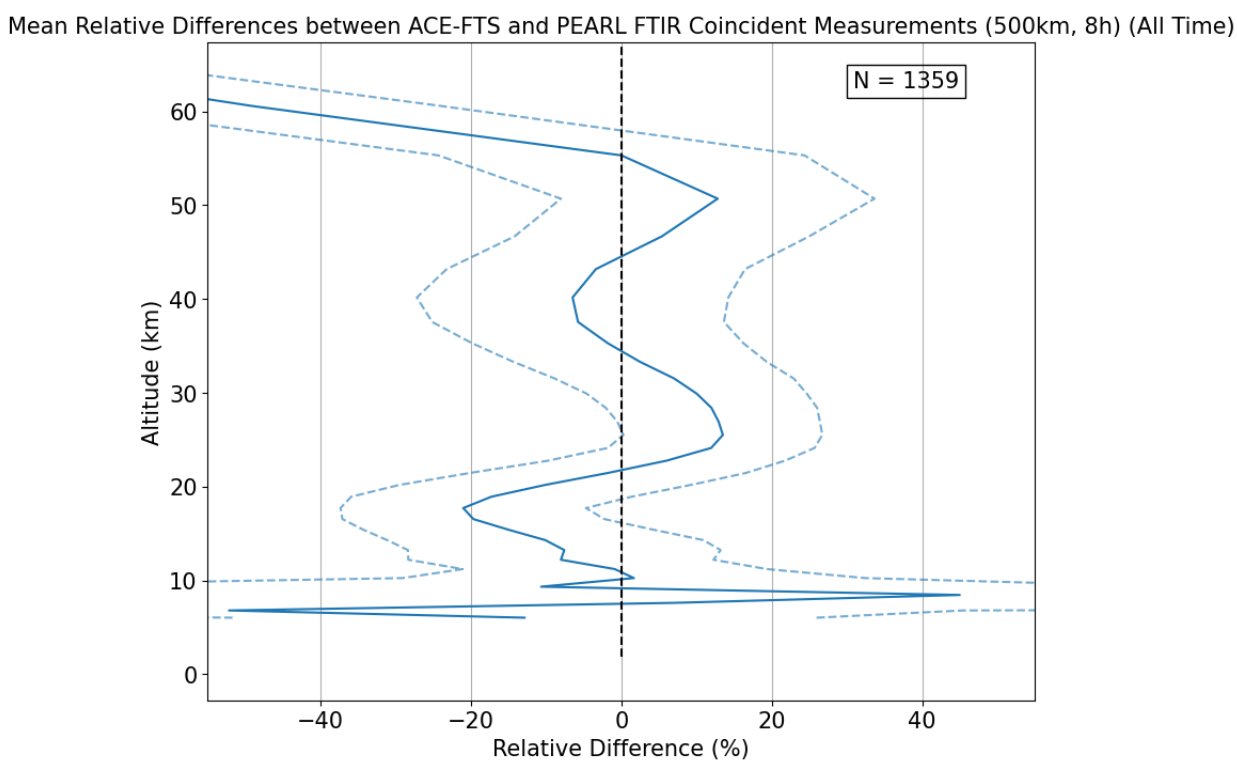

Figure 27. Line plot of the mean relative difference of all ACE-FTS and PEARL FTIR coincident ozone measurements at each altitude.

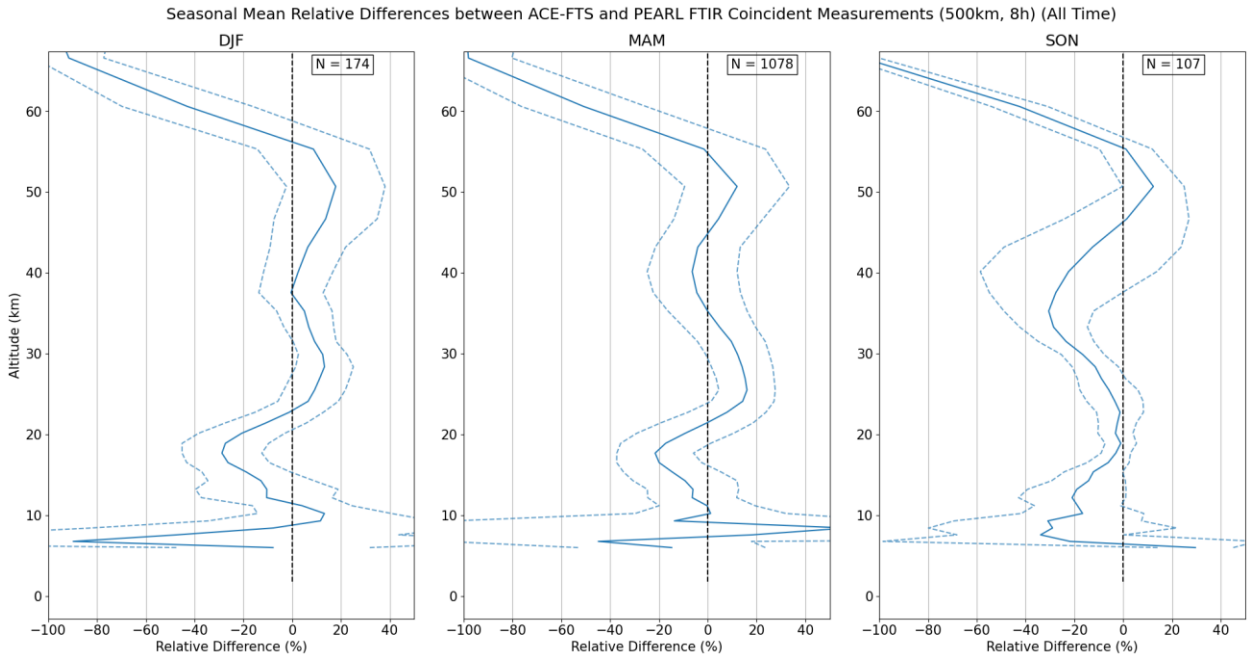

Figure 28. Seasonal line plots of the mean relative difference of all ACE-FTS and PEARL FTIR coincident ozone measurements at each altitude.

The relative difference plots in Figures 27 and 28 mirror the same pattern observed in the absolute difference plots like the peak in Northern Hemisphere fall. Most of the relative differences are confined between -20% to 20% which indicates that the measurements mostly agree with each other.

Figures 29 and 30 all indicate that the measurements are not very correlated using the Pearson correlation coefficient as the only metric for correlation. However, considering the other metrics, it seems like on average the measurements tend to be similar. The higher variability of ACE-FTS measurements is a probable cause of the Pearson correlation coefficient plots suggesting low correlation at higher stratospheric altitudes.

In comparison to the ACE-FTS and PEARL FTIR individual coincident measurements, the peaks and variability of OSIRIS and PEARL FTIR plots in Figures 31 and 32 seem to align more closely. Most of the coincident measurements occur in Northern Hemisphere spring and summer due to the orbital path of ODIN.

As Figures 31 and 32 suggest, the instruments do indeed have very good agreement, with mean absolute difference being mostly confined between -0.25 to 0.25 ppmv shown in Figure 33. Figure 34 also has a peak like the one seen in Figure 26 in the same season. The mean absolute difference in the rest of the seasons oscillate around 0 and are mostly confined between -0.5 and 0.5 ppmv. Overall, these plots show good agreement between the measurements, on average.

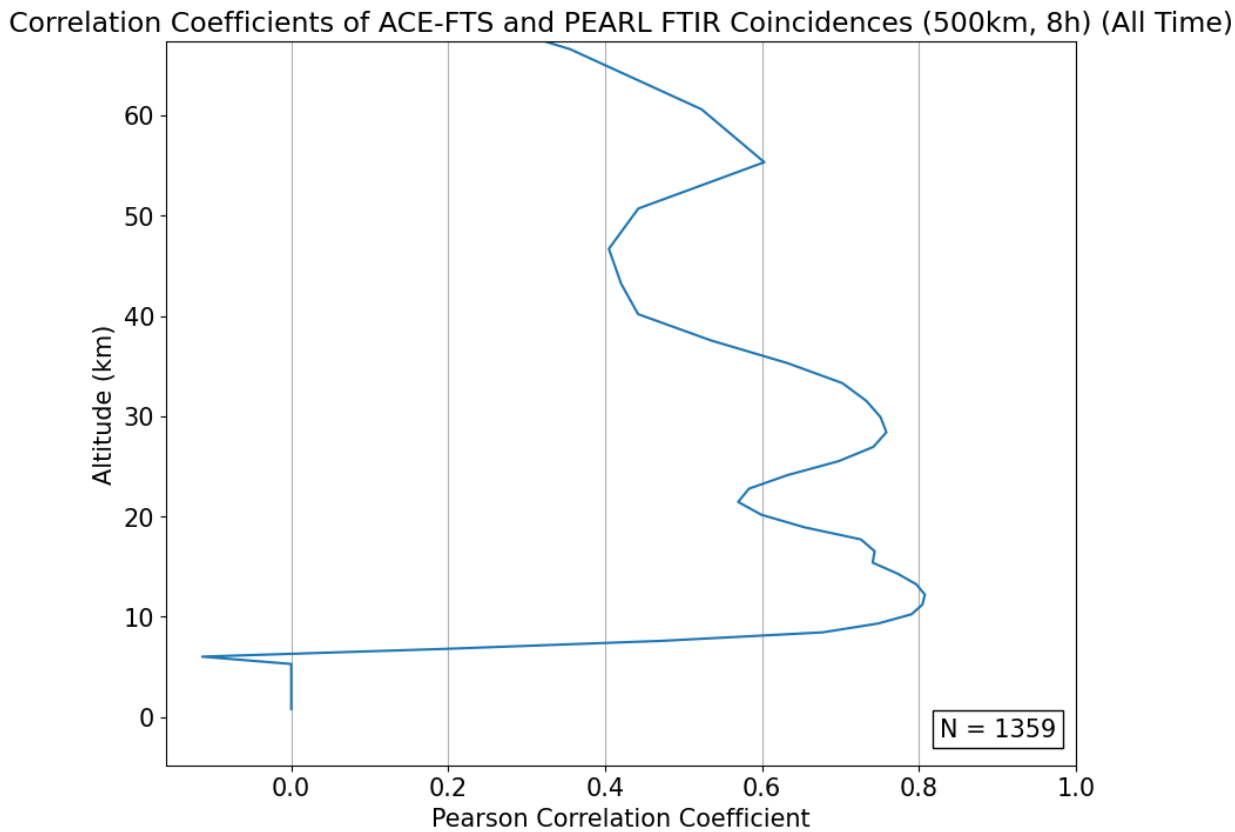

Figure 29. Line plot of the Pearson correlation coefficient of all ACE-FTS and PEARL FTIR coincident ozone measurements at each altitude.

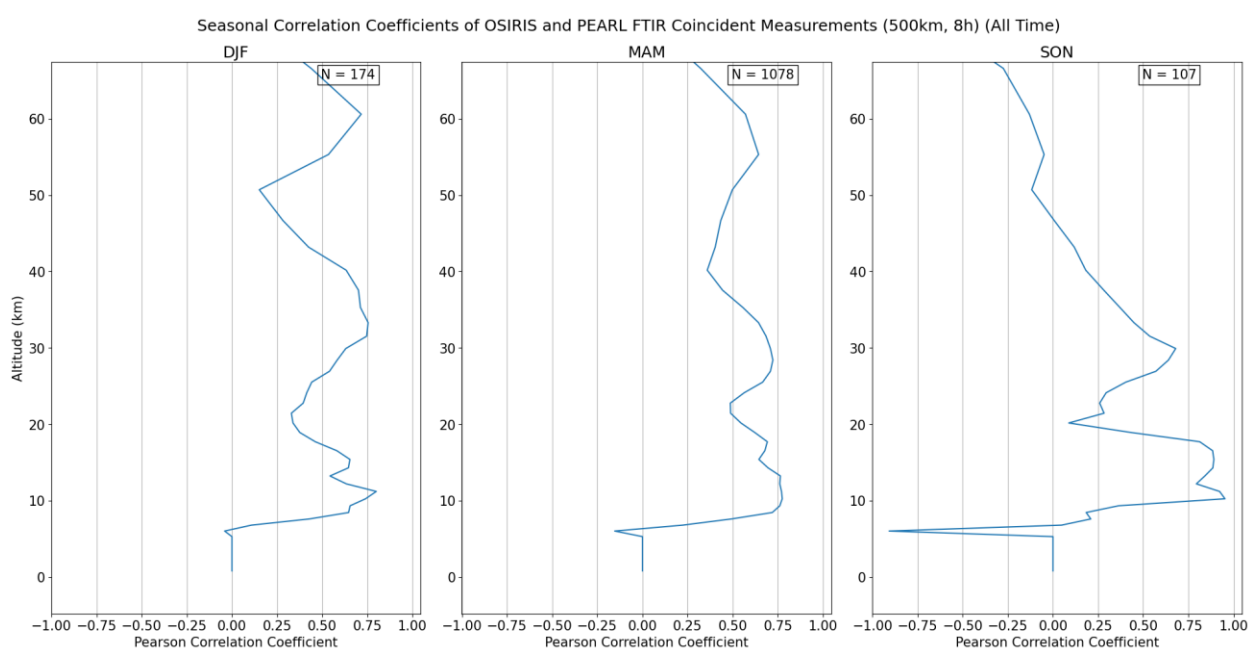

Figure 30. Seasonal line plots of the Pearson correlation coefficient of all ACE-FTS and PEARL FTIR coincident ozone measurements at each altitude.

3.2.2.2 OSIRIS vs PEARL FTIR Profile Comparisons

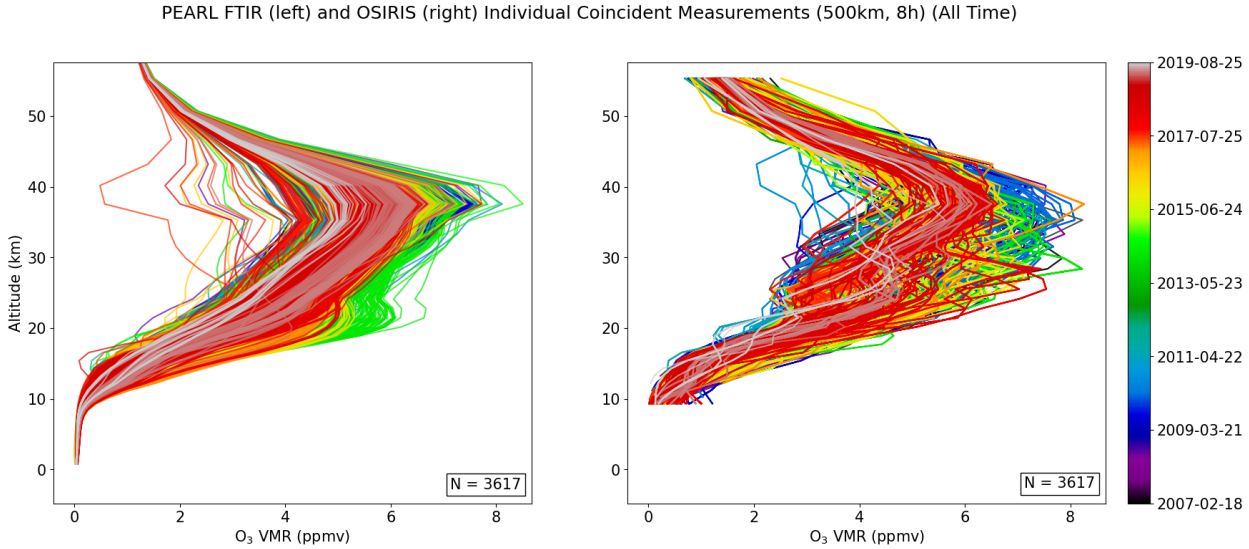

Figure 31. Line plots of individual coincident ozone profiles from PEARL FTIR (left) and OSIRIS (right).

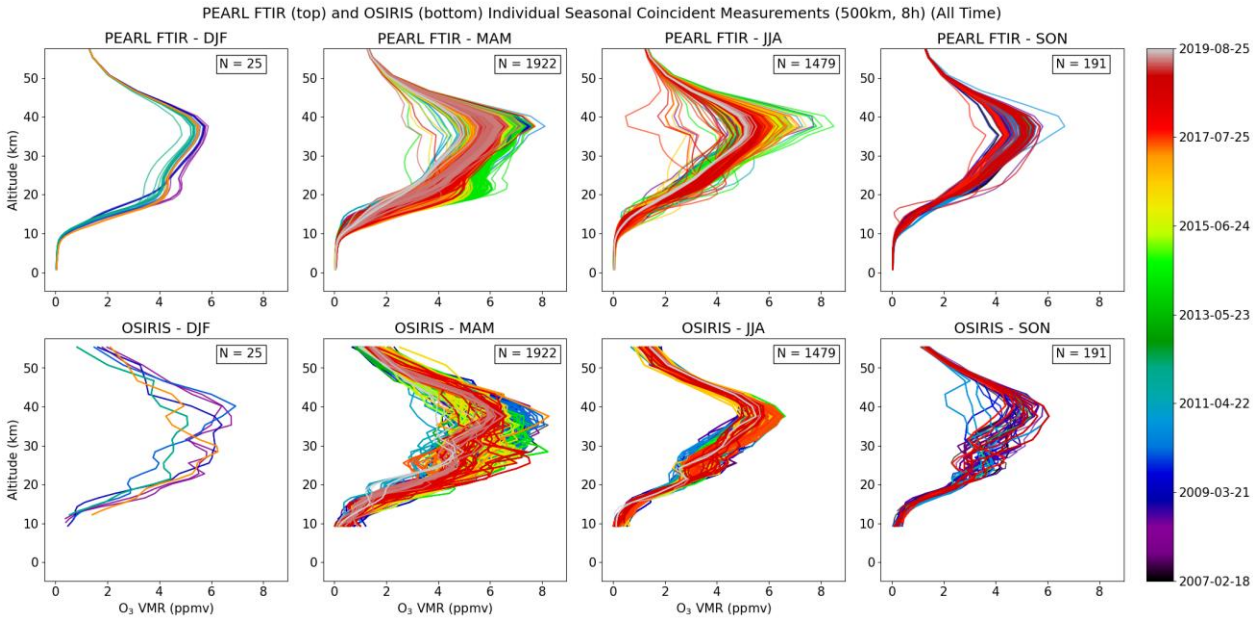

Figure 32. Seasonal line plots of individual coincident ozone profiles from PEARL FTIR (top) and ACE-FTS (bottom).

The relative difference plots in Figures 35 and 36 further affirms that on average, the measurements seem to converge towards each other just as the previous figures suggests. The mean relative difference across altitudes and seasons tends to reside between -12.5 and 12.5%.

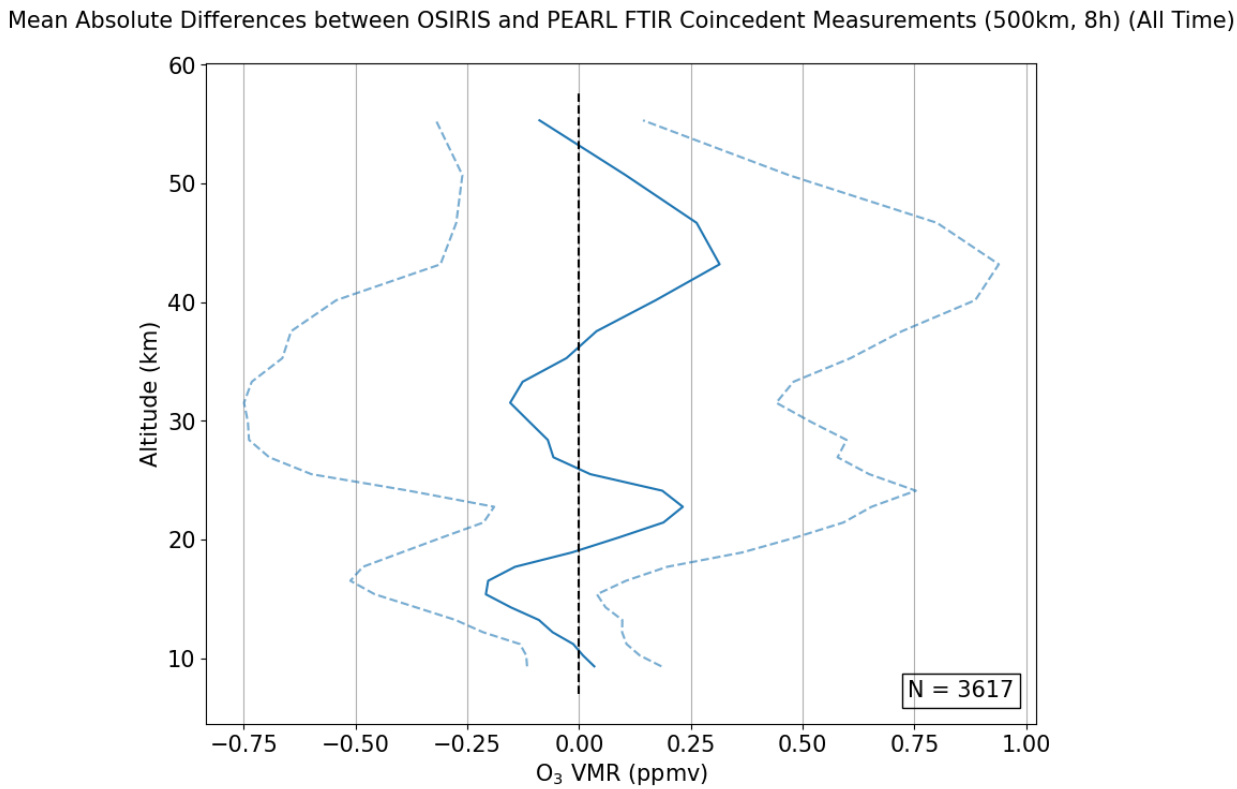

Figure 33. Line plot of the mean absolute difference of all OSIRIS and PEARL FTIR coincident ozone measurements at each altitude.

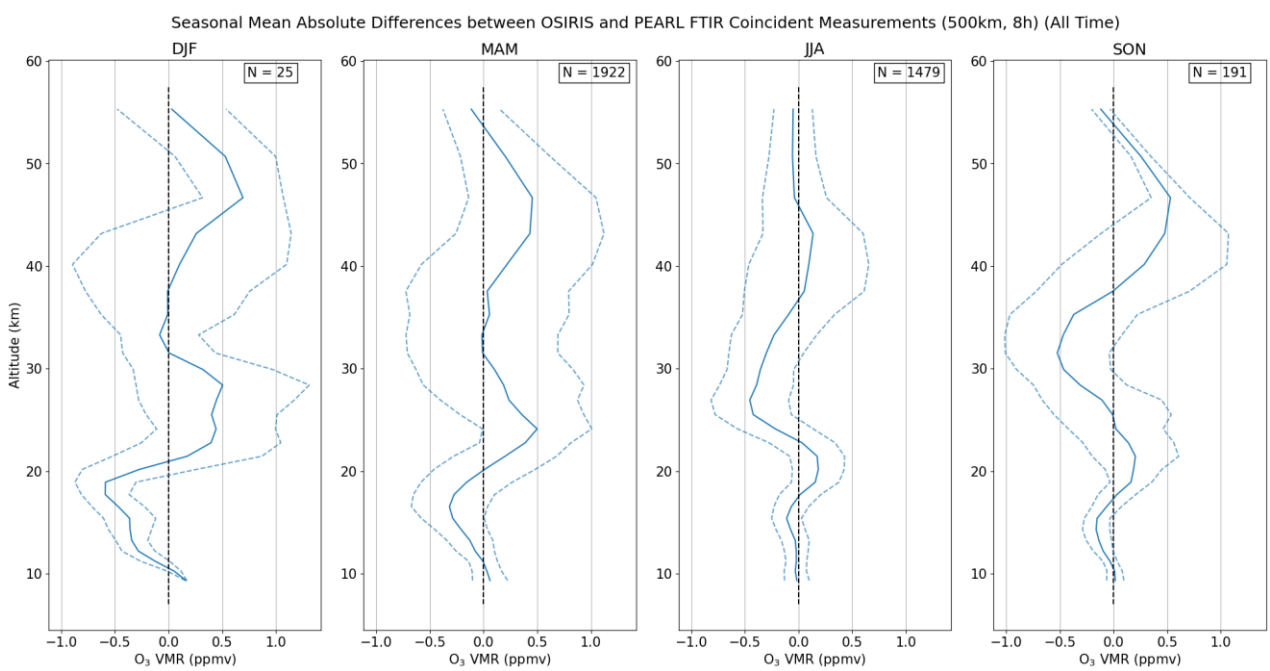

Figure 34. Seasonal line plots of the mean absolute difference of all OSIRIS and PEARL FTIR coincident ozone measurements at each altitude.

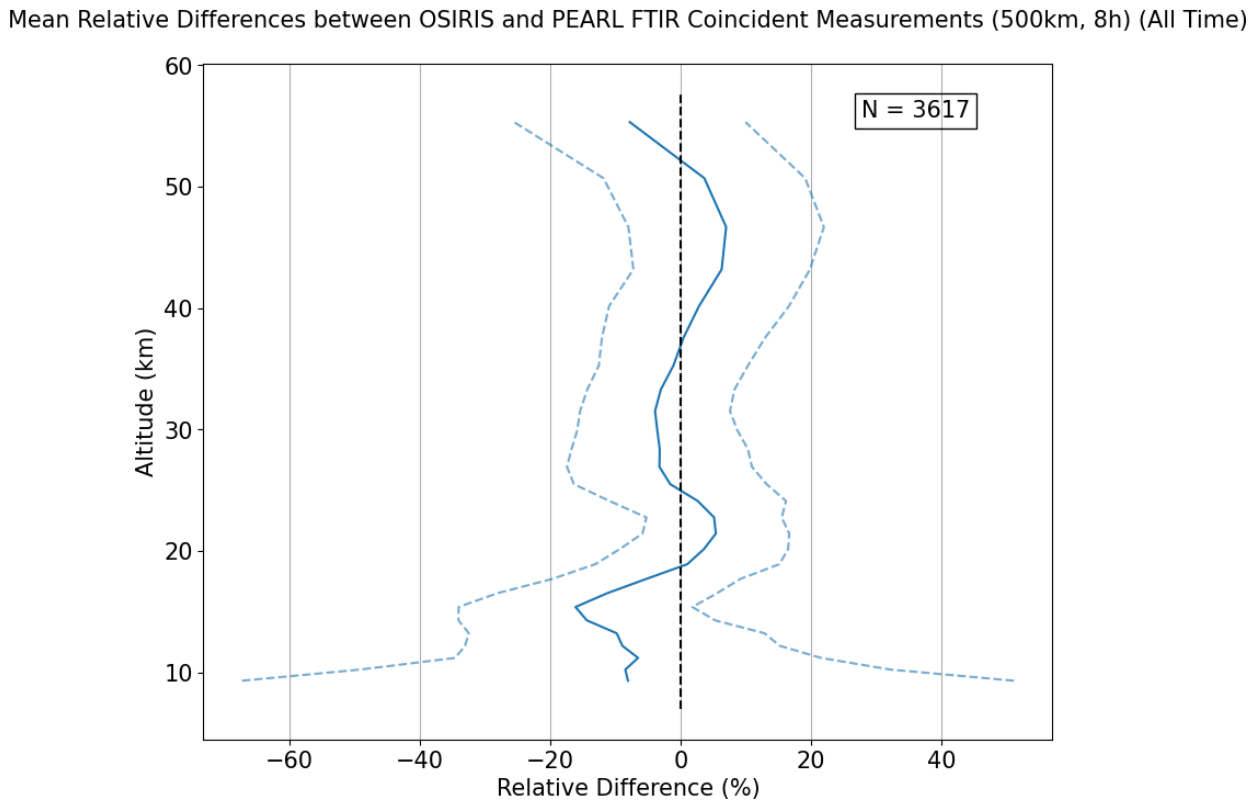

Figure 35. Line plot of the mean relative difference of all OSIRIS and PEARL FTIR coincident ozone measurements at each altitude.

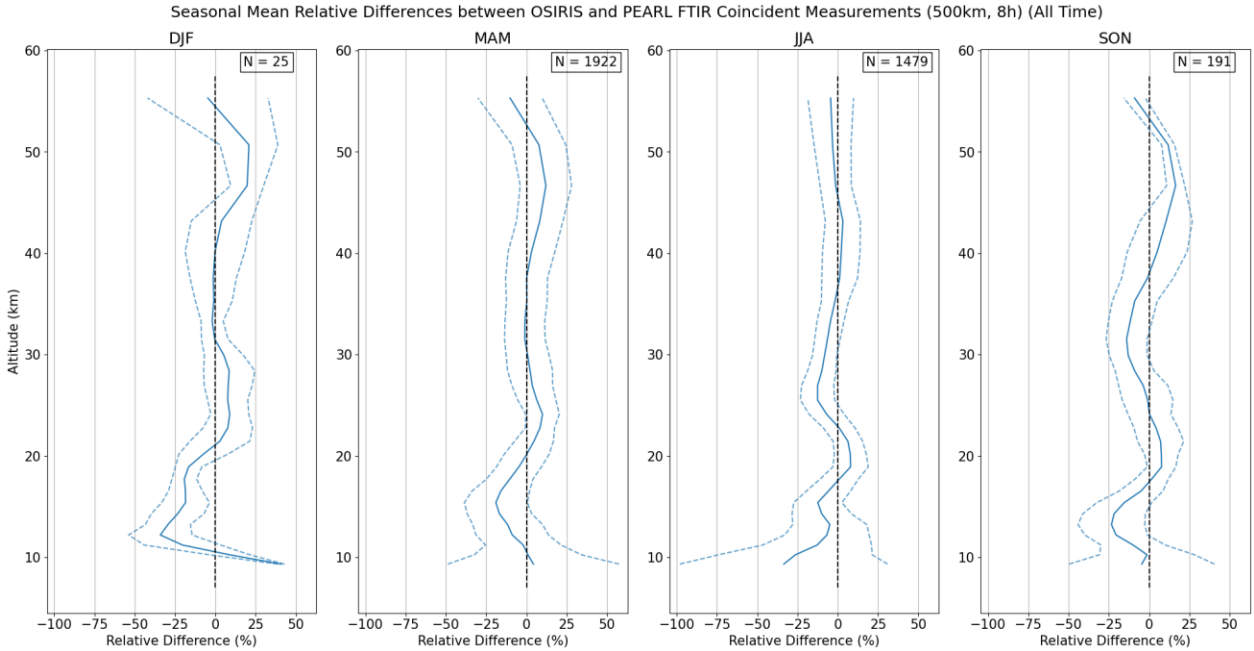

Figure 36. Seasonal line plots of the mean absolute difference of all OSIRIS and PEARL FTIR coincident ozone measurements at each altitude.

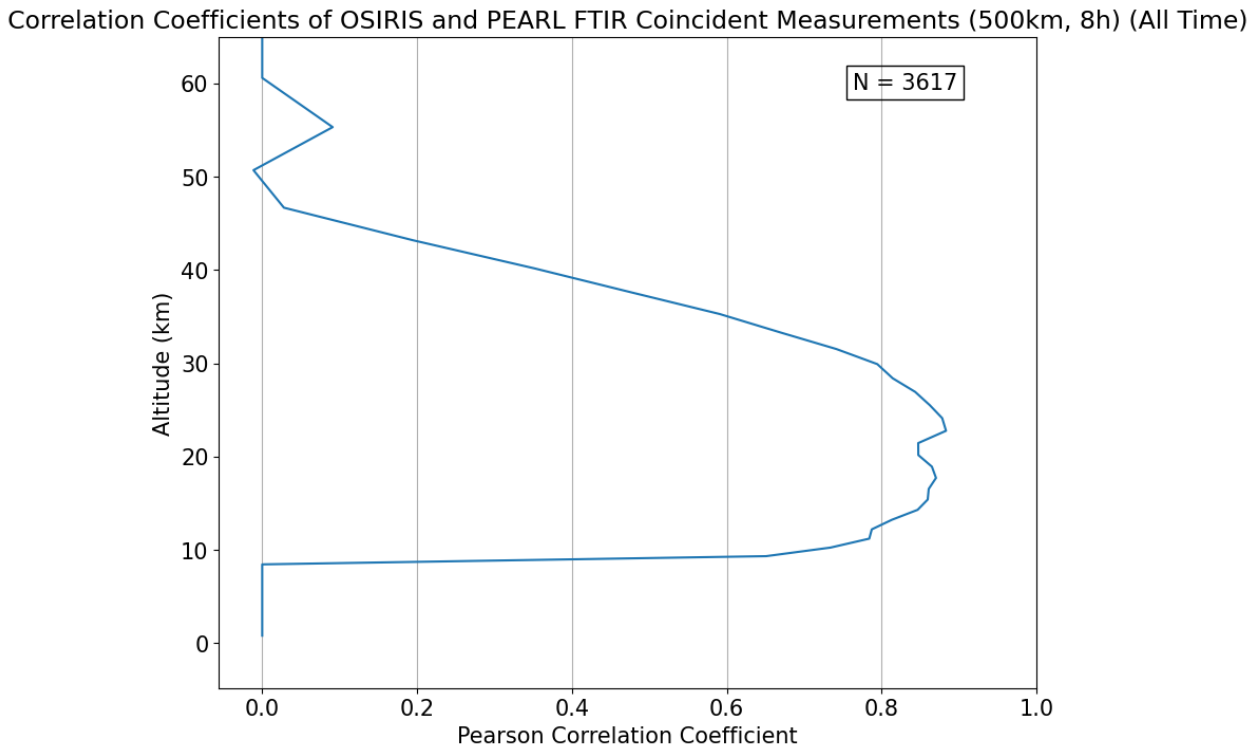

Figure 37. Line plot of the Pearson correlation coefficient of all OSIRIS and PEARL FTIR coincident ozone measurements at each altitude.

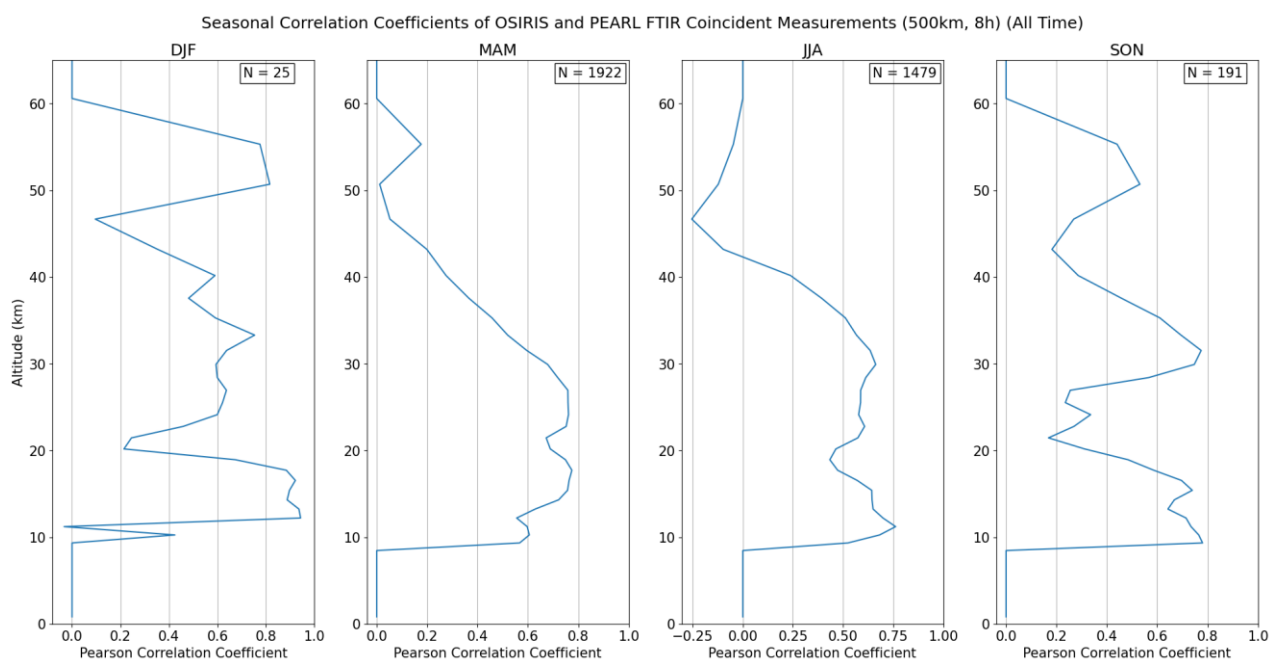

Figure 38. Seasonal line plots of the Pearson correlation coefficient of all OSIRIS and PEARL FTIR coincident ozone measurements at each altitude.

Similar to the Pearson correlation coefficient plots in Figures 29 and 30, Figures 37 and 38 do not seem to yield the same conclusions derived from the previous differences' plots. As before, measurement variability, despite average agreement, appears to drive this discrepancy. Although, the correlation coefficient plots all report higher correlations at lower altitudes compared to higher altitudes.

3.3 Column comparisons

Columns were calculated by converting the ozone VMR profiles to ozone number density profiles, multiplying by the appropriate altitude widths, then summing up these values for each altitude which yields ozone columns. Unlike ozone profile comparisons, column comparisons were not done with interpolation. To ensure column comparisons were accurate, all columns calculated from a profile with a null value at any altitude were discarded. This filtering led to a lower number of coincidences for column comparisons compared to profile coincidences. The units used to represent ozone columns in this paper is Dobson Units.

Each instrument pair will be presented with scatter plots of individual pairs of measurements along with a seasonal perspective and a fitted line in all scatter plots. Subsequently, individual absolute and relative column differences plotted against their measurement month will be presented. The end of this section will be assessing the extent to which the instruments' column measurements diverge over time.

3.3.1 Partial Column Altitude Range

The choice of partial column range was consistent for all instrument pairs and can be divided into 2 different choices: upper bound choice and lower bound choice.

3.3.1.1 Partial Column Upper Bound Choice

The partial column upper bound of 51km was chosen based on analysis of the Averaging Kernel Matrix (AVK) of the PEARL FTIR retrievals. The AVK of retrievals provides additional information about the retrievals such as the sensitivity of the retrieval to various altitudes which is the sum of the rows of the AVK at each altitude layer (Jeffery, 2022, p. 49). AVK plots are included in the Appendix. The maximum altitude whereby the mean sensitivity of all PEARL FTIR retrievals had a sensitivity greater than or equal to 0.1 was the metric used for the choice of an upper bound. This ensures that the altitudes used in the columns had an impact on the retrieval and does not significantly limit the altitude range of the columns.

3.3.1.2 Partial Column Lower Bound Choice

The lower bound of 10km was chosen to ensure a decently large, representative sample size for each instrument while maintaining data integrity. The filtration process when used on a lower bound lower than 10km significantly reduced the amount of data available for analysis and higher lower bounds had diminishing returns in terms of how much more data is recovered.

3.3.2 OSIRIS vs ACE-FTS Column Comparisons

Similar to profile comparisons, OSIRIS vs ACE-FTS column comparisons will be divided into coincident comparisons globally and coincident comparisons above PEARL.

3.3.2.1 Global OSIRIS vs ACE-FTS Column Comparisons

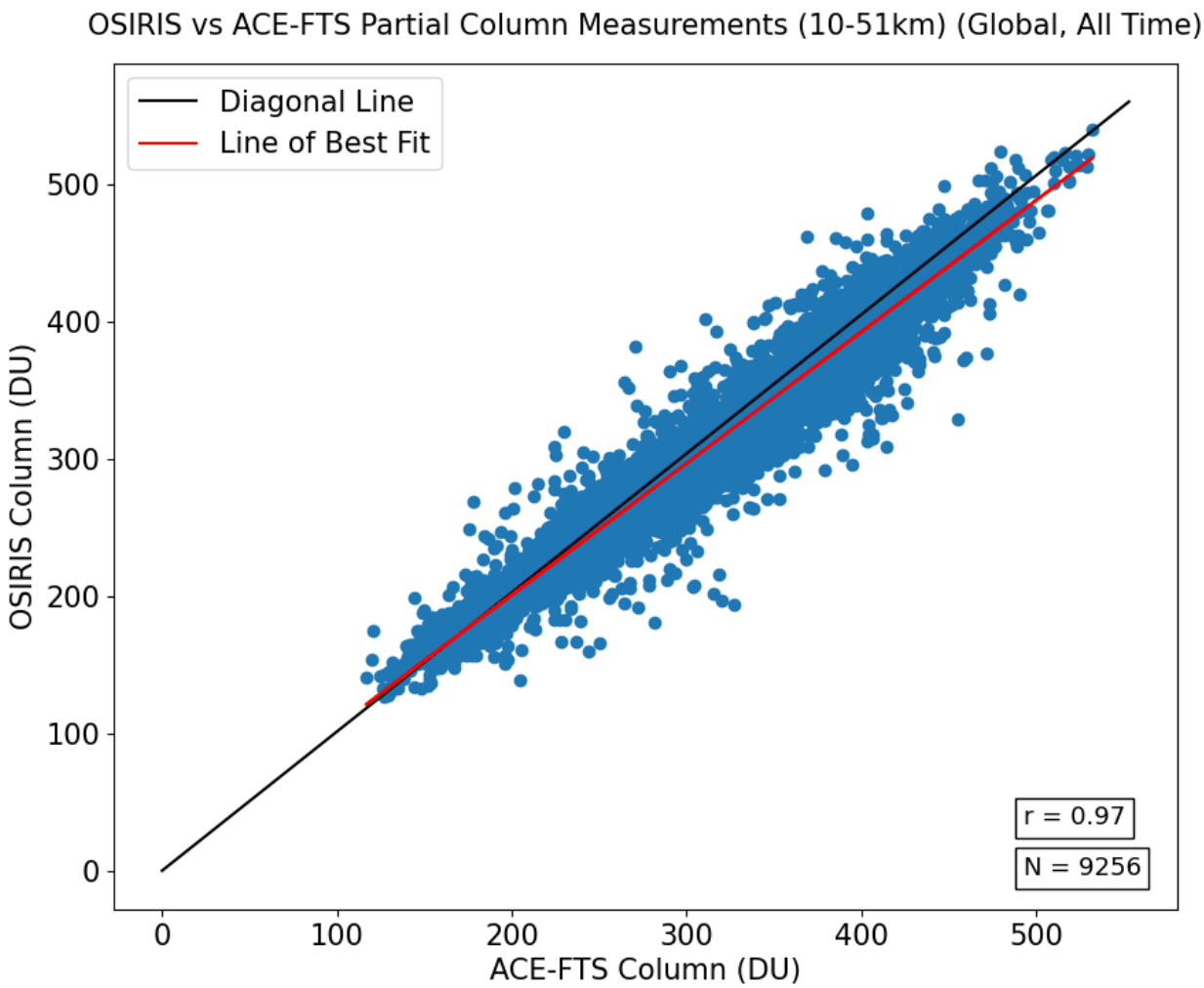

Figure 39. Scatter plot of OSIRIS and ACE-FTS global coincident ozone column measurements.

Figures 39 and 40 show that the column measurements of OSIRIS and ACE-FTS globally are almost perfectly correlated. This high correlation is also present in all seasons with Northern Hemisphere winter having the highest correlation and Northern Hemisphere summer having the least correlation.

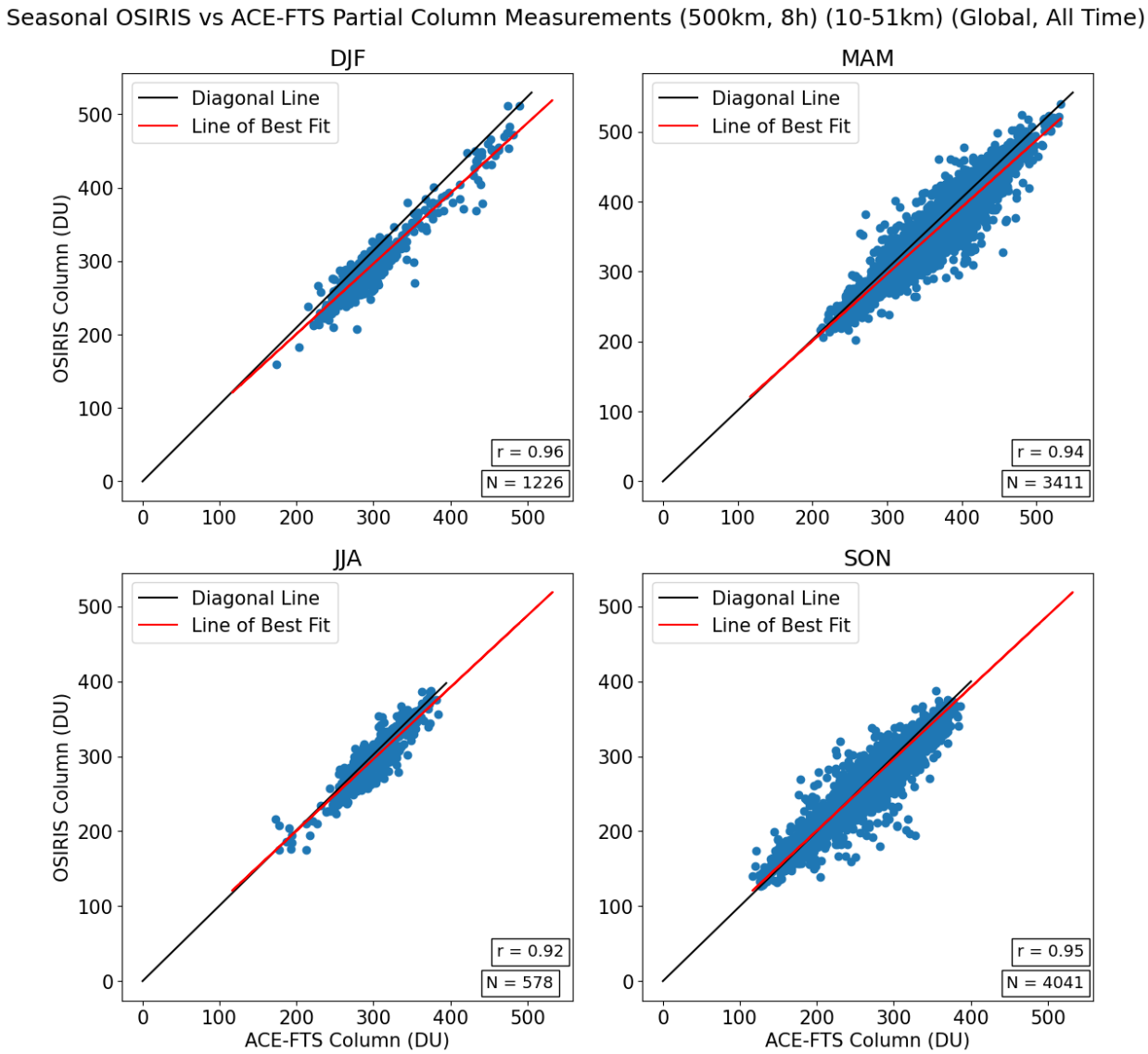

Figure 40. Seasonal scatter plots of OSIRIS and ACE-FTS global coincident ozone column measurements.

Figures 41 and 42 further supports the conclusion that the instruments' column measurements are very similar. Most of the differences in both plots are concentrated close to 0, including the mean differences, indicating high consistency. This trend is consistent across all months, although, more measurements made in March and November disagree more compared to other months.

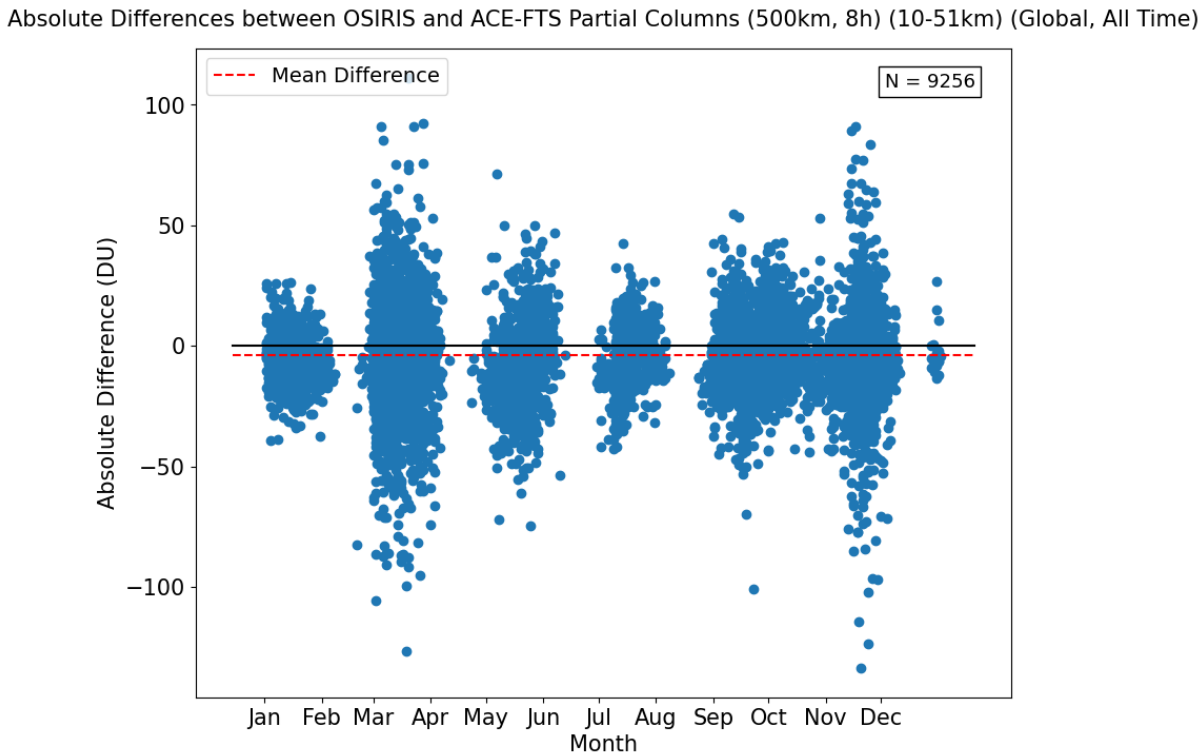

Figure 41. Scatter plot of absolute differences between OSIRIS and ACE-FTS global coincident ozone column measurements.

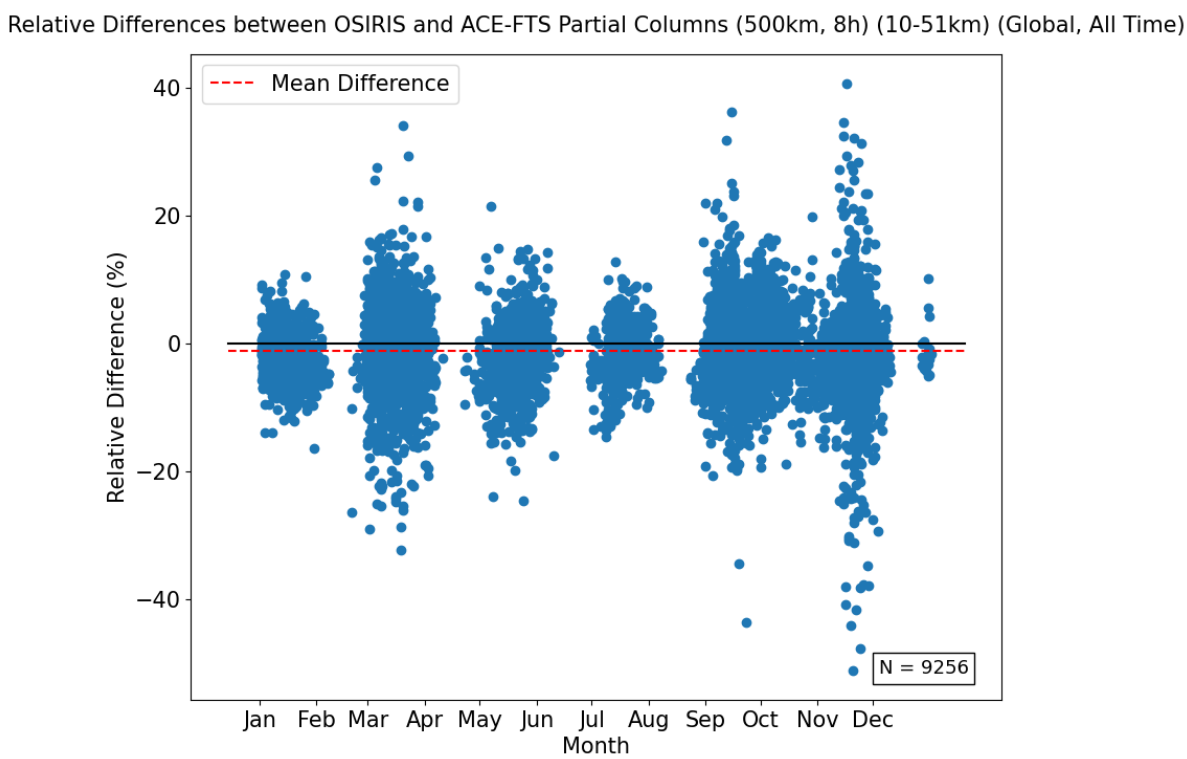

Figure 42. Scatter plot of relative differences between OSIRIS and ACE-FTS global coincident ozone column measurements.

3.3.2.2 Above PEARL OSIRIS vs ACE-FTS Column Comparisons

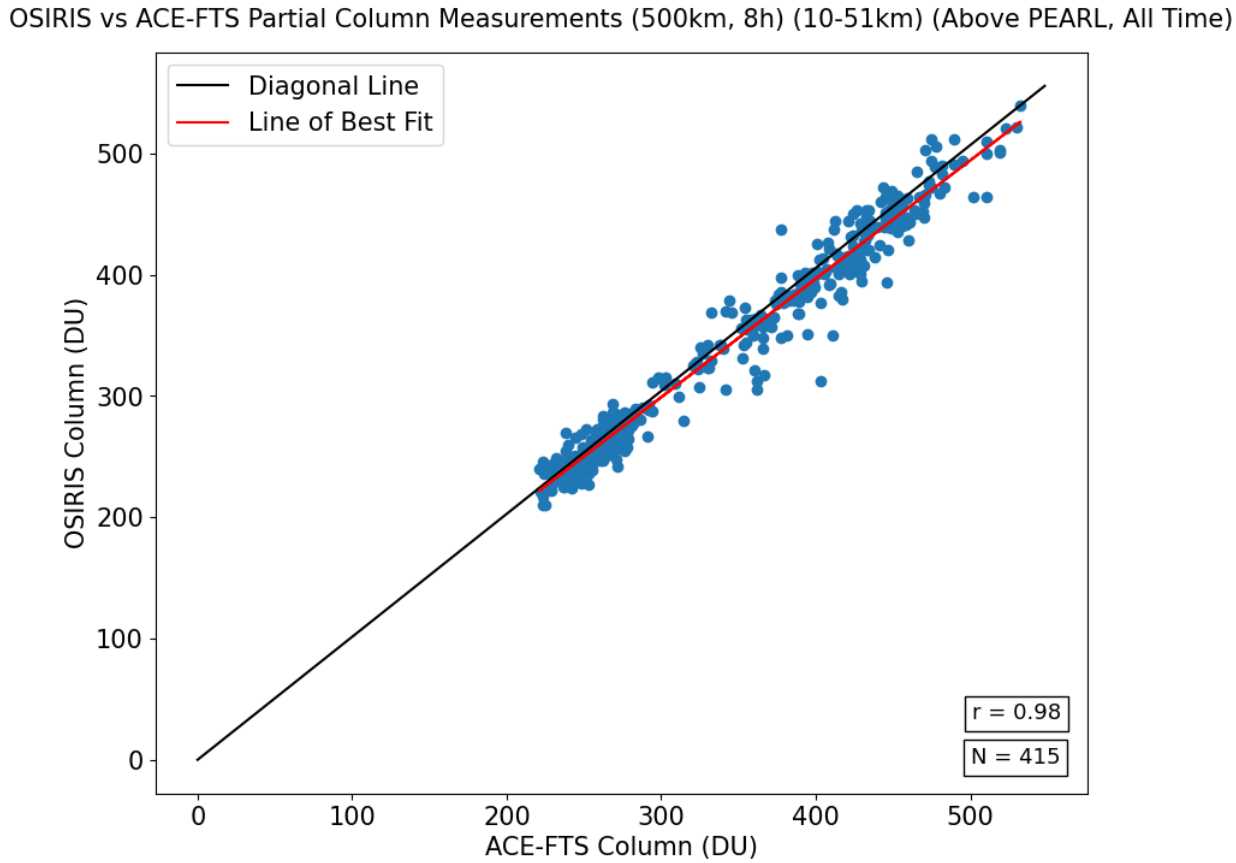

Figure 43. Scatter plot of OSIRIS and ACE-FTS coincident ozone column measurements above PEARL.

Similar to Figures 39 and 40, Figures 43 and 44 show significant agreement between column measurements across all seasons. However, there is a noteworthy decrease in correlation in the Northern Hemisphere fall season compared to the other seasons. The measurements seem to have better agreement above PEARL than globally.

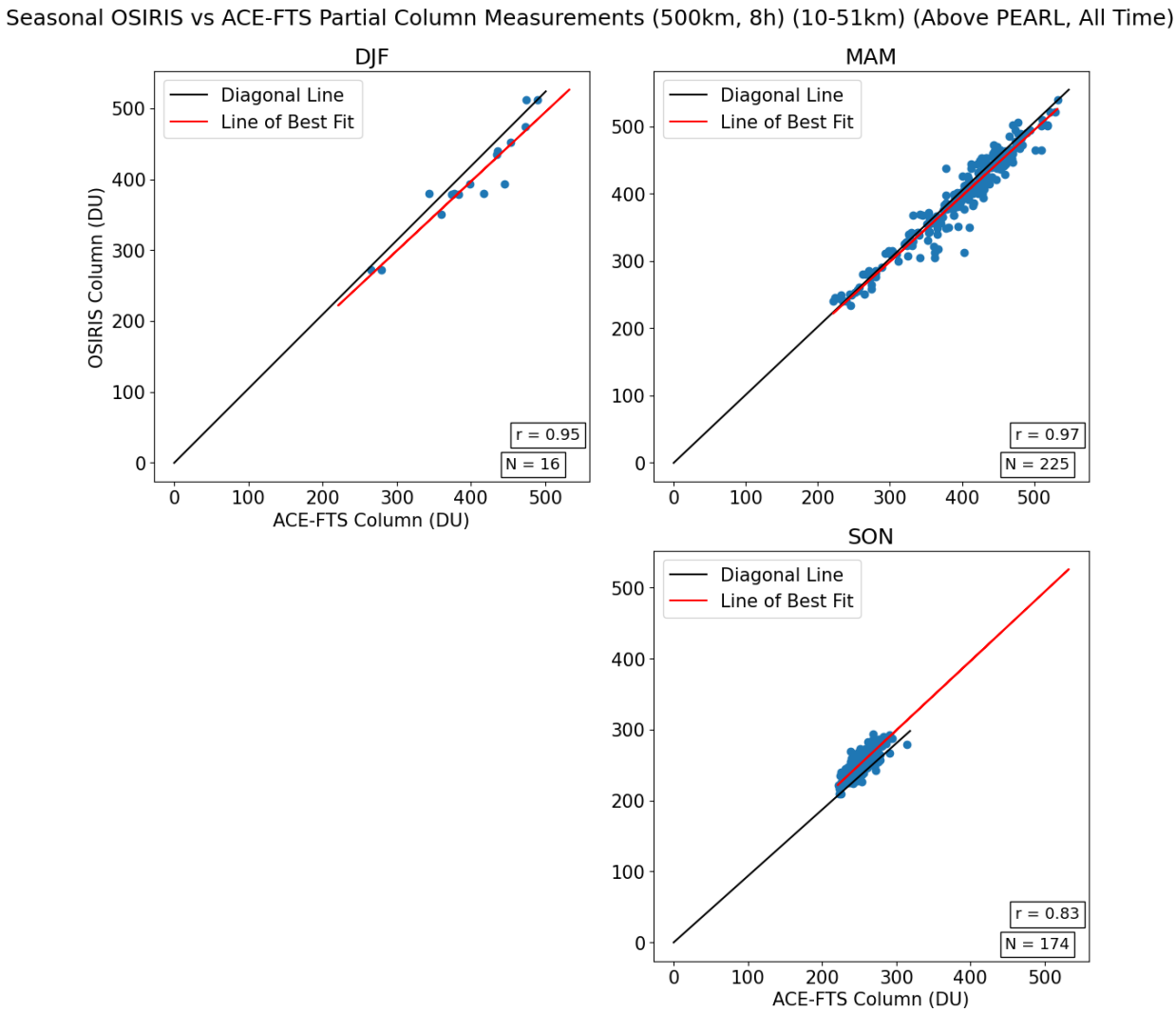

Figure 44. Seasonal scatter plots of OSIRIS and ACE-FTS coincident ozone column measurements above PEARL.

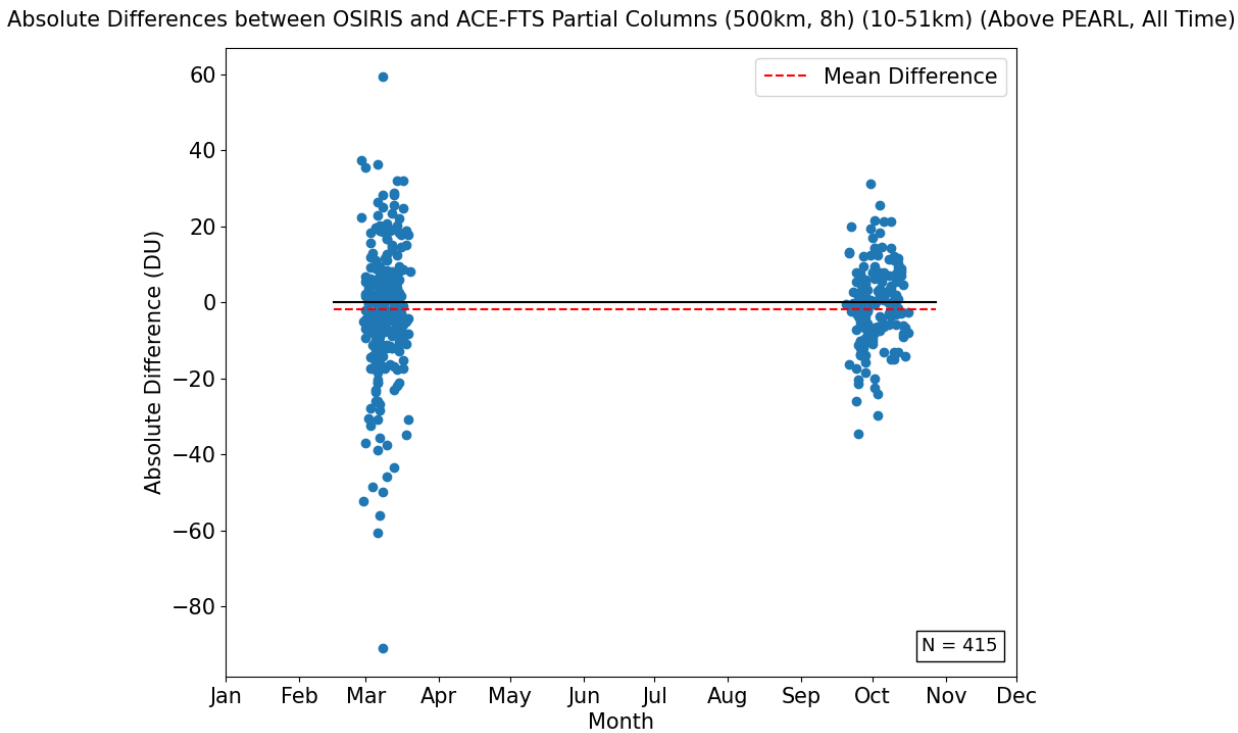

Figure 45. Scatter plot of absolute differences between OSIRIS and ACE-FTS coincident ozone column measurements above PEARL.

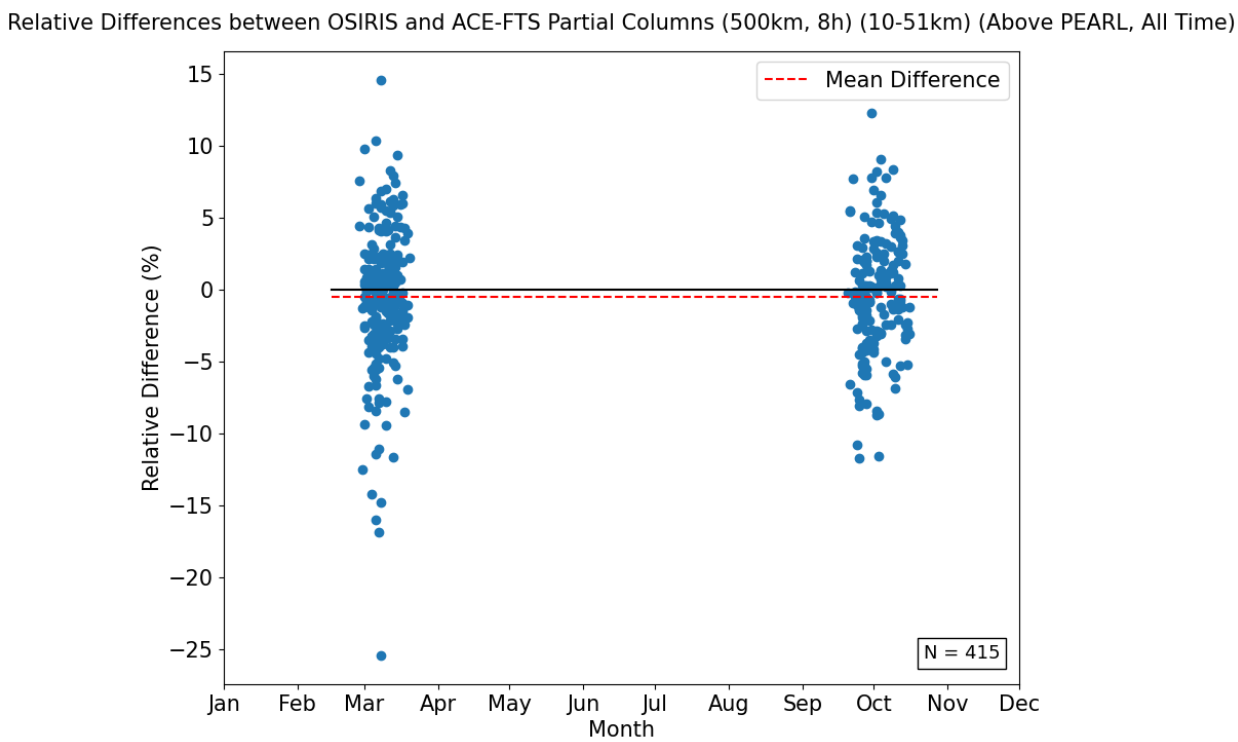

Figure 46. Scatter plot of relative differences between OSIRIS and ACE-FTS coincident ozone column measurements above PEARL.

Due to the requirement that measurements are above PEARL, the coincident measurement differences in Figures 45 and 46 are sparser throughout the year. During the months where coincident measurements occur above PEARL, the differences are more concentrated and less scattered around zero compared to global comparisons. The differences plots demonstrate that the measurements are close in agreement due to most individual differences and the mean difference being close to 0.

3.3.3 Satellite-based vs PEARL FTIR Column Comparisons

3.3.3.1 ACE-FTS vs PEARL FTIR Column Comparisons

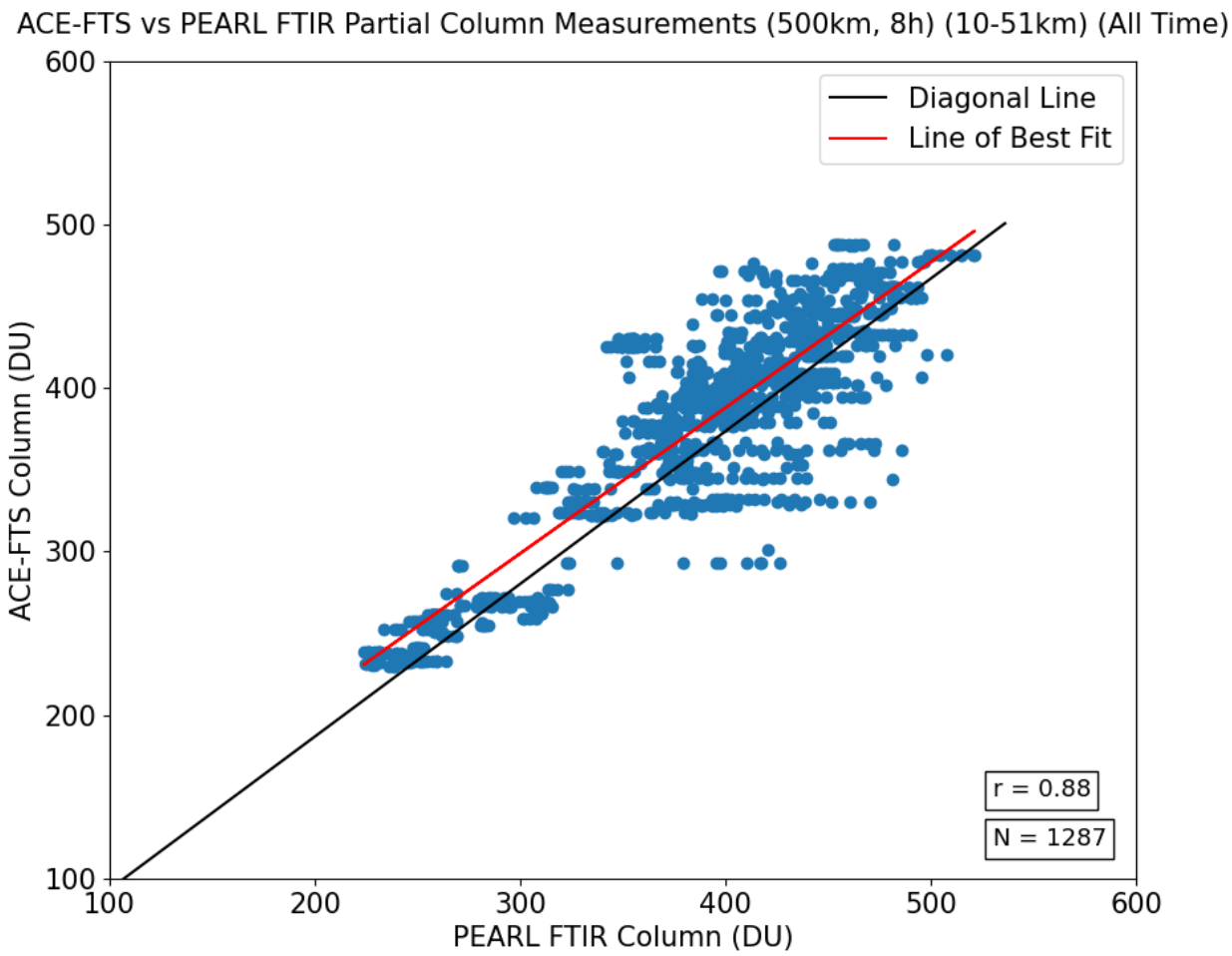

Figure 47. Scatter plot of ACE-FTS and PEARL FTIR coincident ozone column measurements.

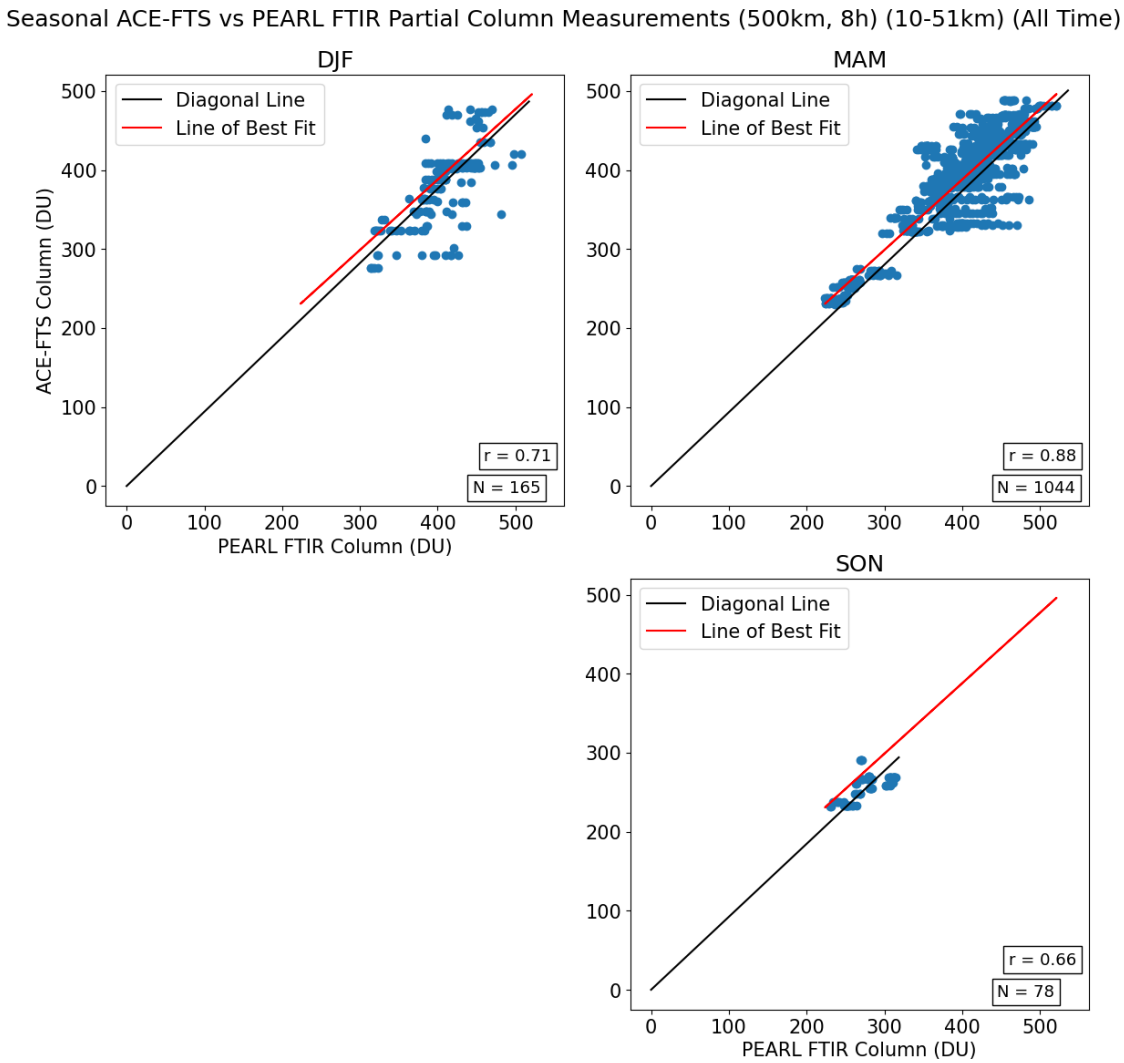

Figure 48. Seasonal scatter plots of ACE-FTS and PEARL FTIR coincident ozone column measurements.

Figures 47 and 48 shows close agreement between ACE-FTS and PEAR FTIR measurements. Although, less correlated than OSIRIS and ACE-FTS column measurements and more variable between different seasons. Northern Hemisphere fall measurements are the least correlated, followed by Northern Hemisphere winter. On the aggregate, the measurements are shown to be highly correlated in Figure 47. The reduced seasonal correlation might be due to lack of a representative sample size.

Figures 49 and 50 depict the high variability of the measurements, although, the measurements mostly agree since the differences are concentrated around zero along with the mean difference. These plots affirm the trends observed from the previous plots.

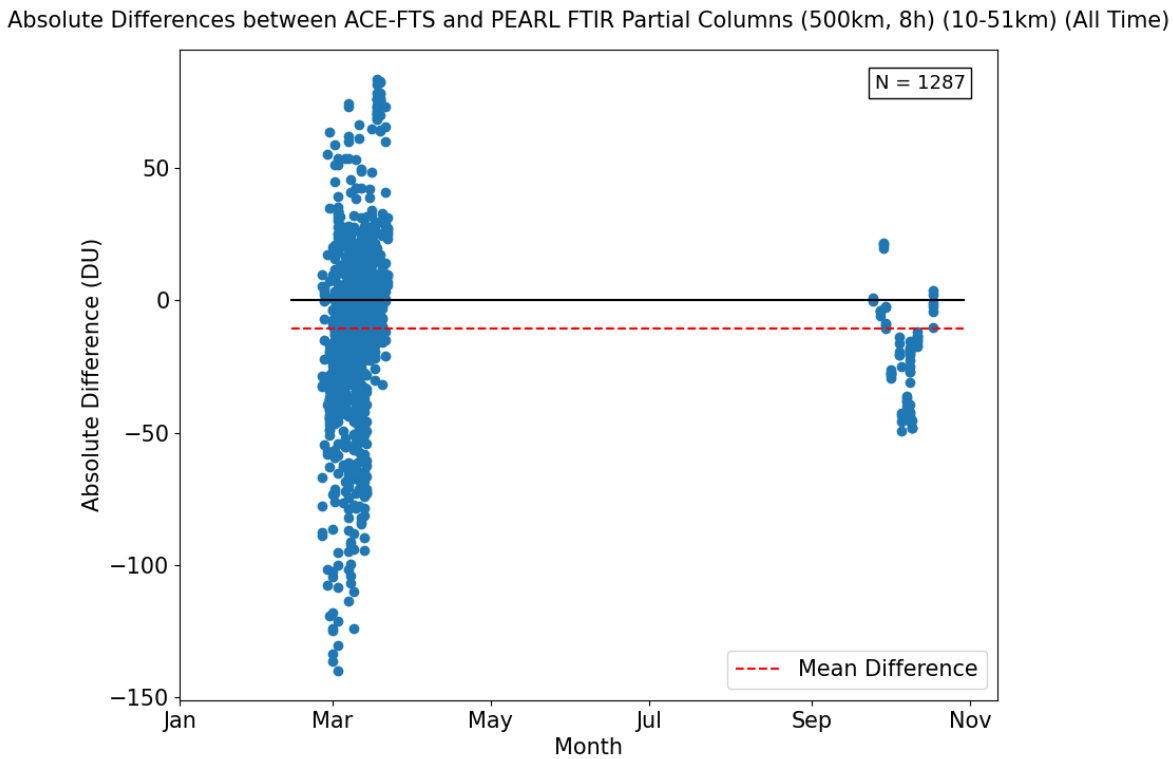

Figure 49. Scatter plot of absolute differences between ACE-FTS and PEARL FTIR coincident ozone column measurements.

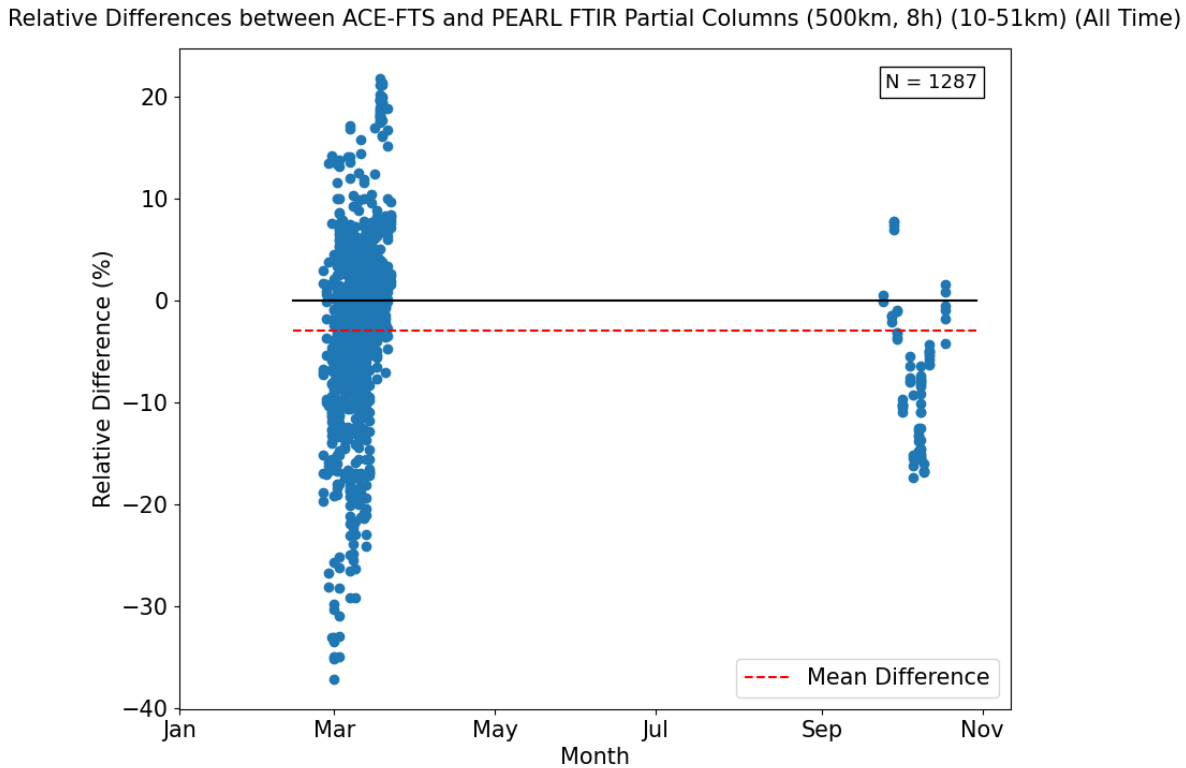

Figure 50. Scatter plot of relative differences between ACE-FTS and PEARL FTIR coincident ozone column measurements.

3.3.3.2 OSIRIS vs PEARL FTIR Column Comparisons

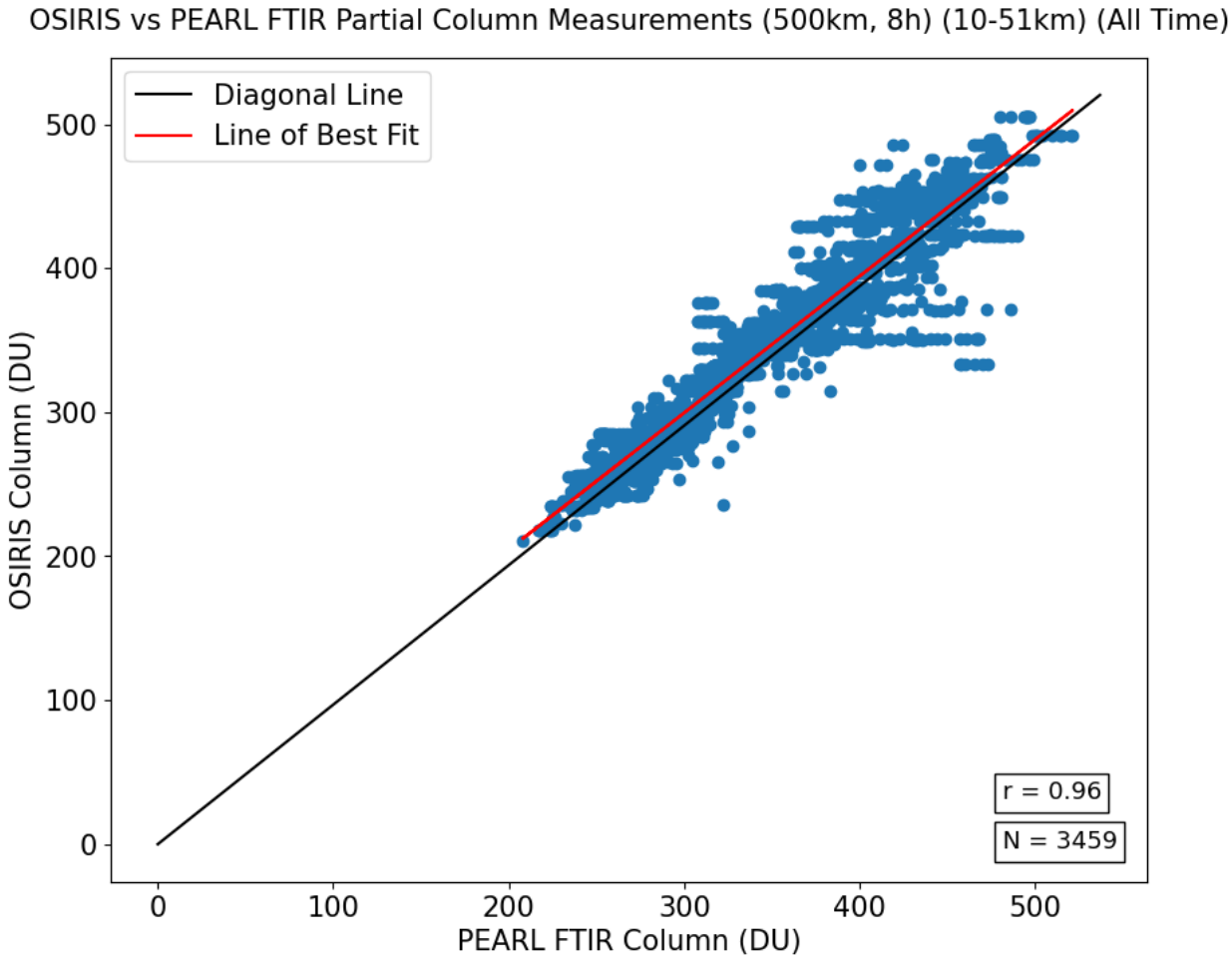

Figure 51. Scatter plot of OSIRIS and PEARL FTIR coincident ozone column measurements.

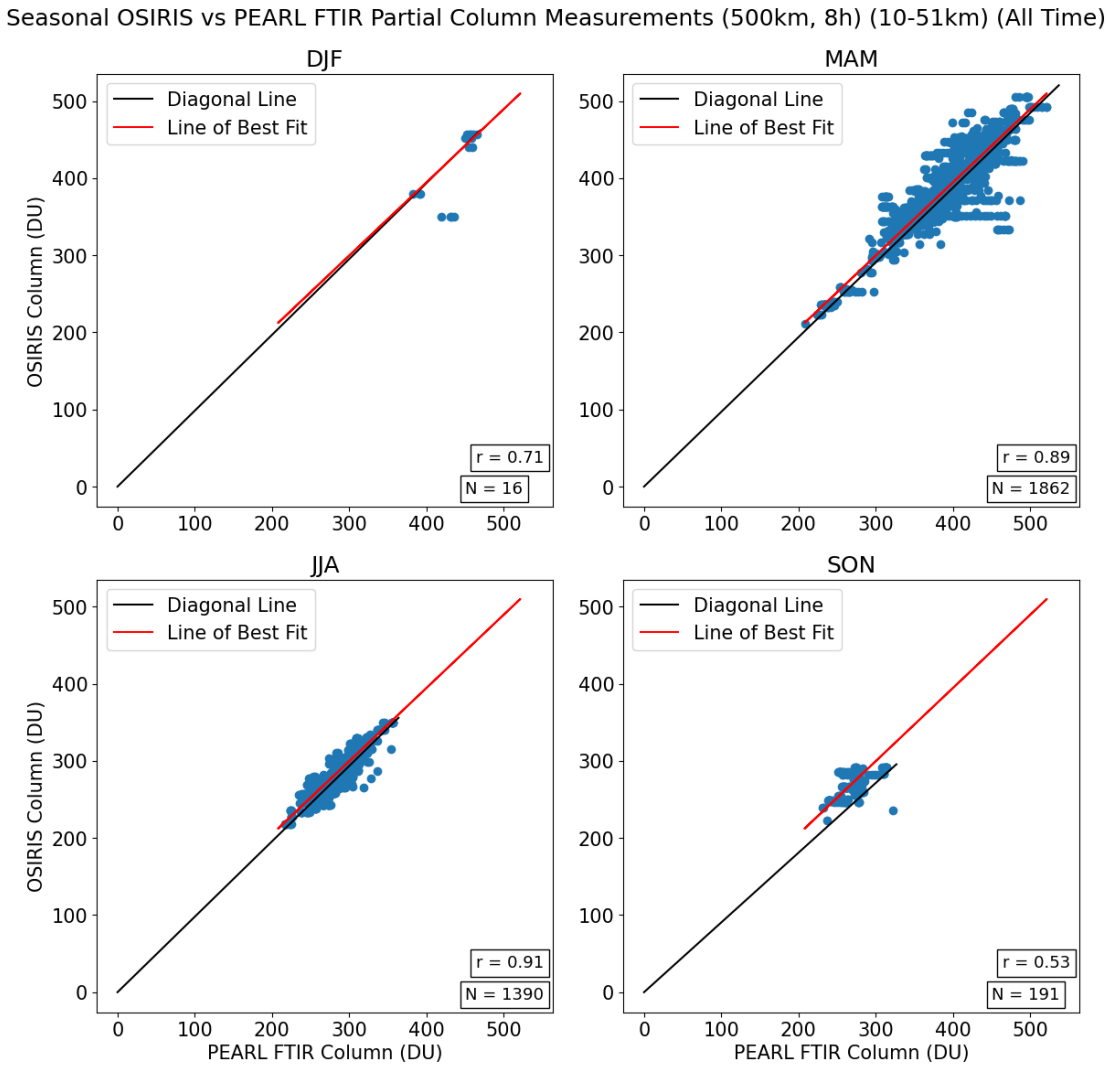

Figure 52. Seasonal scatter plots of OSIRIS and PEARL FTIR coincident ozone column measurements.

Resembling previous column comparisons, OSIRIS and PEARL FTIR show good agreement with very high correlation as seen in Figure 51. Figure 52 shows that the high correlation occurs mostly during Northern Hemisphere spring and summer. The other seasons have significantly lower correlation which possibly due to their lower sample sizes.

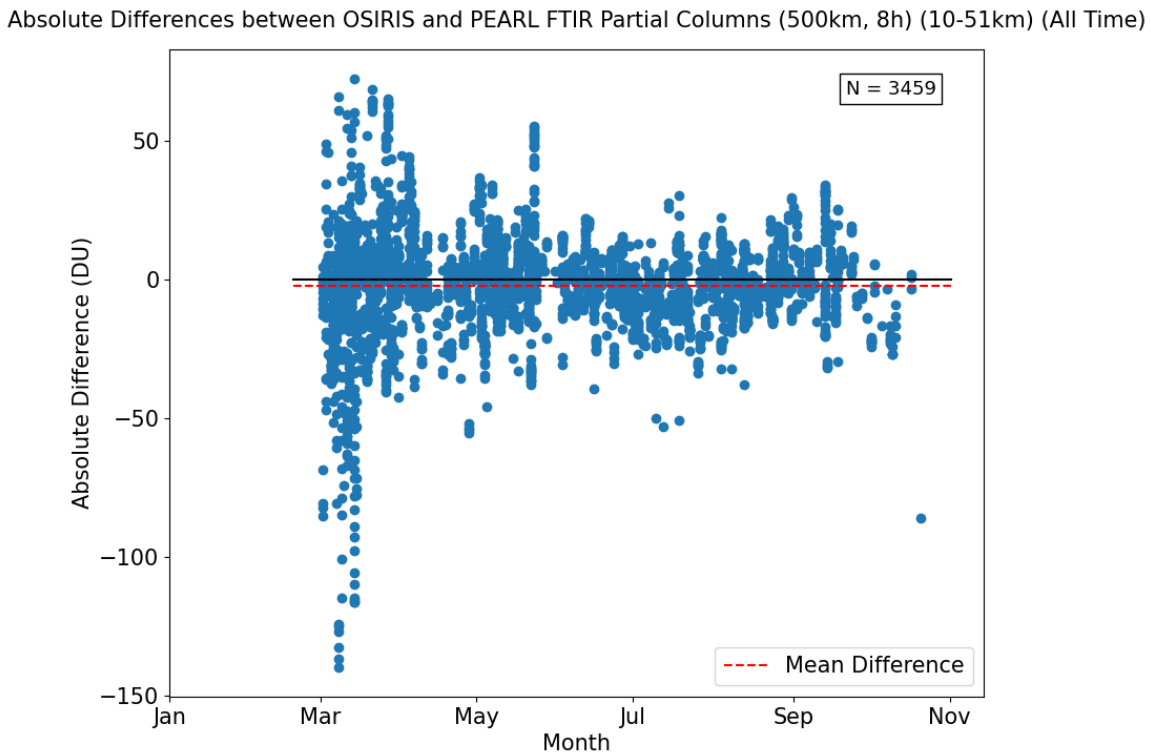

Figure 53. Scatter plot of absolute differences between OSIRIS and PEARL FTIR coincident ozone column measurements.

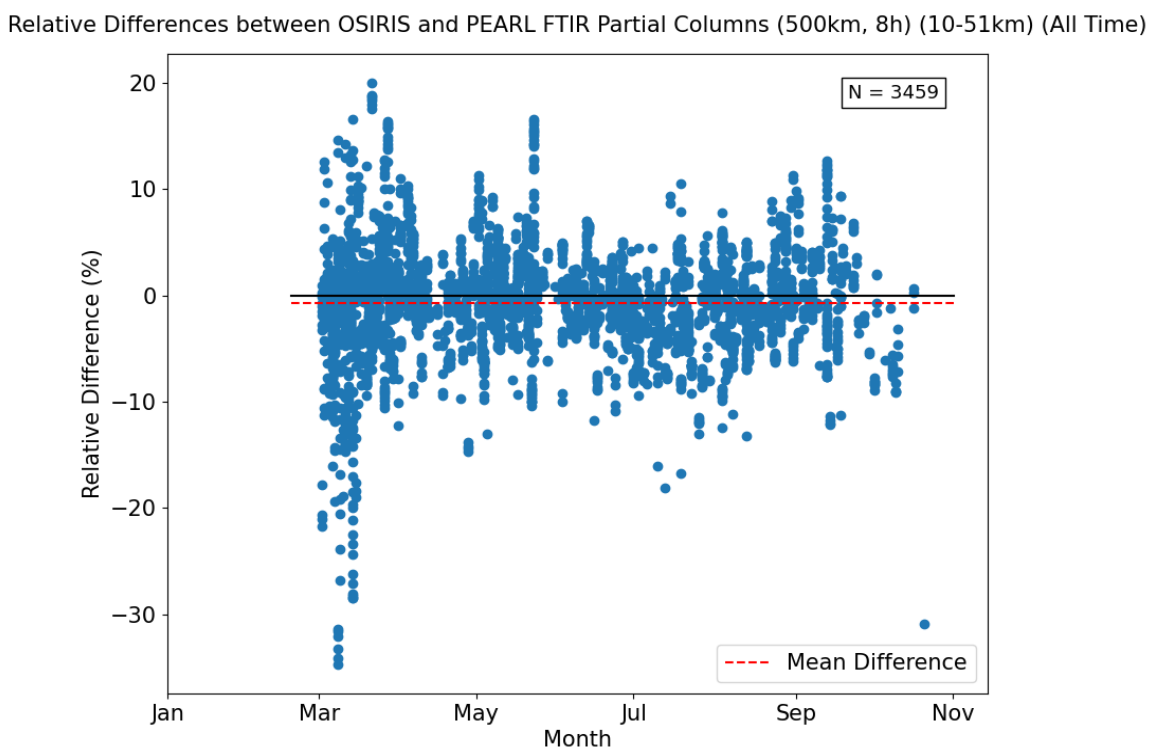

Figure 54. Scatter plot of relative differences between OSIRIS and PEARL FTIR coincident ozone column measurements.

These differences plot show that most differences are scattered around zero, including the mean difference, confirming the result seen in previous plots that the measurements are mostly correlated. The month of March shows more divergence away from zero, however, most of the other measurements being close to zero compensates for these outliers.

3.3.4 Time Series Column Comparisons

A regression line was fit to Time Series plots of absolute and relative column differences for each pair of measurement. The slope of this fitted line is used to infer the divergence of the instrument's measurements over time along with its 95% confidence interval. The slopes and their confidence intervals are included in Table 2 and discussed subsequently. The confidence intervals for the OSIRIS vs ACE-FTS (Above PEARL) and ACE-FTS vs PEARL FTIR pairs include 0, indicating that it is safe to assume the measurements are not significantly diverging. The other instrument pairs have confidence intervals not including 0 but very close to 0, furthermore, the slopes do not indicate a very significant divergence of measurement over time. For example, a slope value of 0.00032 indicates that it would take 10 years for the relative/absolute difference to change by about one unit which is not an urgent concern. The Time Series plots are included in the Appendix for a closer observation.

Instrument Pair	Difference Type	Fitted Slope	Margin of Error	95% Confidence Interval	Units
OSIRIS vs ACE-FTS (Global)	Relative Difference	-0.00009	0.00007	(-0.00015, -0.00002)	1%/day
OSIRIS vs ACE-FTS (Global)	Absolute Difference	-0.00025	0.00019	(-0.00044, -0.00006)	1DU/day
OSIRIS vs ACE-FTS (Above PEARL)	Relative Difference	0.00010	0.00023	(-0.00013, 0.00034)	1%/day
OSIRIS vs ACE-FTS (Above PEARL)	Absolute Difference	0.00033	0.00079	(-0.00046, 0.00112)	1DU/day
ACE-FTS vs PEARL FTIR	Relative Difference	0.00020	0.00035	(-0.00018, 0.00052)	1%/day
ACE-FTS vs PEARL FTIR	Absolute Difference	0.00020	0.00035	(-0.00018, 0.00052)	1DU/day
OSIRIS vs PEARL FTIR	Relative Difference	0.00020	0.00012	(0.00008, 0.00032)	1%/day
OSIRIS vs PEARL FTIR	Absolute Difference	0.00020	0.00012	(0.00008, 0.00032)	1DU/day

Table 2. Relevant values corresponding to Time Series analysis of differences between coincident ozone column measurements of each instrument pair.

4 Conclusion

This paper sought to assess the assess the validity of OSIRIS, ACE-FTS and PEARL FTIR ozone measurements. The assessment focused on comparing individual pairs of measurements within a great-circle distance of 500km and temporal distance of 8 hours using various metrics. For each profile comparison, the relative and absolute differences plots suggest that the measurements between the pairs of instruments are not significantly different, however, Pearson correlation coefficient plots do not always yield the same conclusions for the satellite vs PEARL FTIR comparisons. This discrepancy may be a result of general measurement variability or measurement variability intrinsic to the location of the measurements being above PEARL. Future work could focus on differentiating between measurements inside and outside the Northern Hemisphere polar vortex which may yield higher correlation for measurements above PEARL. Overall, there is good agreement between the profile measurements of all pairs of instruments on average. Column measurements for all pairs of instruments show significant correlation, also indicating good agreement. Some inconsistencies arose when assessing seasonal correlation, however, this could be attributed to those seasons having a non-representative sample size. Lastly, the instruments' column measurements do not seem to be significantly diverging over time, so, it can be assumed that none of these instruments has had any major issues develop over time.

5 Appendix

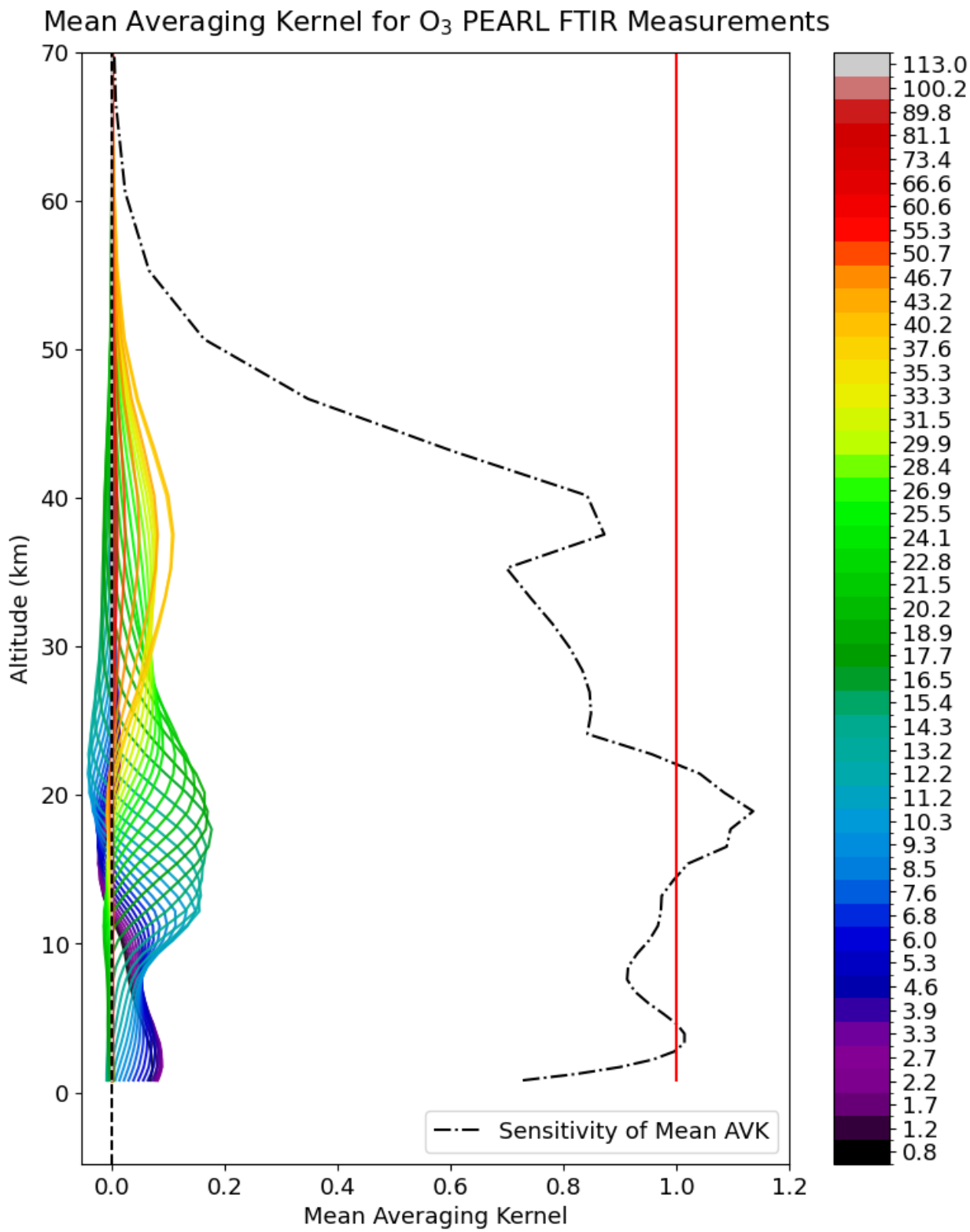
Mean Averaging Kernel for O_3 PEARL FTIR Measurements
Altitude (km)
Mean Averaging Kernel
Sensitivity of Mean AVK
0
10
20
30
40
50
60
70
0.0
0.2
0.4
0.6
0.8
1.0
1.2
113.0
100.2
89.8
81.1
73.4
66.6
60.6
55.3
50.7
46.7
43.2
40.2
37.6
35.3
33.3
31.5
29.9
28.4
26.9
25.5
24.1
22.8
21.5
20.2
18.9
17.7
16.5
15.4
14.3
13.2
12.2
11.2
10.3
9.3
8.5
7.6
6.8
6.0
5.3
4.6
3.9
3.3
2.7
2.2
1.7
1.2
0.8

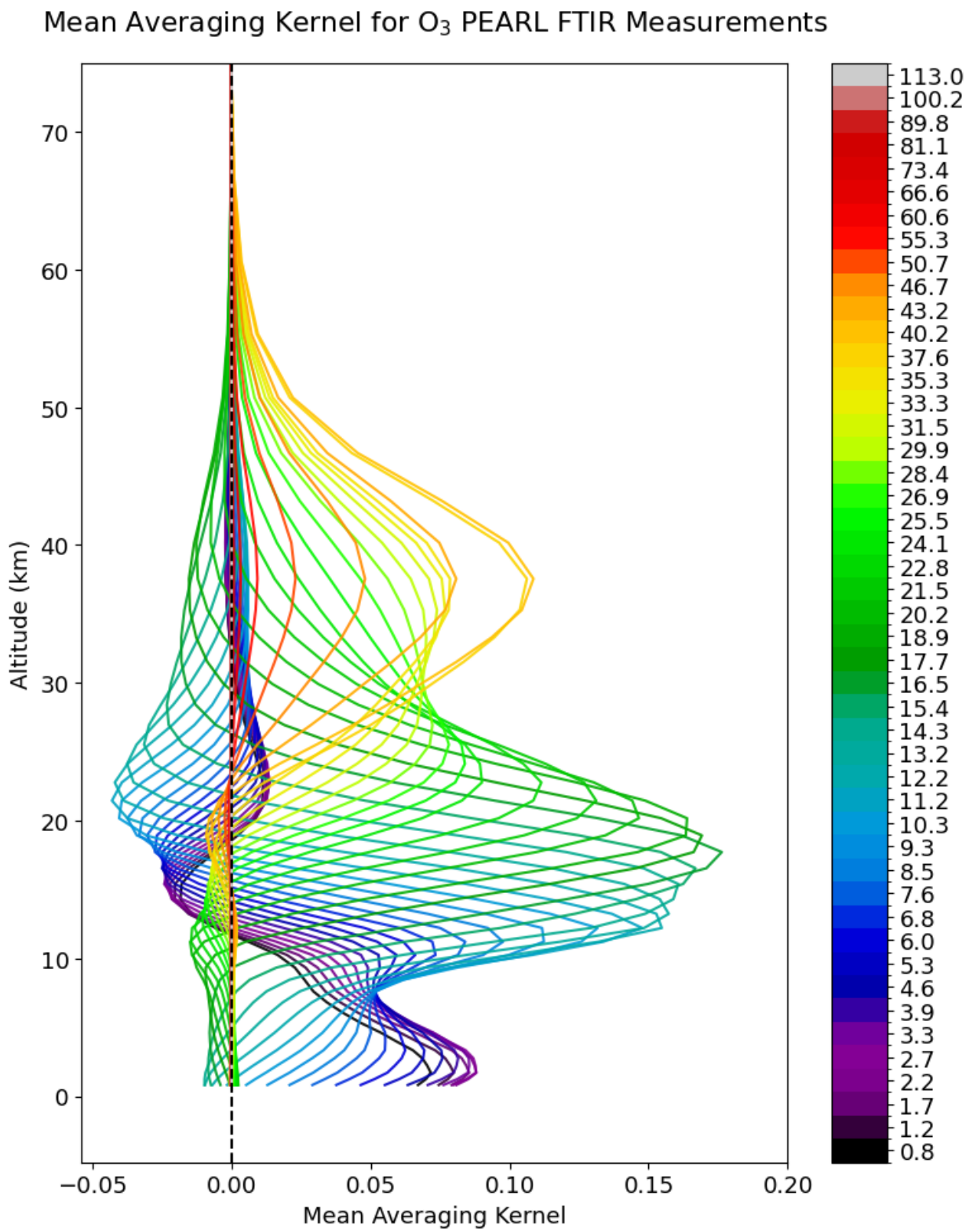
Mean Averaging Kernel for O_3 PEARL FTIR Measurements
Altitude (km)
Mean Averaging Kernel
−0.05
0.00
0.05
0.10
0.15
0.20
0
10
20
30
40
50
60
70
113.0
100.2
89.8
81.1
73.4
66.6
60.6
55.3
50.7
46.7
43.2
40.2
37.6
35.3
33.3
31.5
29.9
28.4
26.9
25.5
24.1
22.8
21.5
20.2
18.9
17.7
16.5
15.4
14.3
13.2
12.2
11.2
10.3
9.3
8.5
7.6
6.8
6.0
5.3
4.6
3.9
3.3
2.7
2.2
1.7
1.2
0.8

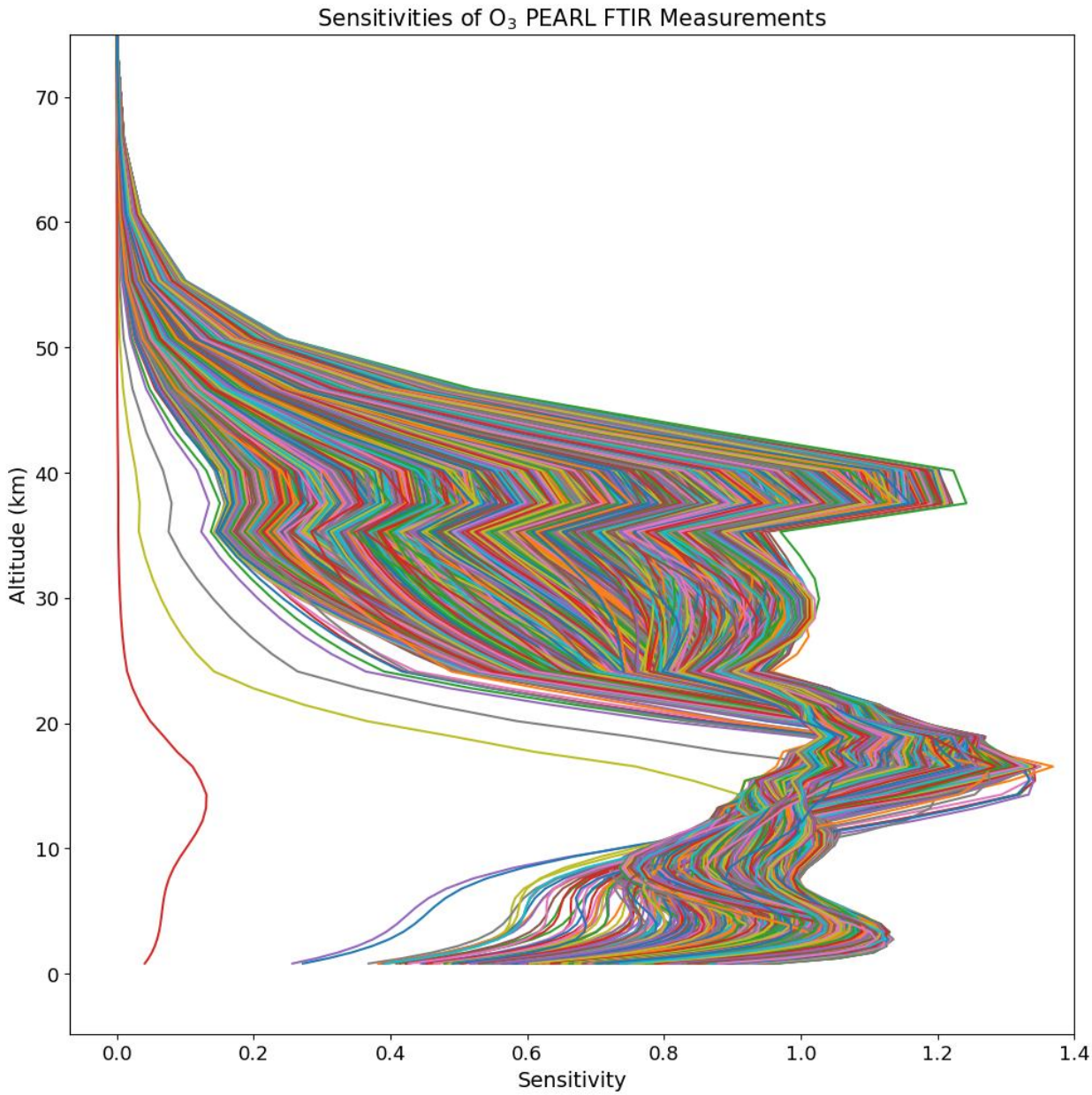
Sensitivities of O_3 PEARL FTIR Measurements
Altitude (km)
Sensitivity
0
10
20
30
40
50
60
70
0.0
0.2
0.4
0.6
0.8
1.0
1.2
1.4

Absolute Differences between OSIRIS and ACE-FTS Partial Columns Over Time (500km, 8h) (10-51km) (Global, All Time)

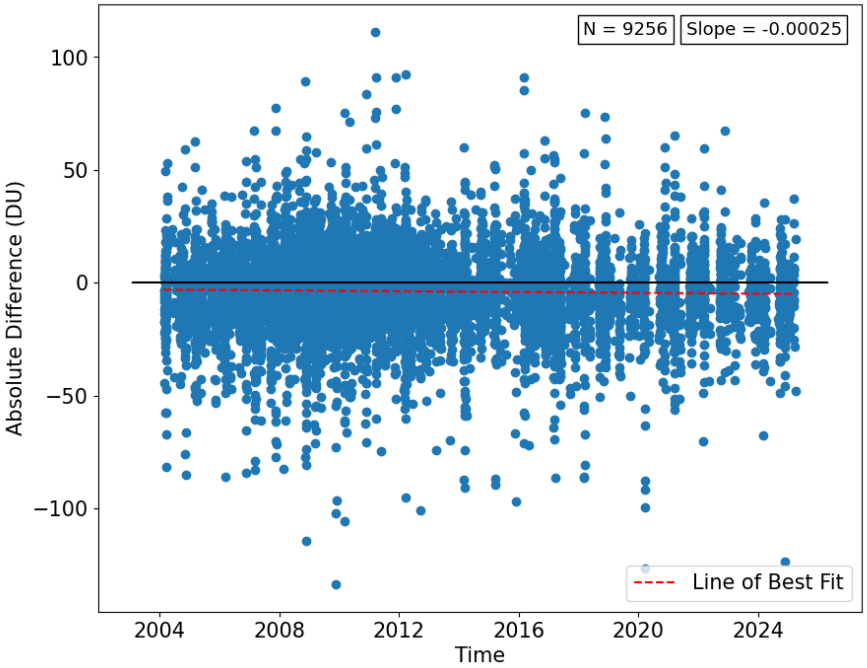

Relative Differences between OSIRIS and ACE-FTS Partial Columns Over Time (500km, 8h) (10-51km) (Global, All Time)

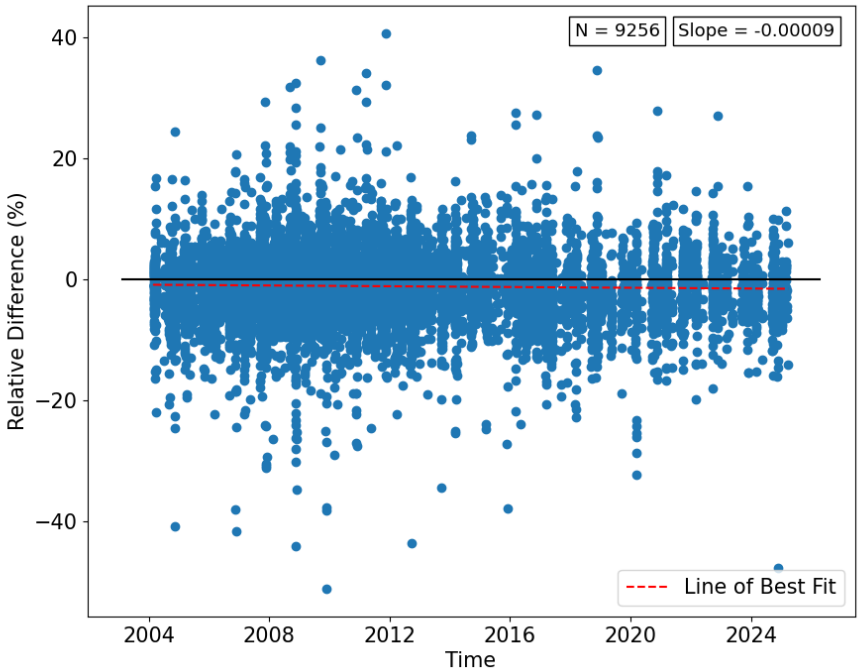

Absolute Differences between OSIRIS and ACE-FTS Partial Columns Over Time (500km, 8h) (10-51km) (Above PEARL, All Time)

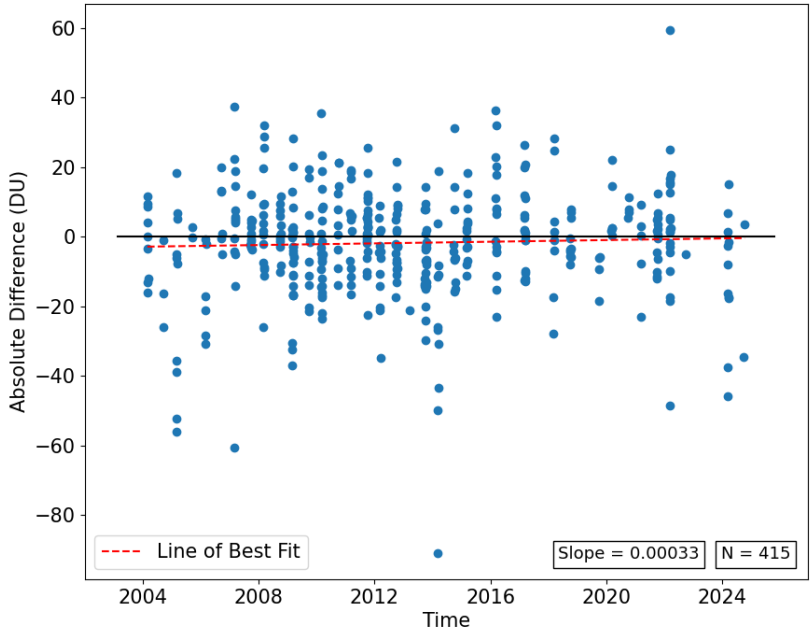

Relative Differences between OSIRIS and ACE-FTS Partial Columns Over Time (500km, 8h) (10-51km) (Above PEARL, All Time)

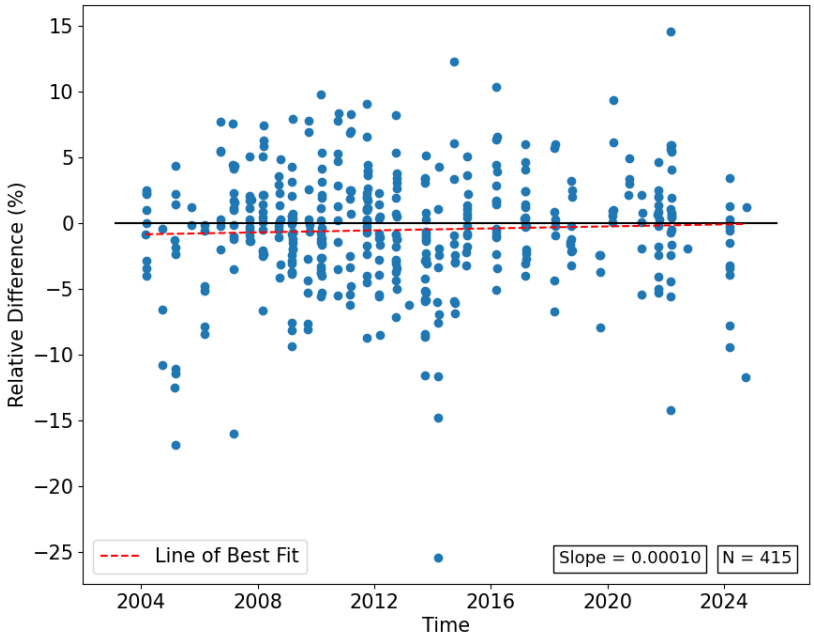

Absolute Differences between ACE-FTS and PEARL FTIR Partial Columns Over Time (500km, 8h) (10-51km) (All Time)

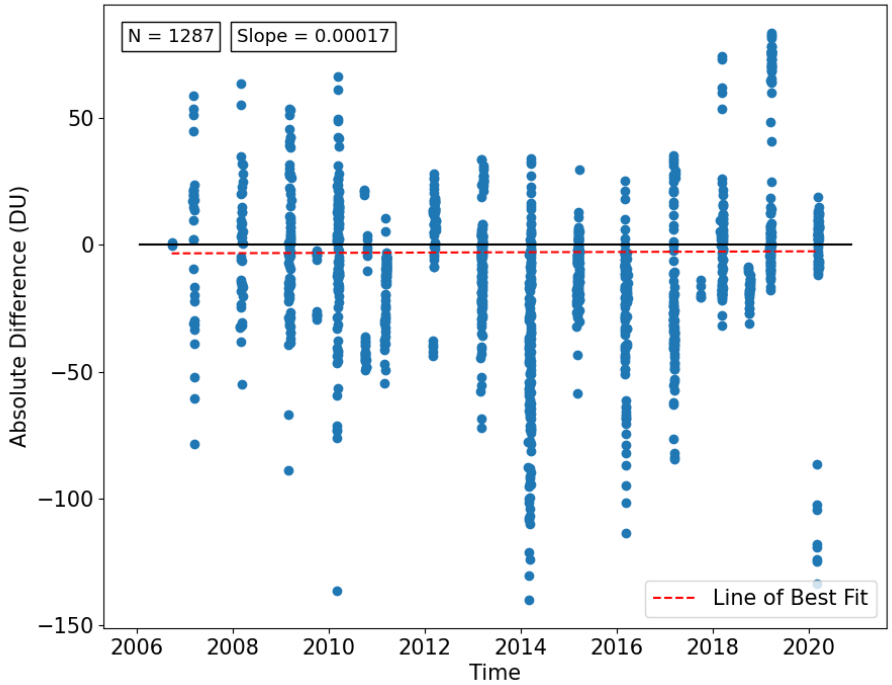

Relative Differences between ACE-FTS and PEARL FTIR Partial Columns Over Time (500km, 8h) (10-51km) (All Time)

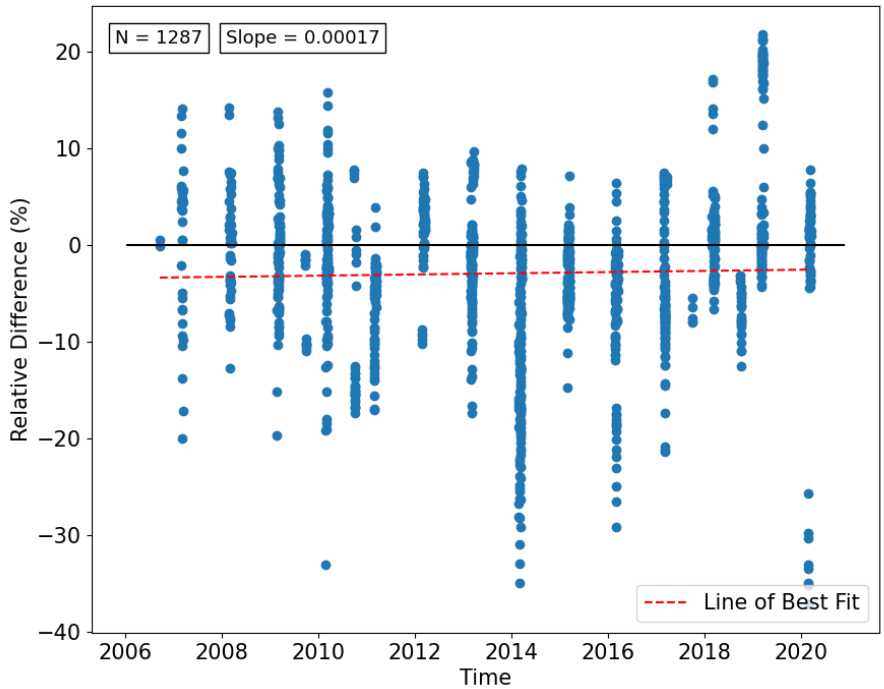

Absolute Differences between OSIRIS and PEARL FTIR Partial Columns Over Time (500km, 8h) (10-51km) (All Time)

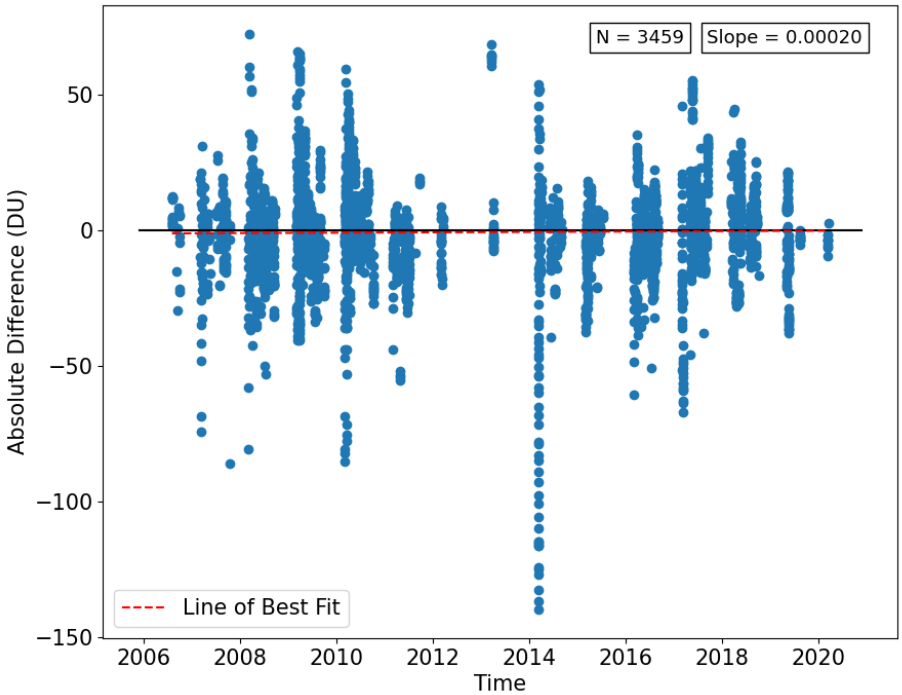

Relative Differences between OSIRIS and PEARL FTIR Partial Columns Over Time (500km, 8h) (10-51km) (All Time)

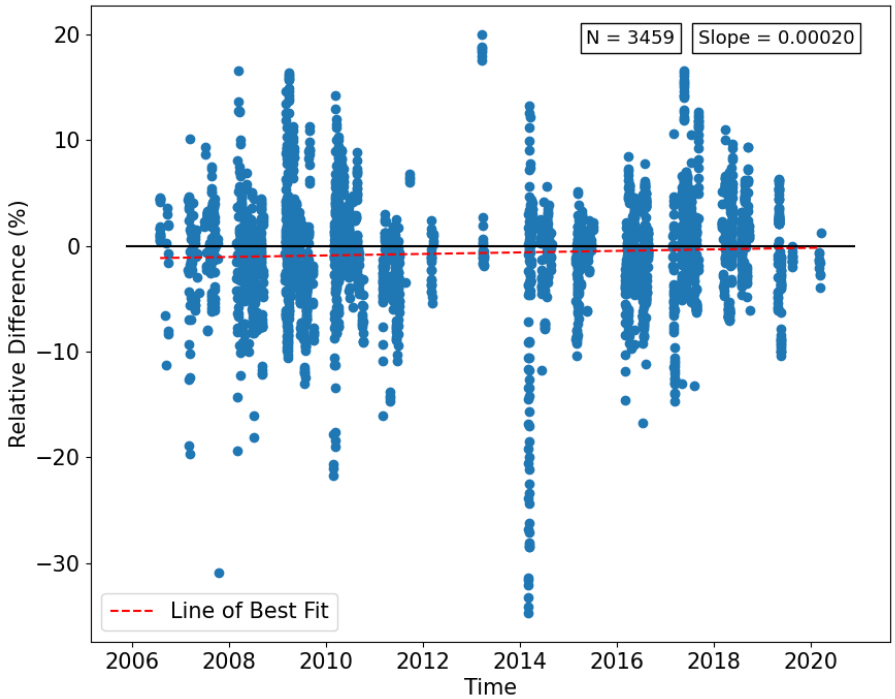

6 References

Adams, C., Strong, K., Batchelor, R. L., Bernath, P. F., Brohede, S., Boone, C., Degenstein, D., Daffer, W. H., Drummond, J. R., Fogal, P. F., Farahani, E., Fayt, C., Fraser, A., Goutail, F., Hendrick, F., Kolonjari, F., Lindenmaier, R., Manney, G., McElroy, C. T., … Zhao, X. (2012). Validation of ACE and OSIRIS ozone and NO_2 measurements using ground-based instruments at 80° N. *Atmospheric Measurement Techniques*, *5*(5), 927–953. https://doi.org/10.5194/amt-5-927-2012

Batchelor, R. L., Kolonjari, F., Lindenmaier, R., Mittermeier, R. L., Daffer, W., Fast, H., Manney, G., Strong, K., & Walker, K. A. (2010). Four Fourier transform spectrometers and the Arctic polar vortex: Instrument intercomparison and ACE-FTS validation at Eureka during the IPY springs of 2007 and 2008. *Atmospheric Measurement Techniques*, *3*(1), 51–66. https://doi.org/10.5194/amt-3-51-2010

Batchelor, R. L., Strong, K., Lindenmaier, R., Mittermeier, R. L., Fast, H., Drummond, J. R., & Fogal, P. F. (2009). *A New Bruker IFS 125HR FTIR Spectrometer for the Polar Environment Atmospheric Research Laboratory at Eureka, Nunavut, Canada: Measurements and Comparison with the Existing Bomem DA8 Spectrometer*. https://doi.org/10.1175/2009JTECHA1215.1

Bernath, P. F., McElroy, C. T., Abrams, M. C., Boone, C. D., Butler, M., Camy-Peyret, C., Carleer, M., Clerbaux, C., Coheur, P.-F., Colin, R., DeCola, P., DeMazière, M., Drummond, J. R., Dufour, D., Evans, W. F. J., Fast, H., Fussen, D., Gilbert, K., Jennings, D. E., … Zou, J. (2005). Atmospheric Chemistry Experiment (ACE): Mission overview. *Geophysical Research Letters*, *32*(15). https://doi.org/10.1029/2005GL022386

Department of Physics, University of Toronto. (n.d.). *Eureka Physics*. Retrieved July 31, 2025, from https://eureka.physics.utoronto.ca/

Griffin, D., Walker, K. A., Conway, S., Kolonjari, F., Strong, K., Batchelor, R., Boone, C. D., Dan, L., Drummond, J. R., Fogal, P. F., Fu, D., Lindenmaier, R., Manney, G. L., & Weaver, D. (2017). Multi-year comparisons of ground-based and space-borne Fourier transform spectrometers in the high Arctic between 2006 and 2013. *Atmospheric Measurement Techniques*, *10*(9), 3273–3294. https://doi.org/10.5194/amt-10-3273-2017

Jeffery, P. S. (2022). *Water Vapour and Ozone: Measuring Key Trace Gases in Challenging Regions*. http://hdl.handle.net/1807/123476

Kerzenmacher, T. E., Walker, K. A., Strong, K., Berman, R., Bernath, P. F., Boone, C. D., Drummond, J. R., Fast, H., Fraser, A., MacQuarrie, K., Midwinter, C., Sung, K., McElroy, C. T., Mittermeier, R. L., Walker, J., & Wu, H. (2005). Measurements of O3, NO2 and Temperature during the 2004 Canadian Arctic ACE Validation Campaign. *Geophysical Research Letters*, *32*(16). https://doi.org/10.1029/2005GL023032

Llewellyn, E. J., Lloyd, N. D., Degenstein, D. A., Gattinger, R. L., Petelina, S. V., Bourassa, A. E., Wiensz, J. T., Ivanov, E. V., McDade, I. C., Solheim, B. H., McConnell, J. C., Haley, C. S., von Savigny, C., Sioris, C. E., McLinden, C. A., Griffioen, E., Kaminski, J., Evans, W. F., Puckrin, E., … Nordh, L. (2004). The OSIRIS instrument on the Odin spacecraft. *Canadian Journal of Physics*, *82*(6), 411–422. https://doi.org/10.1139/p04-005

McElroy, C. T., Nowlan, C. R., Drummond, J. R., Bernath, P. F., Barton, D. V., Dufour, D. G., Midwinter, C., Hall, R. B., Ogyu, A., Ullberg, A., Wardle, D. I., Kar, J., Zou, J., Nichitiu, F., Boone, C. D., Walker, K. A., & Rowlands, N. (2007). The ACE-MAESTRO instrument on SCISAT: Description, performance, and preliminary results. *Applied Optics*, *46*(20), 4341–4356. https://doi.org/10.1364/ao.46.004341

Murtagh, D., Frisk, U., Merino, F., Ridal, M., Jonsson, A., Stegman, J., Witt, G., Eriksson, P., Jiménez, C., Megie, G., Noë, J. de la, Ricaud, P., Baron, P., Pardo, J. R., Hauchcorne, A., Llewellyn, E. J., Degenstein, D. A., Gattinger, R. L., Lloyd, N. D., … Oikarinen, L. (2002). An overview of the Odin atmospheric mission. *Canadian Journal of Physics*, *80*(4), 309–319. https://doi.org/10.1139/p01-157

National Oceanic and Atmospheric Administration. (2024, July 2). *The Atmosphere*. https://www.noaa.gov/jetstream/atmosphere

Salawitch, R. J., McBride, L. A., Thompson, C. R., Fleming, E. L., McKenzie, R. L., Rosenlof, K. H., Doherty, S. J., & Fahey, D. W. (2023). *Twenty questions and answers about the ozone layer: 2022 update* (Scientific Assessment of Ozone Depletion: 2022; 75 pp.). World Meteorological Organization.

Sheese, P. E., Boone, C. D., & Walker, K. A. (2015). Detecting physically unrealistic outliers in ACE-FTS atmospheric measurements. *Atmospheric Measurement Techniques*, *8*(2), 741–750. https://doi.org/10.5194/amt-8-741-2015